ฟลูออเรสเซนต์คีโมเซ็นเซอร์จากอนุพันธ์บิส (1,4-ไดไฮโดรพิริดีน) ที่มีตัวเชื่อมออลิโกเอทิลีนไกลคอล

นายณัฐพงษ์ ศรีเมือง

วิทยานิพนธ์นี้เป็นส่วนหนึ่งของการศึกษาตามหลักสูตรปริญญาวิทยาศาสตรมหาบัณฑิต
สาขาวิชาเคมี ภาควิชาเคมี
คณะวิทยาศาสตร์ จุฬาลงกรณ์มหาวิทยาลัย
ปีการศึกษา 2557

FLUORESCENT CHEMOSENSORS FROM BIS(1,4-DIHYDROPYRIDINE) DERIVATIVES WITH OLIGOETHYLENE GLYCOL LINKER

Mr. Nattapong Srimuang

A Thesis Submitted in Partial Fulfillment of the Requirements
for the Degree of Master of Science Program in Chemistry
Department of Chemistry
Faculty of Science
Chulalongkorn University
Academic Year 2014

Thesis Title	FLUORESCENT CHEMOSENSORS FROM BIS(1,4-DIHYDROPYRIDINE) DERIVATIVES WITH OLIGOETHYLENE GLYCOL LINKER
By	Mr. Nattapong Srimuang
Field of Study	Chemistry
Thesis Advisor	Assistant Professor Anawat Ajavakom, Ph.D.
Thesis Co-Advisor	Associate Professor Mongkol Sukwattanasinitt, Ph.D.

Accepted by the Faculty of Science, Chulalongkorn University in Partial Fulfillment of the Requirements for the Master's Degree

.....Dean of the Faculty of Science
(Professor Supot Hannongbua, Dr.rer.nat.)

THESIS COMMITTEE

.....Chairman
(Associate Professor Vudhichai Parasuk, Ph.D.)

.....Thesis Advisor
(Assistant Professor Anawat Ajavakom, Ph.D.)

.....Thesis Co-Advisor
(Associate Professor Mongkol Sukwattanasinitt, Ph.D.)

.....Examiner
(Associate Professor Paitoon Rashatasakhon, Ph.D.)

.....External Examiner
(Assistant Professor Nantanit Wanichacheva, Ph.D.)

ณัฐพงษ์ ศรีเมือง : ฟลูออเรสเซนต์คีโมเซ็นเซอร์จากอนุพันธ์บิส (1,4-ไดไฮโดรพิริดีน) ที่มีตัวเชื่อมออลิโกเอทิลีนไกลคอล (FLUORESCENT CHEMOSENSORS FROM BIS(1,4-DIHYDROPYRIDINE) DERIVATIVES WITH OLIGOETHYLENE GLYCOL LINKER) อ.ที่ปรึกษาวิทยานิพนธ์หลัก: ผศ. ดร.อนวัช อาชวาคม, อ.ที่ปรึกษาวิทยานิพนธ์ร่วม: รศ. ดร.มงคล สุขวัฒนาสินิทธิ์, 124 หน้า.

เพื่อศึกษาความเป็นไปได้ในการนำอนุพันธ์ 1,4-ไดไฮโดรพิริดีน (DHP) มาใช้เป็นฟลูออเรสเซนต์คีโมเซ็นเซอร์และศึกษาเพิ่มเติมถึงลักษณะเชิงอัลโลสเตอริกของคีโมเซ็นเซอร์ดังกล่าว ดังนั้นอนุพันธ์ DHP ชนิดใหม่ (1c และ 1d) จึงได้รับการสังเคราะห์ขึ้นจาก 4-อะมิโนฟีนอลผ่านปฏิกิริยาไซโคลไตรเมอไรเซชั่นของสารมัธยันต์เบต้าอะมิโนอะคริเลต อนุพันธ์ดังกล่าวมีคุณสมบัติการเรืองแสงที่ดีและง่ายต่อการนำไปเชื่อมต่อกับสายโอลิโกเอทิลีนไกลคอลที่มีความยาวสายต่างๆกัน และได้เป็น bis DHP (5a-d) และ mono DHP (6c, 7 and 8) เพื่อพัฒนาเป็นฟลูออเรสเซนต์คีโมเซ็นเซอร์ สายไกลคอลโดยหลักการแล้วนอกจากจะช่วยเพิ่มสมบัติการละลายน้ำแล้วยังอาจใช้เป็นหน่วยตรวจจับสารได้เมื่อจัดตัวอยู่ในตัวทำละลายอินทรีย์ จากนั้นนำเอาอนุพันธ์ที่ได้มาศึกษาสมบัติการดูดกลืนแสงและการคายแสงทั้งในน้ำและตัวทำละลายอินทรีย์ ในตัวทำละลายเมทานอลทุกอนุพันธ์ให้ค่าการดูดกลืนแสงสูงสุดอยู่ในช่วงความยาวคลื่น 360 ถึง 368 นาโนเมตร การคายแสงสูงสุดอยู่ในช่วง 454 ถึง 466 นาโนเมตร และให้ประสิทธิภาพการคายแสง (Φ_f) เท่ากับ 0.32 ถึง 0.74 ยิ่งไปกว่านั้นการศึกษาคุณสมบัติในการตรวจวัดไอออนโลหะพบว่า สารทุกตัวตอบสนองอย่างจำเพาะกับไอออนทอง(III) ในน้ำ และดับสัญญาณการคายแสงลงตามเวลา โดยสาร 5d พบค่าการตรวจวัดต่ำสุดอยู่ที่ 2.65 μM พฤติกรรมดังกล่าวคาดว่ามาจากปฏิกิริยาออกซิเดชั่นที่เปลี่ยนวงไพริดีนไปเป็นวงไพริดิเนี่ยมโดยมีไอออนทอง(III) เป็นตัวเร่งปฏิกิริยาอย่างจำเพาะ นอกจากนี้การทดลองในระบบที่มีสารลดแรงตึงผิว (Triton X-100) พบว่ามีเพียงสารกลุ่ม bis DHP (5a-d) เท่านั้นที่มีการเพิ่มสัญญาณการเรืองแสง ซึ่งสาร 5d ในระบบนี้ให้ความจำเพาะกับไอออนเหล็ก(II) และให้ค่าการตรวจวัดต่ำสุดอยู่ที่ 1.69 μM และยังได้ทำการทดลองในระบบที่ควบคุมค่า pH ซึ่งพบว่าสาร 1c และ 1d เท่านั้นที่ตอบสนองด้วยการลดลงของสัญญาณการเรืองแสงในช่วงที่มีฤทธิ์เป็นด่าง โดยสาร 1d นั้นมีค่า pK_a เท่ากับ 9.23 ± 0.03 ซึ่งสามารถนำไปใช้เป็นพีเอชเซ็นเซอร์ได้ในช่วง 8.6 ถึง 9.8 ผู้วิจัยยังได้ศึกษาการนำไปประยุกต์ใช้ในด้านอื่นๆอีกเช่น โปรตีนเซ็นเซอร์และออกซิแดนท์เซ็นเซอร์

ภาควิชา เคมี ลายมือชื่อนิสิต .....

สาขาวิชา เคมี ลายมือชื่อ อ.ที่ปรึกษาหลัก .....

ปีการศึกษา 2557 ลายมือชื่อ อ.ที่ปรึกษาร่วม .....

5471966723 : MAJOR CHEMISTRY

KEYWORDS: 1,4-DIHYDROPYRIDINE / FLUORESCENT CHEMOSENSOR / ALLOSTERIC / OLIGOETHYLENE GLYCOL / METAL ION

NATTAPONG SRIMUANG: FLUORESCENT CHEMOSENSORS FROM BIS(1,4-DIHYDROPYRIDINE) DERIVATIVES WITH OLIGOETHYLENE GLYCOL LINKER. ADVISOR: ASST. PROF. ANAWAT AJAVAKOM, Ph.D., CO-ADVISOR: ASSOC. PROF. MONGKOL SUKWATTANASINITT, Ph.D., 124 pp.

To study the possibility of using the 1,4-dihydropyridine (DHP) derivatives as fluorescent sensor and comprehend their allosteric property, novel DHP derivatives (1c and 1d) thus were synthesized from 4-aminophenol via cyclotrimerization reaction of β-amino acrylate intermediate. These compounds offer great fluorescent properties and were easy to linked with various lengths of oligoethylene glycol to gain bis DHPs (5a-d) and mono DHPs (6c, 7 and 8) for the development as fluorescent chemosensor. Glycol chain conceptually did not only enhance its water solubility but also acted as a receptor unit in organic media. The target compounds were studied in terms of absorption and emission properties in both aqueous and organic solutions. In MeOH, all substances reveal the maximum absorption wavelengths at around 360-366 nm, the maximum emission wavelengths at 454-466 nm and fluorescent quantum efficiencies in the value of 0.74-0.32. Moreover, metal ion sensing properties were ascertained and exposed that all compounds selected with gold(III) ion (Au^{3+}) in aqueous media. Their fluorescent signals were quenched as a proportion of time and the probe 5d exhibited the limit of detection of 2.65 μM. These behaviors are expected from the oxidation reaction that converts DHP ring into pyridinium ring by Au^{3+} specific catalyst. Furthermore, the experiments in surfactant system (Triton X-100) illustrated that there are only a group of bis DHPs (5a-d) that their fluorescent intensities were enhanced, and compound 5d was selectively quenched against iron(II) ion (Fe^{2+}) with the limit of detection of 1.69 μM. In pH buffer, only DHP-4AP probes (1c and 1d) responded by decreasing the fluorescent intensity in base region. Compound 1d exhibited the pK_a value of 9.23 ± 0.03 and could be applied as a pH sensor in range of 8.6 to 9.8. Other applications of DHP probes such protein sensor and oxidant sensor were also studied.

Department:	Chemistry	Student's Signature	.....
Field of Study:	Chemistry	Advisor's Signature	.....
Academic Year:	2014	Co-Advisor's Signature	.....

ACKNOWLEDGEMENTS

The accomplishment of this thesis can be attributed to the assistance and support from Dr. Anawat Ajavakom as my thesis advisor. I would like to express my sincere gratitude to him for valuable advice, guidance and encouragement throughout the course of this research.

I would like to deeply thank my co-advisor, Associate Professor Dr. Mongkol Sukwattanasinitt for his generous assistance, precious guidance and kindness throughout this research. I also would like to thank Associate Professor Dr. Paitoon Rashatasakhon and Assistant Dr. Sumrit Wacharasindhu for their attentions and suggestions in our group meeting.

I would like to appreciate many members of Material Advancement and Proficient Synthesis (MAPS) Group; Mr. Thirawat Sirijindalert, Mr. Oran Pinrat, Ms. Daranee Homraruen, Mr. Watcharin Ngampueng, Ms. Pornpat Sam-ang and Ms. Kanoktorn Boonkitpatarakul for their helpful suggestions, Mr. Akachai Khumsri, and everyone in MAPS group for a greatest relationship and kind encouragement.

In particular, I am thankful to the Development and Promotion of Science and Technology Talents Project (DPST) and the National Nanotechnology Center for supporting my thesis.

Finally, I would like to specially thank my family and friends for their encouragements and understanding throughout. I would not be able to reach this success without them.

CONTENTS

Page

Page

Page

Page

Page

LIST OF TABLE

LIST OF FIGURE

LIST OF SCHEME

LIST OF ABBREVIATIONS

a.u.	arbitrary unit
Ab	absotption
ACN	acetonitrile
ALS	ammonium lauryl sulfate
Ar	aryl group
BR	Britton-Robinson
BSA	bovine serum albumin
^{13}C NMR	carbon-13 nuclear magnetic resonance
calcd	calculated
CD_3CN	deuterated acetonitrile
CD_3OD	deuterated methanol
$CDCl_3$	deuterated chloroform
$CHCl_3$	chloroform
CMC	critical micelle concentration
CTAB	cetyl trimethylammonium bromide
d	doublet (NMR)
D_2O	deuterium oxide
DCE	1,2-dichloroethane
DCM	dichloromethane
dd	doublet of doublet (NMR)
DHP	1,4-dihydropyridine

DMF	dimethylformamide
DMSO	dimethylsulfoxide
DTAB	dodecyltrimethylammonium bromide
em	emission
equiv	equivalent (s)
ESI	electrospray ionization mass spectrometry
EtOAc	ethyl acetate
EtOH	ethanol
ex	excitation
FT-IR	fourier transform infrared spectroscopy
g	gram (s)
^{1}H NMR	proton nuclear magnetic resonance
h	hour (s)
His	Histone
HRMS	high resolution mass spectrum
Hz	hertz
I	intensity
I_0	initial intensity
IR	Infrared
J	coupling constant
K_{sv}	Stern-Volmer constant
M	molar
m	multiplet (NMR)
M.W.	molecular weight

m/z	mass per charge
MALDI-TOF	matrix-assisted laser desorption/ionization-time of flight
MeOH	methanol
mg	milligram (s)
MHz	megahertz
mL	milliliter (s)
mM	millimolar
mmol	millimole (s)
MS	mass spectrometry
Myo	myoglobin
nm	nanometer (s)
pH	potential of hydrogen ion
ppb	parts per billion
q	quartet (NMR)
R	alkyl group
R_f	Rate of flow
rt	room temperature
s	singlet (NMR)
SDS	sodium dodecyl sulfate
SOS	1-octanesulfonic acid sodium salt
t	triplet (NMR)
THF	tetrahydrofuran
TLC	thin layer chromatography
TsCl	tosyl chloride

TTAB	tetradecyltrimethylammonium bromide
TX	triton X-100
UV	ultraviolet
δ	chemical shift
ε	molar absorptivity
λ	wavelength
μM	micromolar (s)
μL	microliter (s)
℃	degree Celsius
Φ	quantum yield
% yield	percentage yield

CHAPTER I

INTRODUCTION

1.1 Introduction of 1,4-dihydropyridines

The 1,4-dihydropyridine (DHP) is a heterocyclic molecule semi-saturated with two hydrogens replacing one double bond at the position of 1 and 4 of the pyridine ring, as shown in **Figure 1.1**.

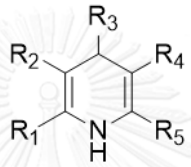

Figure 1.1 Basic structure of 1,4-dihydropyridine (DHP)

DHP was successfully synthesized for the first time by Hantzsch in 1882 [1]. Since then their derivatives have been used for a variety of applications; e.g. modeling NADH in biochemistry (diludine and lacidipine) [2], photosensitive polymers (nifedipine and ac- nifedipine), pharmaceutical medicines (nitrendipine) (**Figure 1.2**) [3-8]. Some of these bioactive DHPs are applied in the class of pharmacological agent known as an antioxidant and calcium channel blocker (CCB) [3, 4]. For instance, the inhibition of calcium ion cell penetration by several DHP-CCBs was reported to weaken the contractility of the cardiac muscle [5]. These compounds were also proven to be effective vasodilators and useful in the treatment of hypertension, ischemic heart disease and other cardiovascular disorders [6, 7].

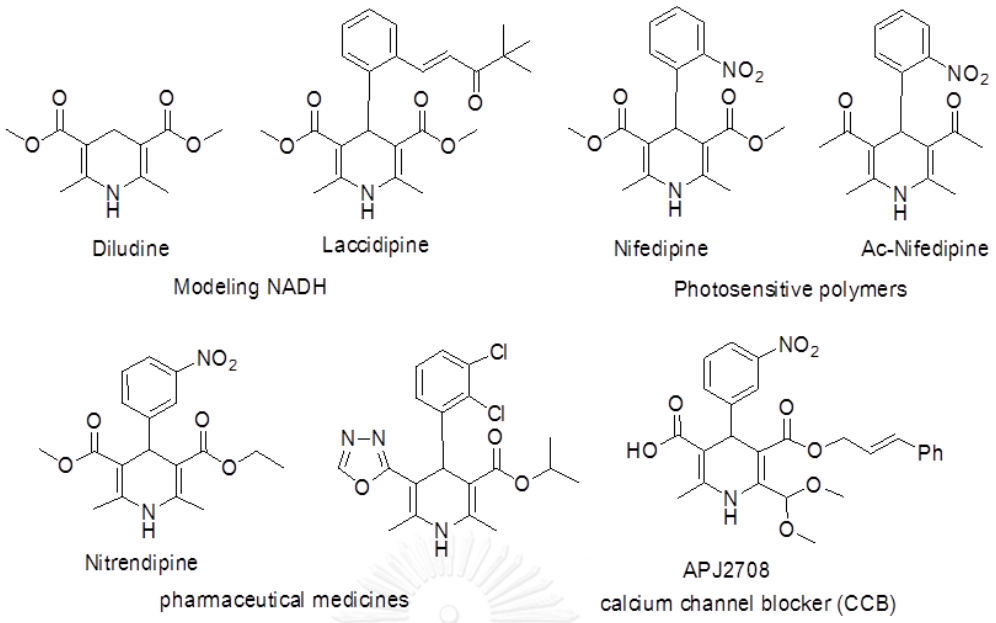

Figure 1.2 DHP derivatives for various applications.

1,4-DHP structure consist of the **π**-conjugated chromophores is endowed by a strongly allowed absorption with the maximum round 350 nm and maximum emission around 450 nm [9-12]. Their optical and photophysical properties of DHP have been rather reported [13-15].

In 2005, Ko and co-workers [16] have developed an easy and efficient method to prepare a variety of DHPs (**Figure 1.3**) from aryl aldehyde, 1,3-cyclohexanedione, ethyl acetoacetate and ammonium acetate in the presence of catalytic amount of iodine at room temperature. Iodine is widely used in the commercial level as catalyst, and gained DHPs in excellent yields. Interestingly, these was no explanation concerning to the asymmetric synthesis.

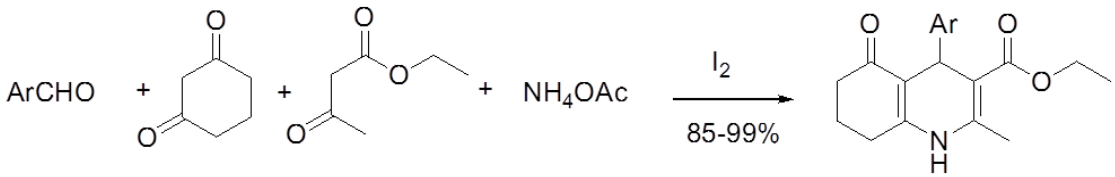

Figure 1.3 The synthetic scheme of Ko and co-workers's DHPs

In 2010, Cheung and co-workers [17] successfully synthesized DHP derivatives by also using modified Hantzsch reaction (**Figure 1.4**). This coupling reaction

consumed methyl acetoacetate or ethyl acetoacetate, ammonium acetate, and formaldehyde at 80 °C for 10 minutes, leading to symmetric DHP in range of 30-95%. This work has overcome the difficult and uncontrollable use of formaldehyde by using 36% aqueous formaldehyde.

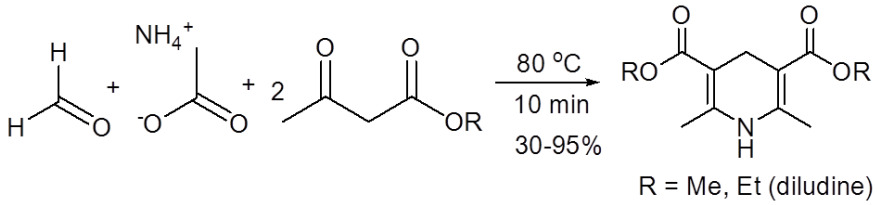

Figure 1.4 The synthetic scheme of Cheung and co-workers's DHP derivatives.

In 2011, Sueki and colleagues [18] reported an efficient one-pot reaction to synthesize the 2,6-unsubstituted DHP derivatives (**Figure 1.5**). Various Lewis acids were attempted for the condensation reaction of aniline, aldehyde and acetal protected β-ketoester and $Yb(OTf)_3$ gave the best yield. The favorable conditions for the syntheses was the catalytic use of 2.5 mol% $Yb(OTf)_3$ in 1,4-dioxane at 90 °C for 16 hours. The proposed reaction mechanism of these DHP derivatives started from the formation of imine intermediate followed by imine-enamine tautomerization and Michael-type annulation, respectively.

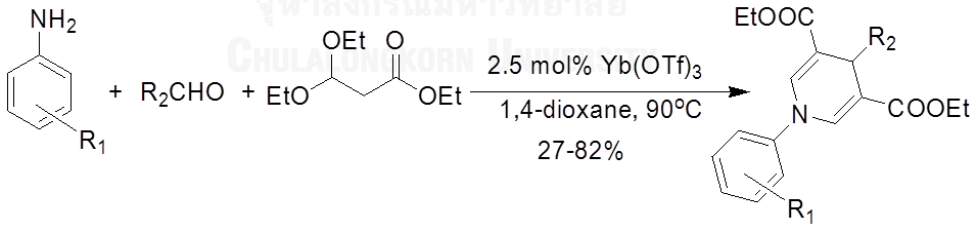

Figure 1.5 The synthetic scheme of Sueki and co-workers's DHP derivatives.

In 2010, Sirijindalert and Ajavakom group [19] demonstrated that DHPs can be easily obtained from the cyclotrimerization of β-amino acrylates under facile conditions by treatment with $TiCl_4$ in CH_2Cl_2 at room temperature (**Figure 1.6**). The convertion of β-amino acrylates to *N*-substituted DHP **1** was achieved in high yields (70–83%) through two Michael additions followed by cyclization. One year after,

Homraruen [20] developed DHP derivatives with better water solubility by basic hydrolysis changing triester to triacid **2** as the selective Hg^{2+} fluorescent sensor.

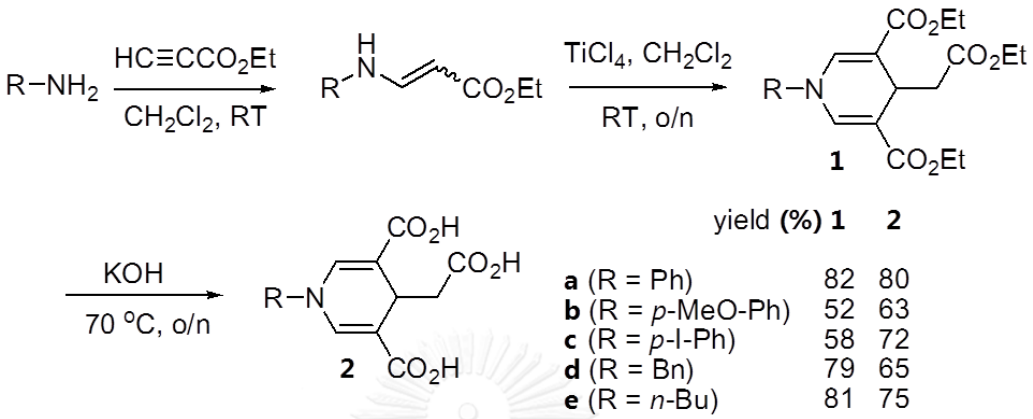

Figure 1.6 The synthetic scheme of DHP tri acid derivatives.

1.2 Introduction of fluorescence and fluorometry

Fluorescence is a photon emission process that occurs when a molecule absorbs photons from the UV visible light, known as an excitation, and then rapidly emits light photons when return to its ground state. The phenomenon is usually illustrated by the Jablonski diagram [21], which offers a convenient representation of the excited state structure and the relevant transitions, to illustrate possible various molecular processes. According to Franck-Condon principle, most molecules absorb light much rapidly (10^{-15} s) than molecular vibration (10^{-8} s). A simplified Jablonski diagram (**Figure 1.7)** demonstrates that, this light absorption causes electrons to become excited to second electronic state (S_2), then the electrons lose the energy by internal conversion (vibration or rotation) decaying to first excited state (S_1). After that, the fluorescence signal is observed when the electrons relax to singlet ground electronic state (S_0) via photon emission (radiative decay). The time required to complete the whole process takes only around nano-second.

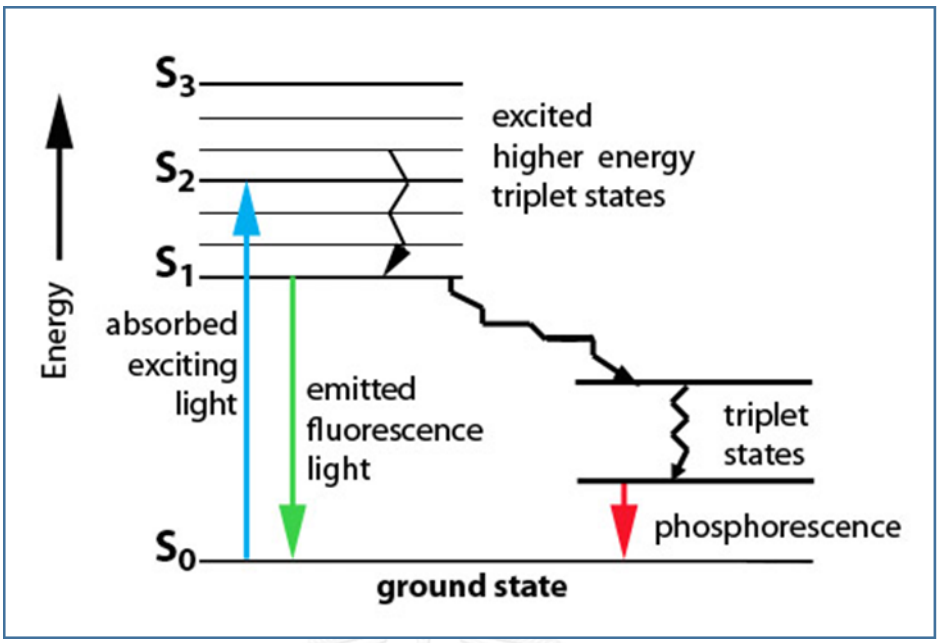

Figure 1.7 Jablonski diagram illustrating the fluorescence processes.

Fluorometry is an important analytical technique which works on the principle of fluorescence. This method can be used to assay the state of a biological chemical system by studying its interaction with fluorescence probe molecules. This interaction is monitored by measuring the changes of the optical properties of fluorescence probe. The fluorescence characterizes the relationship between absorbed and emitted photons at specific wavelength. It is a precise quantitative and qualitative analytical technique that is not only highly sensitive and specific but with even greater advantages of rapid testing, inexpensive and easy-to-use [22-25]. The development of selective and trustworthy methods for the quantification of environmentally toxic heavy metal of wastewater by using fluorescence spectroscopy was reported [24, 26-29].

1.3 Fluorescence chemosensor

Chemical sensor based on the principle of fluorescence signal change is generally called “Fluorescent chemosensor” [30-34] which basically consists of two main parts: receptor unit and signaling unit. In some cases, spacer may be added as

linker between two main units (**Figure 1.8**). In principle, when the analyte, which is either cation, anion or neutral molecule, interacts with the sensor, the fluorescence signal from signaling unit is changed. Fluorescence signal change can occur in various forms, for instance, quenching or enhancement of fluorescent intensity, maximum emission wavelength shift and decay lifetime which can be detectable by fluorescent spectrometer. There are several mechanisms to control the quenching response of a fluorophore to substrate binding which are photo-induced electron transfer (PET), intramolecular charge transfer (ICT), fluorescence (FÖrster) resonance energy transfer (FRET), and excimer/exciplex formation or extinction. Advantages of Fluorescent chemosensor are high sensitivity, high specificity and low limit of detection. Importantly, the fluorescent chemosensor can be applied in a wide range of fields such as industry, environment, and biology.

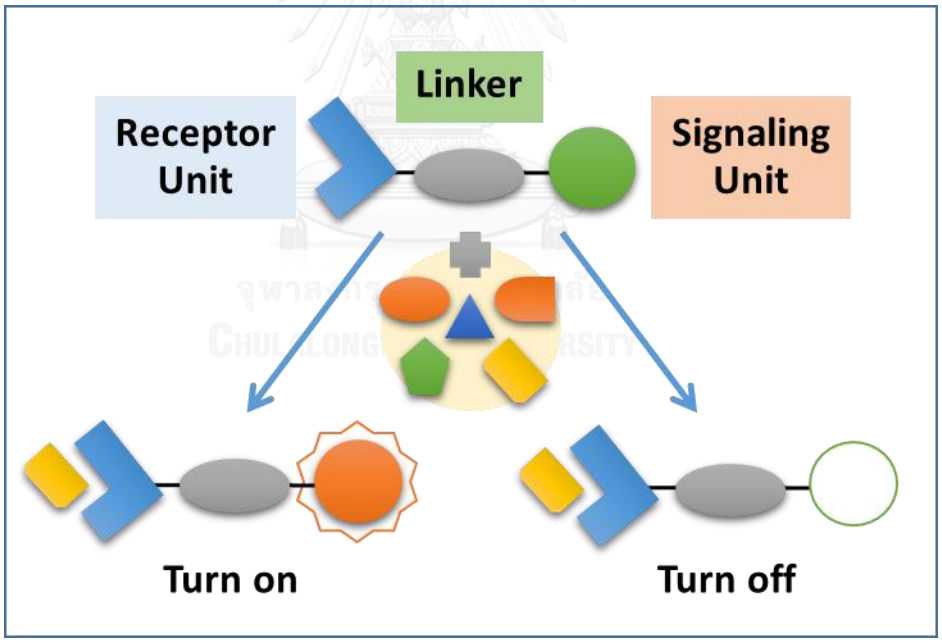

Figure 1.8 Schematic illustration of a fluorescence sensor device.

1.3.1 Metal ion sensor

In 2011, Hsieh and co-workers [35] designed and synthesized a new fluorescent chemosensor from coupling reaction of sugar-aza-crown (SAC) ether and anthracene triazolymethyl moieties (**Figure 1.9**). This sugar-aza-crown ether sensor

shows high selectivity for Cu^{2+} ion over other metal ions. On addition of Cu^{2+} ion into a MeOH solution, the fluorescence intensity of the sensor was enhanced because of the PET process operating between the amino group of the SAC ether and the anthracene fluorophore.

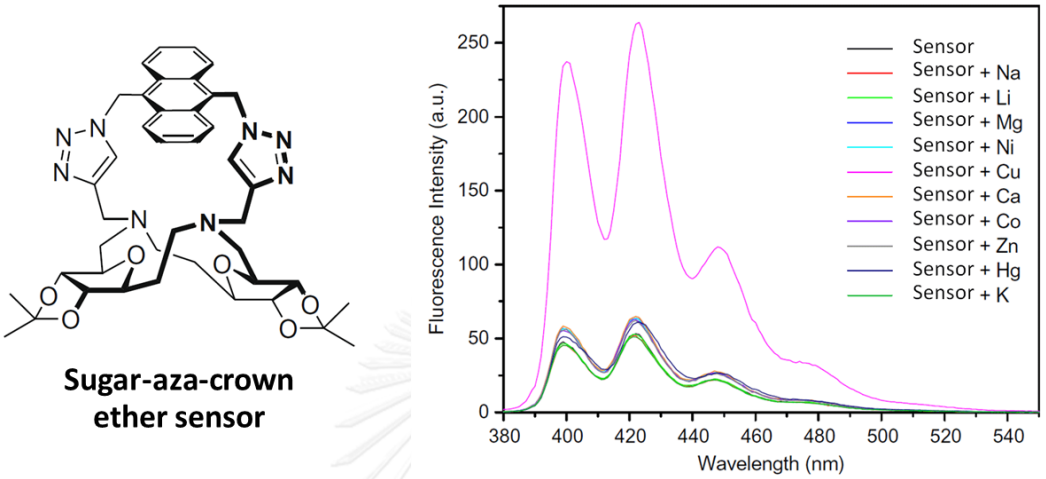

Figure 1.9 Structure of sugar-aza-crown ether sensor and fluorescent respond over other metal ions.

In 2009, Huang and colleagues [29] demonstrated that a rhodamine derivative can be used as a selective and sensitive chemosensor for Hg^{2+}. This probe could specifically recognize Hg^{2+} ion in aqueous buffer solution by the “naked eye”, UV/vis, and fluorescent responses (**Figure 1.10**). This chemosensor reduced the amount of organic co-solvent in detecting media and improved sensitivity and selectivity through a rational incorporation of sulfur containing receptor to the rhodamine structure due to the thiophilic nature of mercury. In addition, the spectral response toward Hg^{2+} was established to be reversible by the EDTA-titration experiments.

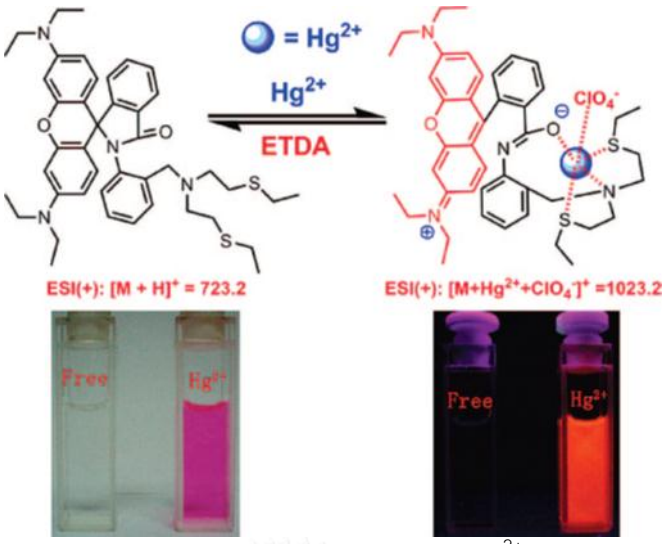

Figure 1.10 Proposed binding mode between sensor/Hg^{2+} and color change upon addition Hg^{2+}.

In 2011, Tang and co-workers [29] designed and synthesized a new pyrrole Schiff base-containing rhodamine B derivative as a dual sensor for Cu^{2+} and Hg^{2+} ions (**Figure 1.11, a**). This sensor exhibits selective recognition of Cu^{2+} with UV–vis spectroscopy and selective recognition of Hg^{2+} (**Figure 1.11, b**). The colorimetric recognition of Cu^{2+} and fluorescent recognition of Hg^{2+} by this probe are free from the interference of Hg^{2+} and Cu^{2+}, respectively.

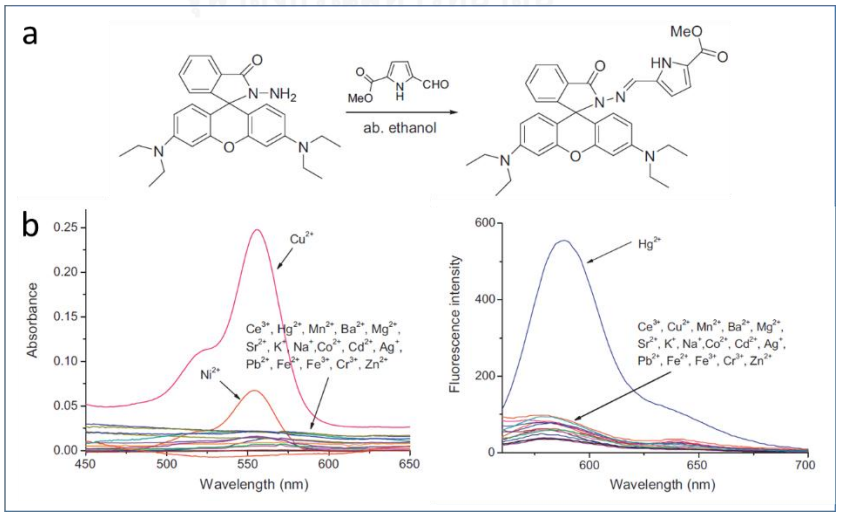

Figure 1.11 (**a**) Synthesis of rhodamine B derivative sensor. (**b**) UV–vis and Fluorescence spectral changes of receptor 2 upon addition of various metals.

1.3.2 Au^{3+} sensor

In 2009, Egorova and colleagues [36] developed a fluorescence sensing system for Au(I)/Au(III) species for the first time based on their alkynophilicity. A rhodamine-derived alkyne probe undergoes a spirolactam ring opening and concomitant heterocyclic formation upon coordination with the gold species (**Figure 1.12**), resulting in both color and turn-on fluorescence changes.

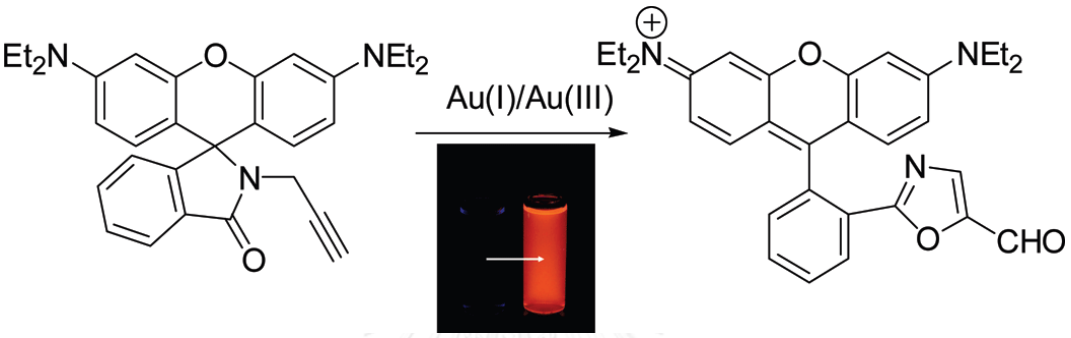

Figure 1.12 Structure of rhodamine derived alkyne probe when added Au(I)/Au(III) and its image under black light.

In 2010, Dong and co-workers [37] demonstrated a highly selective ratiometric fluorescent probe for Hg^{2+} or Au^{3+} in aqueous media depending on detection conditions (**Figure 1.13**). Upon the addition of various metal ions in HEPES buffer (0.01 M, pH=7.4) (0.05% DMSO, v/v), only Hg^{2+} caused the change of the maximum fluorescence emission band of this naphthalimide probe. However, when tested in MeOH-H_2O (95:5 v/v, pH=9.0) solution, only Au^{3+} caused the change of its fluorescent signal. The rational analysis of selective recognition of Hg^{2+} and Au^{3+} is accommodated in the well-established Kucherov reaction mechanism. This work provides a novel non-sulfur approach for selective recognition of these two ions with significant change of fluorescence color and constitutes the first ratiometric case for Au^{3+}.

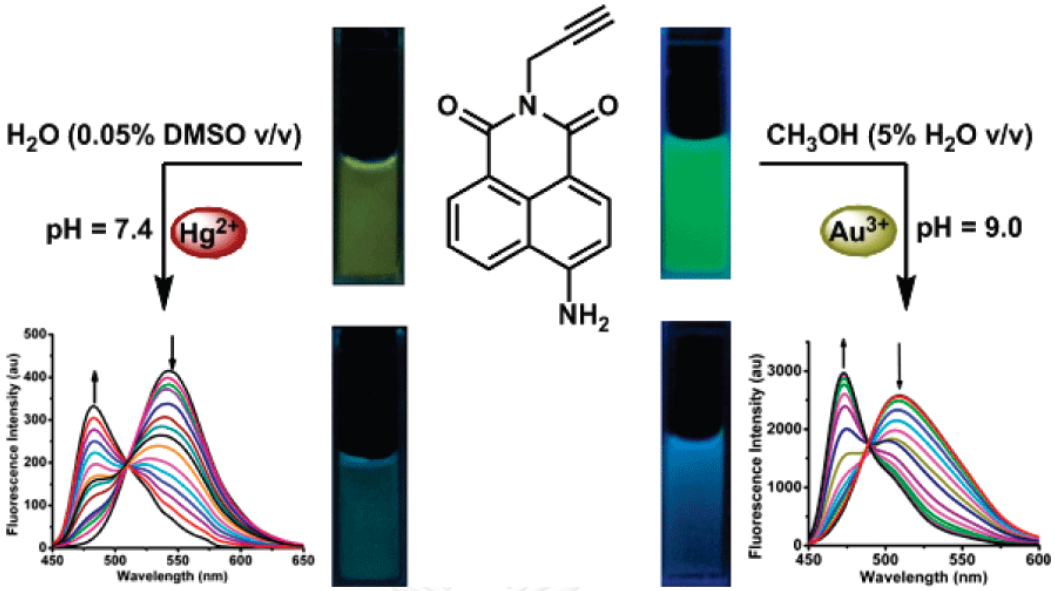

Figure 1.13 Color and structural change of naphthalimide derivative toward Hg^{2+} and Au^{3+}.

In 2012, Park and his research group [38] synthesized a simple thiocoumarin derivative, developed for a gold selective chemosignaling system. Au^{3+}-induced desulfurization of thiocarbonyl function resulted in a colorimetric and an "off–on"-type fluorescence signaling of Au^{3+} ions in a 50% aqueous acetonitrile (**Figure 1.14**). Marked color change from pink to yellowish green allowed naked-eye detection of Au^{3+} with the detection limit of 1.1×10^{-7} M. Interference from Hg^{2+} ions was successfully eliminated by using a chelating agent *N,N,N′,N′*-Tetrakis-(2-pyridylmethyl)ethylenediamine (TPEN). The postulated conversion was evidenced by ^{1}H NMR, UV–vis, and fluorescence measurements.

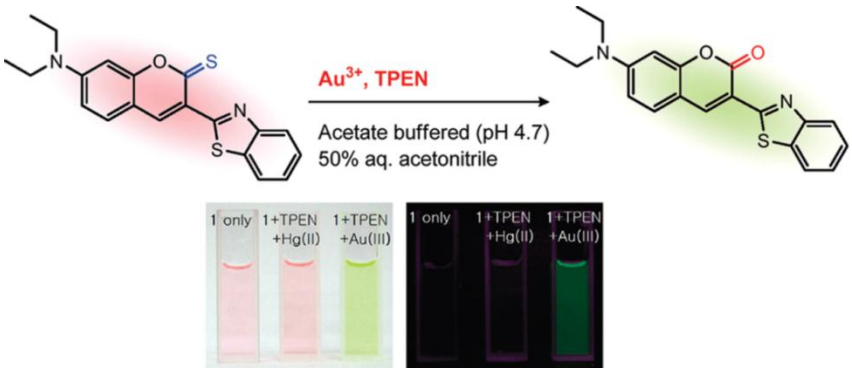

Figure 1.14 Au^{3+}- Selective Signaling of Thiocumarin derivative and its color change

1.3.3 Glycol-based fluorescent sensor

In 2005, Liu and his group [39] synthesized a new podand **1** possessing plural imidazo-[4,5-f]-1,10-phenanthroline groups. The addition of alkali metal and alkaline earth metal ions to its DMF solution leads to fluorescence quenching of the podand. Because of the good complementarity between the pseudo-cavity of the podand and the ionic radii of Mg^{2+}, the compound showed the specific responses for only Mg^{2+} (**Figure 1.15, a**), readily distinguished by naked-eye (**Figure 1.15, b**).

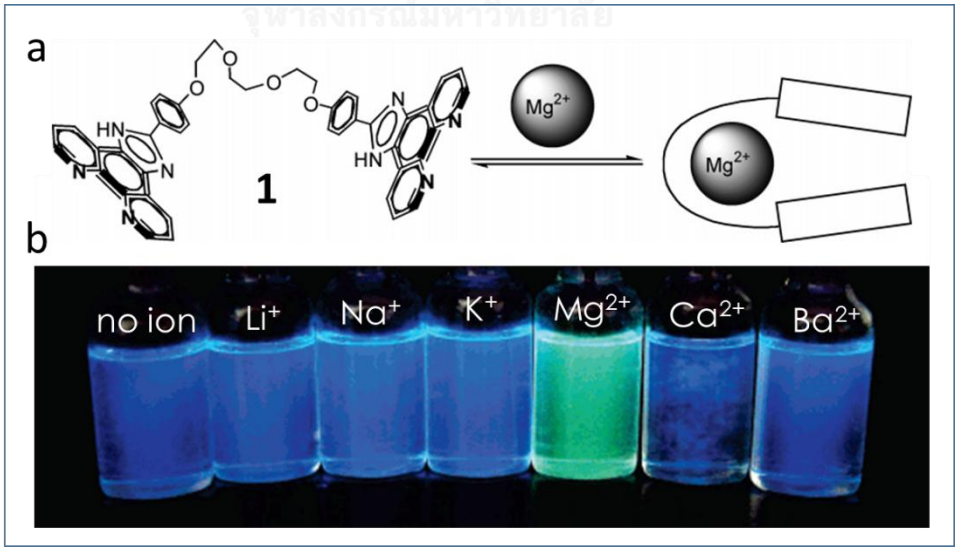

Figure 1.15 (**a**) Proposed conformational changes of **1** before and after complex formation with Mg^{2+}. (**b**) Visible emission observed under black light with various alkali and alkaline earth cations.

In 2011, Ashokkumar et. Al. [40] developed an acridinedione derivative (ADD)-based bichromophoric podand systems. This ADD demonstrated the solvent dependent binding mode of the metal ion and the selectivity toward an acyclic polyether-based receptor (**Figure 1.16, a** and **b**). In acetonitrile, Ca^{2+} alone shows the binding at the oxyethylene receptor unit and -OCH3 groups, whereas in low polar aprotic solvents, chloroform, both Ca^{2+} and Na^{+} are involved in the binding at different position resulting in the distinct optical output (**Figure 1.16, c** and **d**).

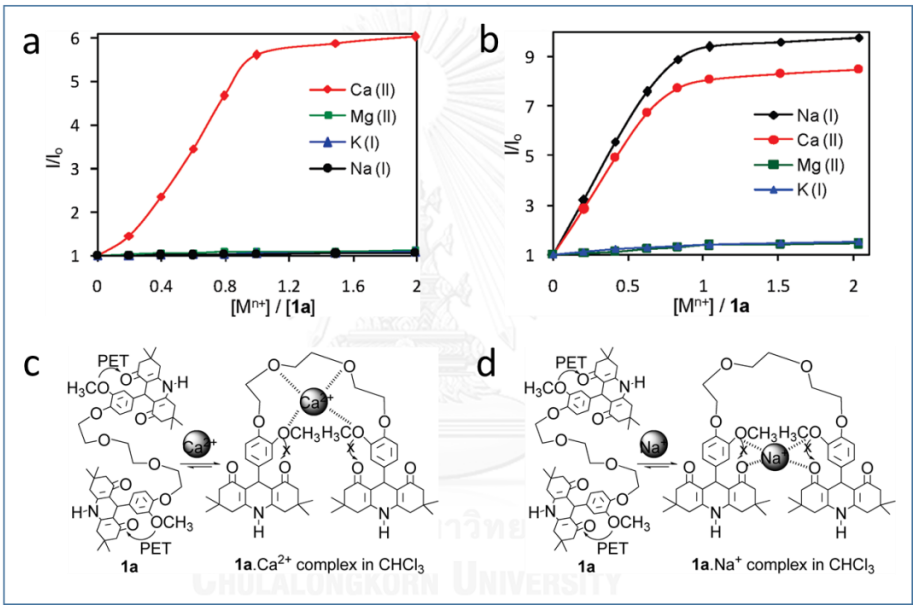

Figure 1.16 Metal ion selectivity (**a**) in acetonitrile, (**b**) in chloroform. (**c** and **d**) Binding Mode of Ca^{+} and Na^{2+} in Chloroform, respectively.

1.3.4 DHP sensors

In 2013, Homraruen and teams [20] reported a new fluorescence 1,4-dihydropyridine (DHP) tricarboxylic acid. This probe is selective chemodosimeter for Hg^{2+} in aqueous solution. The decrease of fluorescence signal was proportional to Hg^{2+} concentration with high quenching efficiency (K_{SV}=78,300) providing a detection limit of 0.2 μM. The quenching process involves an oxidation of the DHP into a

pyridinium ring specifically induced by Hg^{2+} that brought about its remarkable selectivity over other metal ions (**Figure 1.17**).

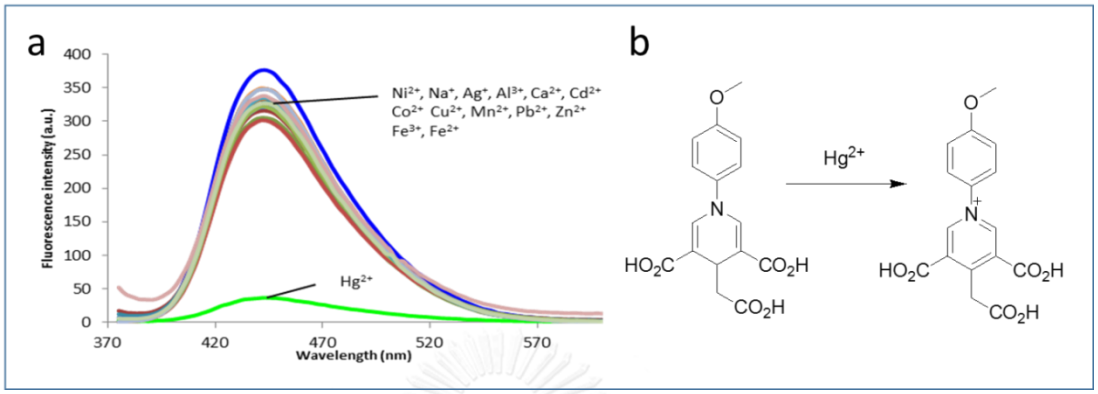

Figure 1.17 (**a**) Selectivity over other metal ions and (**b**) its proposed mechanism toward Hg^{2+} ion.

In 2015, Pinrat and colleages [41] reported a novel fluorescent 1,4-dihydropyridinyl glucosamine (DHP-Glc) as a chemosensor for selective and sensitive detection of TNP in aqueous solution (**Figure 1.18, a**). The decrease of the fluorescence signal was proportional to the TNP concentration with a high quenching efficiency (Ksv = 4.47×10^4) providing a detection limit of 0.94 μM. In addition, a fluorescent paper sensor was fabricated for the on-site convenient in real samples, sensitive and selective naked-eye detection of trace amounts of TNP either in solution or vapor down to the single digit μM level or 0.06 ppb, respectively (**Figure 1.18, b**).

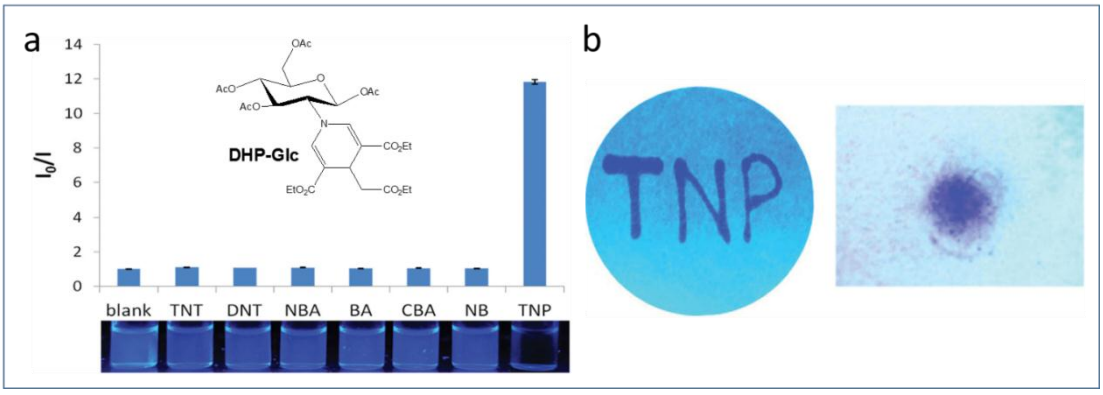

Figure 1.18 (**a**) NAC selectivity of DHP-Glc and (**b**) fluorescent paper sensor for real samples.

1.3.5 pH sensor

In 2014, Mukherjee and colleagues [42] designed and synthesized two new quinoline hydrazones based ratiometric fluorescent pH sensors (**Figure 1.19, a**). The sensors exhibit reversible absorption and emission change in the acidic region (**Figure 1.19, b**) and the consequent color change from yellow to red can easily be detected by the naked eye. The differential pH responsive fluorescent staining ability of these hydrazones toward HeLa cells might be helpful for intracellular pH sensing (**Figure 1.19, c**).

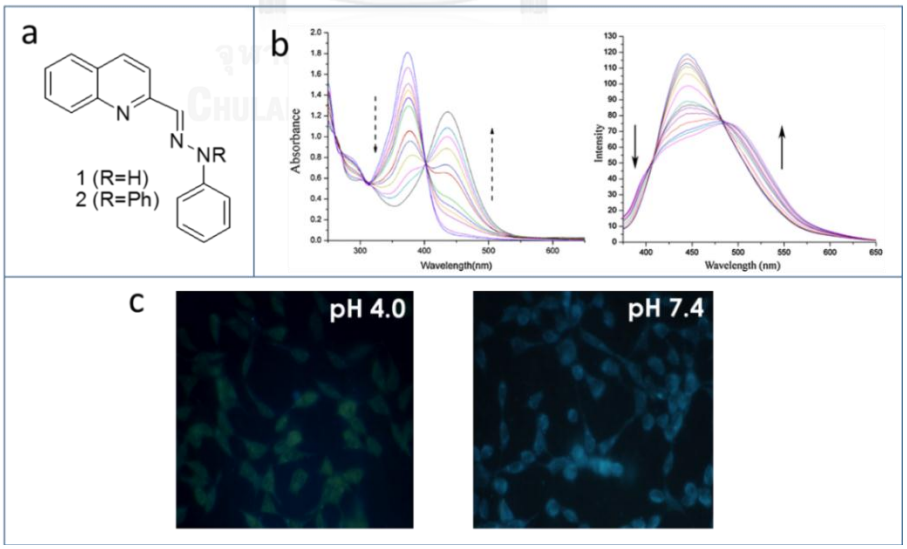

Figure 1.19 (**a**) Structure of this hydrazone pH sensor, (**b**) absorption and emission spectra of at different pH and (**c**) fluorescence images of HeLa cells at pH 4.0 and pH 7.4

In 2014, Shi and colleages [43] reported a new rhodamine–morpholine (RM) fluorescent probe for monitoring of lysosomal pH changes in live cells. RM sensor has high sensitivity and selectivity, as well as high photostability and low cytotoxicity. The fluorescence intensity of RM is sensitive to acidic pH in a short response time with a pKa value of 5.23 (**Figure 1.20**). It shows a 140-fold increase in the emission intensity within the pH range of 7.4–4.5 due to the H^+-triggered "turn-on" fluorescence signal. Importantly, RM was successfully applied to the chloroquine-induced increase in lysosomal pH and monitor the lysosomal pH changes during apoptosis in living cells, demonstrating its value of practical application in biological systems.

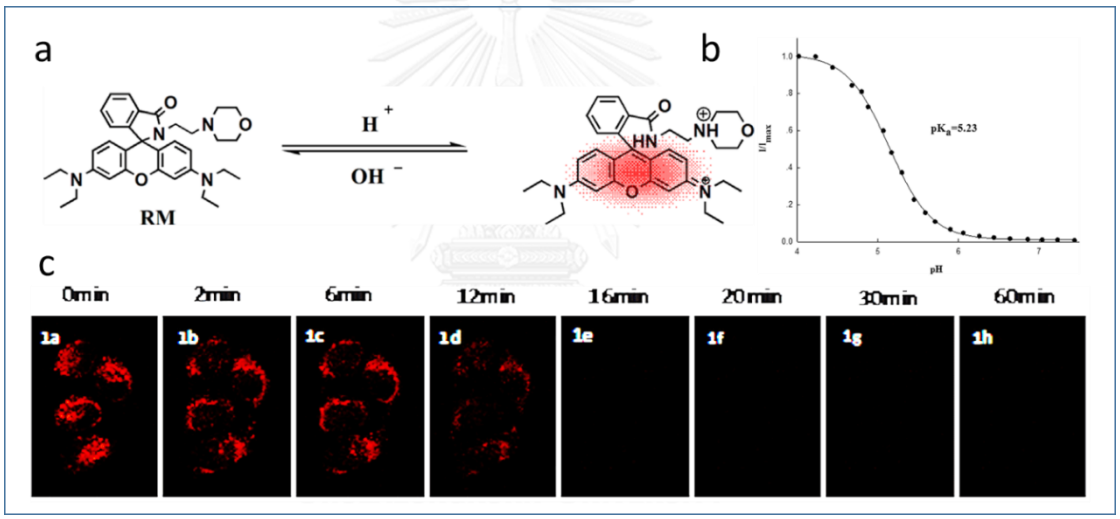

Figure 1.20 (**a**) the response mechanism of RM to pH, (**b**) pH titration curve of RM and (**c**) time dependent fluorescence changes of RM in MCF-7 cells stimulated with chloroquine.

In the same year, Devarayan and colleagues [44] also showed a novel nanocomposite, cellulose electrospun non-woven (Cs-ESNW) nanofibers loaded with red cabbage pigment (RC) and evaluated as a potential material for eco-friendly, economical, and universal pH sensor. The RC/Cs-ESNW nanofibers showed visibly distinct colors at all pH range, indicating its universal pH sensing characteristics

(**Figure 1.21**). The samples also demonstrated a rapid halochromic response in 5 seconds.

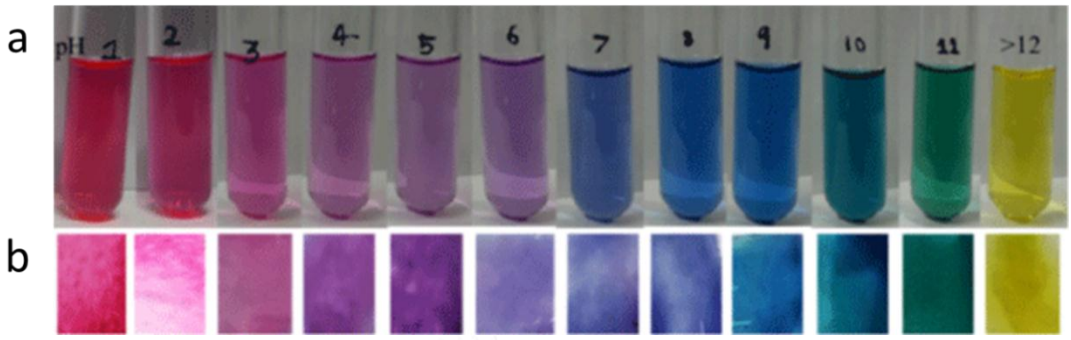

Figure 1.21 The color schemes of (**a**) the RC extract solution and (**b**) dyed RC/Cs-ESNW nanofiber mats at pH 1–14.

1.4 Allosteric System

Allosteric regulation is the operation control process of enzyme or protein molecules system, in with a substance called effector binds with host molecule to trig the operation process. That is, certain enzymes comprise the so-called allosteric site which acts to bind with effector, such binding resulting in the changes within the structure. Occurred structural changes of biomolecule at active site may induce the enzyme to change its role. If the catch of the effector at allosteric site of the enzyme results in better performance, it will be called as positive allosteric modulation or allosteric activation. Conversely, if it results in worse performance, it is called as negative allosteric modulation or allosteric inhibition. In chemistry, allosteric can be seen in the organic molecules that generally has two active sites to capture the target analyte [45]. The compound that two areas both pick the same target molecule is called homotropic host (**Figure 1.22, a**). This picture showed the cerium(IV) bis(porphyrinate) double deckers host could be suppressed the rotation of two porphyrin planes by the first binding of dicarboxylic acid guest, the second one should be bound more efficiently, which clearly observed by circular dichroism spectrometer . While the each site of the molecule selects a different target

compound will be called heterotropic host, with is the simplest mode of allosteric (**Figure 1.22, b**). This image demonstrated the Na^+ ion, positive effector, could repeal an intramolecularly hydrogen-bonded "closed" form to establish "open" form of calix[4]aryl esters that active to second binding with such lactam derivatives via intramolecular hydrogen bonding. In both cases, the compound binds to target at first area will normally affect the binding of the next target compound to the other area.

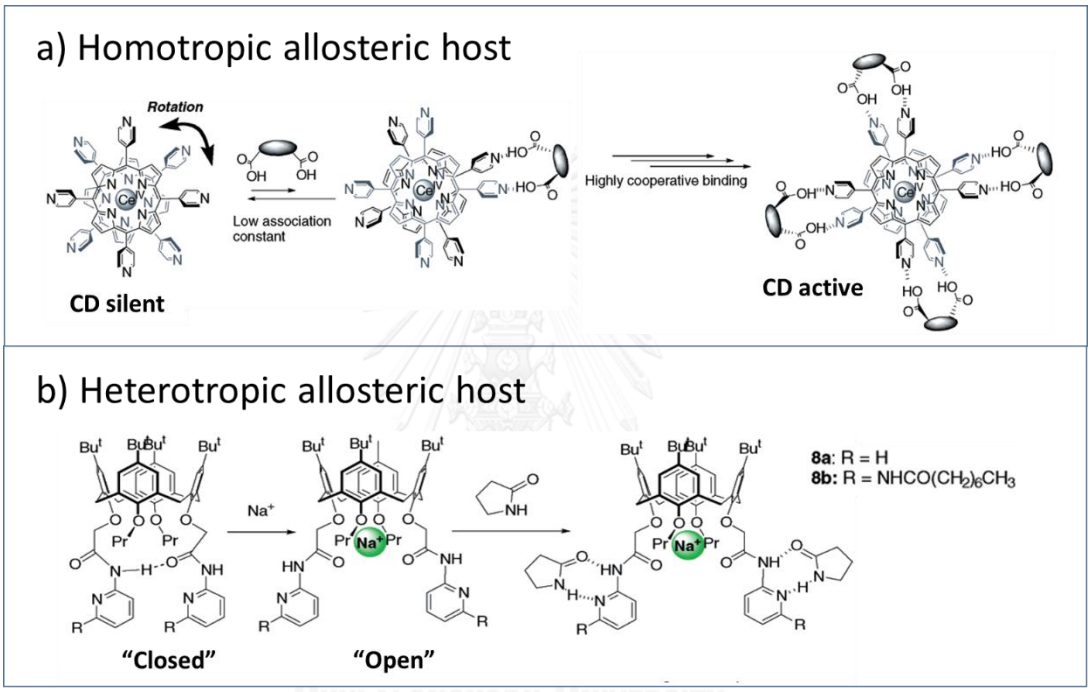

Figure 1.22 Example of (a) homotropic host, (b) heterotropic host and their allosteric behaviors.

In 2000, Ikeda and co-worker [46] synthesized a cerium(IV) double decker porphyrin **1** bearing four 4-methoxyphenyl groups (**Figure 1.23**). This compound shows a positive, homotropic allosteric effect in metal recognition of Ag^+ ion, and the peripheral ***π*** clefts of complex act as effective binding sites for Ag^+ ion.

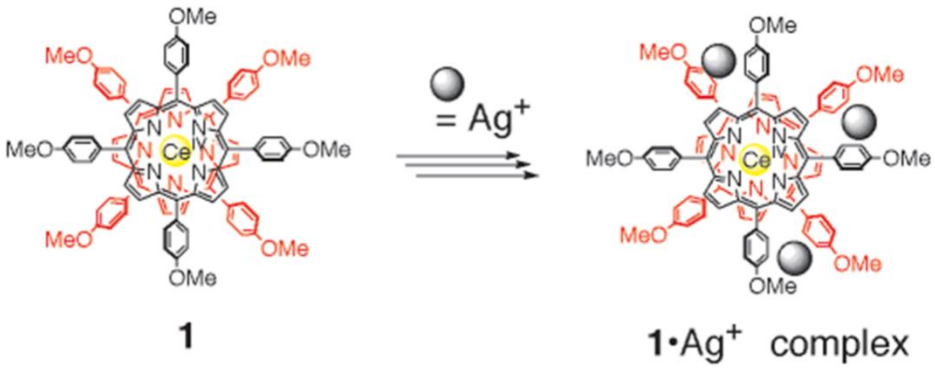

Figure 1.23 Positive homotropic allosteric effect of compound 1 with Ag^{+} ion

In 2012, Kumar and colleagues [47] designed and synthesized a novel ditropic fluorescent chemosensor, based on the 1,3-alternate conformation of thiacalix[4]arene possessing two complexation sites, a crown-4 moiety and an amino moiety appended with pyrenyl groups (**Figure 1.24**). This compound undergoes a selective monomer enhancement and excimer quenching only in the presence of Cu^{2+} ions. Moreover, Li^{+} ion selectively binds to the receptor unit, crown-4 ring, which is responsible for the small enhancement of both monomer and excimer emissions. Interestingly, sequential additions of Cu^{2+} and Li^{+} ions triggers a Cu^{2+}/Li^{+} switchable fluorescent chemosensor with negative allosteric behavior between these ions.

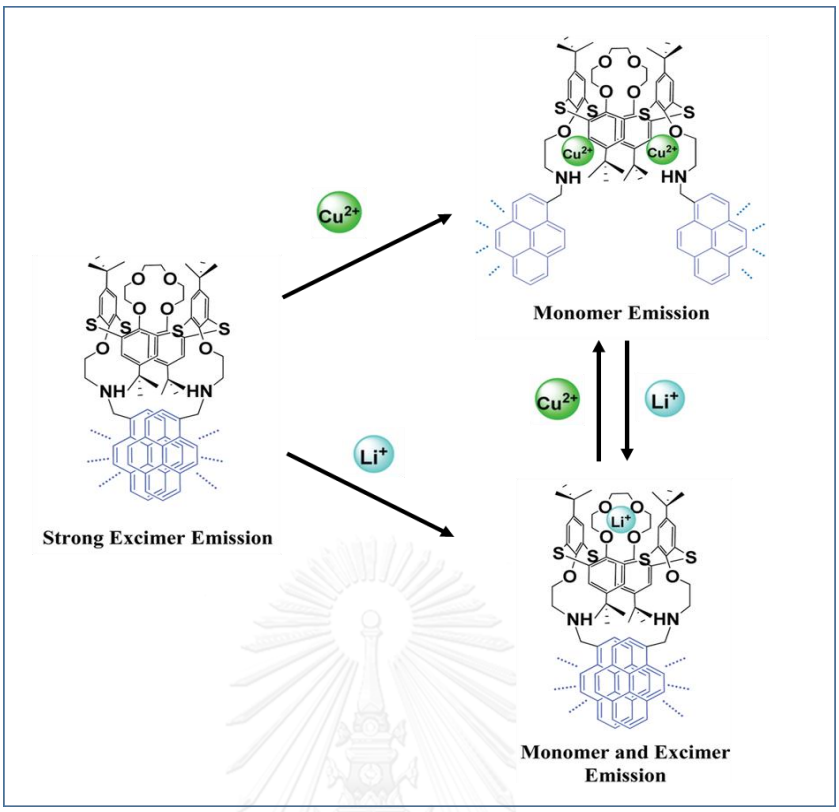

Figure 1.24 Scheme representing relation between monomer and excimer emission along with the ion exchange between metal ions.

1.5 Statement of problem

DHP derivatives were widely utilized in many facets such as biochemistry, photosensitive polymers, pharmaceutical medicines and fluorescent chemosensor. However, these molecules are rarely published as fluorescent sensor application, even these substances have great photophysical properties. This work desired to further study for the sensing property of DHP derivatives that can be easily synthesized via cyclotrimerization of β-amino acrylate by Ajavakom method [19], To make it more interesting, DHP was designed to linked with oligoethylene glycol which could be applied as a receptor unit by changing its conformation to pseudo crown ether in organic media and also enhancing its water solubility. Some metal ion selectivity in pseudo crown cavity was reported with selectivity towards alkali and alkaline earth metal ions. Since our newly designed DHPs have two active sites: DHP

moiety and glycol chain, allosteric modulation that the first site affects to the next interaction on the second one, might be worth exploring. This allosteric behavior is highly expected to be also observed in our system as fluorescent sensor, explicitly at DHP and glycol active sites.

For this reason, we intend to synthesize a series of novel DHP derivatives linked with oligoethylene glycol. These target molecules will be determined the photophysical, sensing and allosteric properties under various conditions. Moreover, our group attends to study other applications such as surfactant sensor, pH sensor, protein sensor and oxidant sensor.

1.6 Objectives of this research

In this study, we focus on the synthesis of novel water soluble 1,4-dihydropyridine (DHP) fluorophores consisting of DHP moiety as fluorophore linked with various lengths of oligoethylene glycol as receptor unit for tuning hetero allosteric modulation (**Figure 1.25**). The photophysical, sensing and allosteric properties will be investigated in various solvent systems. The applications of these new compounds will also be explored such as metal ion, surfactant, pH, protein and oxidant sensors.

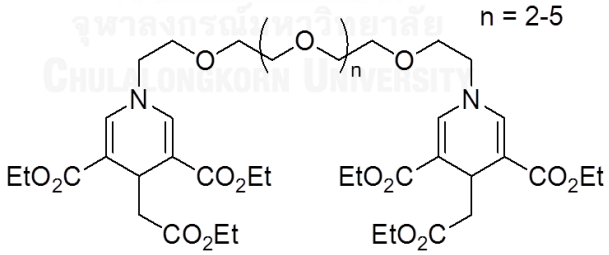

Figure 1.25 The target molecules

CHAPTER II

EXPERIMENTAL

2.1 Chemicals and materials

All reagents were purchased from Sigma-Aldrich and Fluka. Metal ions were prepared from their commercially available inorganic salts purchased from Sigma-Aldrich. For most reactions, solvents such as dichloromethane (DCM), 1,2-dichloroethane (DCE), acetonitrile (ACN) ethanol (EtOH) and methanol (MeOH) were reagent grade stored over molecular sieves and and tetrahydrofuran (THF) for anhydrous reactions were dried over CaH_2 and distilled prior to use. Solvents used for extraction and chromatography such as DCM, hexane, ethyl acetate (EtOAc) and MeOH were commercial grade. Deionized water was used throughout in the precipitation and all extraction procedures. MilliQ water was used to prepare the stock metal and fluorophore solutions. Column chromatography was operated using Merck silica gel 60 (70-230 mesh). Thin layer chromatography (TLC) was performed on silica gel plates (Merck F_{245}). The mixture of acetic acid, H_3PO_4 and boric acid were titrated using 0.2M NaOH to prepare the Britton-Robinson (BR) buffer. Reactions were mostly carried out under positive pressure of N_2 filled in rubber balloons.

2.2 Analytical instruments

Mass spectra were recorded on a Microflex MALDI-TOF mass spectrometer (Bruker Daltonics) using dithanol as a matrix. The HRMS was undertaken on an electrospray ionization mass spectrometer (MicroTOF, Bruker Daltonics). ^{1}H and ^{13}C NMR were acquired from sample solution in $CDCl_3$, CD_3OD and CD_3CN on Varian Mercury NMR spectrometer (Varian, USA) at 400 MHz and Bruker NMR spectrometer at 100 MHz, respectively. The UV-visible absorption spectra were obtained from a Varian Cary 50 UV-visible spectrophotometer (Varian, USA) and the fluorescent

emission spectra were recorded on a Perkin Elmer Precisely LS 45 luminescence spectrometer (Varian, USA).

2.3 Synthetic procedures

2.3.1 General synthesis and characterization of DHP derivatives (1a-d)

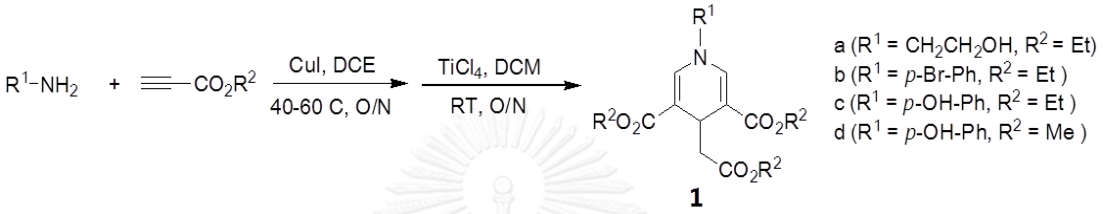

For aromatic amines, alkyl propiolate (1.2 equiv) in DCE (36.63 mM), copper(I) iodide (0.5 equiv) and aromatic amine (1.0 equiv) were dispersed and the reaction mixture was stirred for 10 min. The reaction mixture was then heated at 60°C overnight and filtered. The solvent evaporated to give the corresponding *N*-aromatic β-amino acrylates. Case of aliphatic amines to the solution of aliphatic amine (1 equiv) in CH_2Cl_2, ethyl propiolate (1.2 equiv) was added slowly and the reaction mixture was stirred overnight at room temperature under nitrogen atmosphere. The mixture was evaporated *in vacuo* to obtain the corresponding *N*-aliphatic β-amino acrylates.

To a solution of *N*-substituted β-amino acrylates in CH_2Cl_2 in an ice bath, $TiCl_4$ (0.2 equiv in the case of *N*-aliphatic β-amino acrylates or 0.5 equiv in the case of *N*-aromatic β-amino acrylates) was added rapidly and the reaction mixture was stirred overnight at room temperature under nitrogen atmosphere. After the solution was quenched with ice, deionized water (25 mL) was added and the mixture was extracted with CH_2Cl_2 (25 mL). The organic portions were combined and neutralized by addition of 0.1 M $NaHCO_3$ solution. The organic phase was washed with deionized water (3×25 mL), dried over $MgSO_4$, and evaporated under reduced pressure. The crude product was purified by column chromatography (EtOAc/hexane = 20:80 to 50:50) to provide the corresponding DHP-4AP (**1a-d**)

Diethyl 4-((ethoxycarbonyl)methyl)-1,4-dihydro-1-(2-hydroxyethyl)pyridine-3,5-dicarboxylate (DHP-OH, 1a)

According to above general procedure, **1a** was synthesized from ethanolamine (1.02 mL, 16.6 mmol) and ethyl propiolate (2.02 mL, 19.9 mmol). The crude product was purified to provide **1a** as a pale yellow oil (1.58 g, 81% yield): R_f (50% EtOAc/hexane) 0.20; ^{1}H NMR (400 MHz, $CDCl_3$): δ_H 7.17 (1H, s, C*H*=C), 4.26-4.12 (4H, m, $CO_2CH_2CH_3$), 4.07 (1H, t, *J* 4 Hz, $CHCH_2CO_2$), 4.02 (2H, q, *J* 7 Hz, $CH_2CO_2CH_2CH_3$), 3.75 (2H, dd, *J* 10, 6 Hz, CH_2CH_2OH), 3.40 (2H, t, CH_2CH_2OH), 2.64 (2H, d, *J* 4 Hz, $CH_2CO_2CH_2CH_3$), 1.28 (6H, t, *J* 7 Hz, $CO_2CH_2CH_3$), 1.18 (3H, t, *J* 7 Hz, $CH_2CO_2CH_2CH_3$), The data were agreed with those reported in literature [19].

Diethyl 4-((ethoxycarbonyl)methyl)-1-(4-bromophenyl)-1,4-dihydropyridine-3,5-dicarboxylate (1b)

According to above general procedure, **1b** was synthesized from 2-bromoethanamine (0.454 mL, 5.80 mmol) and ethyl propiolate (0.62 mL, 6.96 mmol). The crude product was purified to provide **1b** as a pale yellow oil (207 mg, 25% yield): R_f (100% CH_2Cl_2) 0.20; ^{1}H NMR (400MHz, $CDCl_3$): δ_H 7.18 (2H, s, NC*H*=C), 4.22-4.17 (4H, m, DHP-$CO_2CH_2CH_3$), 4.08 (1H, t, C*H*CH_2CO_2Et), 4.05-4.00 (2H, q, *J* 6.8 Hz, $CH_2CO_2CH_2CH_3$), 3.75 (2H, t, CH_2CH_2Br), 3.75 (2H, t, CH_2CH_2N), 2.66 (2H, d, *J* 4.2 Hz, CH_2CO_2Et), 1.29 (6H, t, *J* 6.8 Hz, DHP-$CO_2CH_2CH_3$), 1.20 (3H, t, *J* 6.8 Hz, $CH_2CO_2CH_2CH_3$).

Diethyl 4-((ethoxycarbonyl)methyl)-1,4-dihydro-1-(4-hydroxyphenyl)pyridine-3,5-dicarboxylate (DHP(Et)-4AP, 1c)

According to above general procedure, **1c** was synthesized from ethyl propiolate (0.23 mL, 2.21 mmol). The crude product was purified to provide **1C** as a pale yellow oil (175 mg, 72% yield): R_f (50% EtOAc/hexane) 0.37; ^{1}H NMR (400MHz, $CDCl_3$): δ_H 7.41 (2H, s, NC*H*=C), 6.93 (2H, d, *J* 8.0 Hz, Ar*H*), 6.83 (2H, d, *J* 8.0 Hz, Ar*H*)

4.26-4.21(5H, m, DHP-$CO_2CH_2CH_3$ and $CHCH_2CO_2Et$), 4.06 (2H, q, *J* 6.8 Hz, $CH_2CO_2CH_2CH_3$), 2.59 (2H, d, *J* 4.2 Hz, CH_2CO_2Et), 1.30 (6H, t, *J* 6.8 Hz, DHP-$CO_2CH_2CH_3$), 1.20 (3H, t, *J* 6.8 Hz, $CH_2CO_2CH_2CH_3$); ^{13}C NMR (100 MHz, $CDCl_3$) δ_C 172.4, 167.2, 155.7, 138.8, 135.8, 122.9, 116.5, 107.1, 60.5, 40.8, 29.6, 14.3; HRMS (ESI): $[M+Na]^+$, found 426.1553. $C_{21}H_{25}NNaO_7^+$ requires 426.1631.

Dimethyl 4-((methoxycarbonyl)methyl)-1,4-dihydro-1-(4-hydroxyphenyl)pyridine-3,5-dicarboxylate (DHP(Me)-4AP, 1d)

According to above general procedure, **1d** was synthesized from methyl propiolate (92 mg, 2.29 mmol). The crude product was purified to provide **1d** as a pale yellow oil (85 mg, 78% yield): R_f (50% EtOAc/hexane) 0.37; ^1H NMR (400 MHz, $CDCl_3$): δ_H (ppm) 7.42 (2H, s, NC*H*=C), 6.96 (2H, d, J 8.0 Hz, Ar*H*), 6.85 (2H, d, J 8.0 Hz, Ar*H*) 4.24(1H, t, $CHCH_2CO_2Me$), 3.73 (6H, d, J 6.8 Hz, DHP-CO_2CH_3), 3.60 (3H, d, J 6.8 Hz, $CH_2CO_2CH_3$), 2.56 (2H, d, J 4.2 Hz, CH_2CO_2Me; ^{13}C NMR (100 MHz, $CDCl_3$) δ_C (ppm) 172.6, 167.5, 155.8, 139.0, 135.7, 122.9, 116.5, 106.8, 51.5, 40.8, 29.5; HRMS (ESI): $[M+Na]^+$, found 384.1053. $C_{18}H_{19}NNaO_7^+$ requires 384.3460.

2.3.2 Synthesis and characterization of DHP Triacid (2)

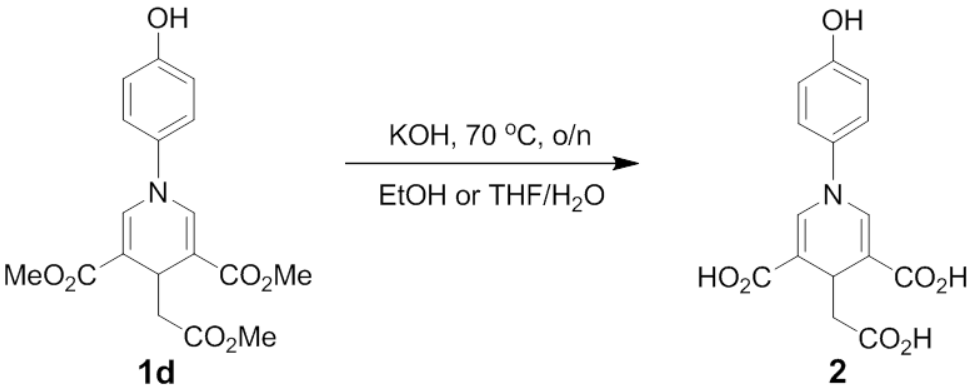

1d **2**

4-(Carboxymethyl)-1,4-dihydro-1-(4-hydroxyphenyl)pyridine-3,5-dicarboxylic acid (DHP Triacid, 2)

Compound **2** was prepared by a simple hydrolysis reaction from DHP(Me)-4AP (**1d**) (510 mg, 1.41 mmol) in KOH pellets (5 g, excess)in THF or EtOH (10 mL) and water (10 mL) was stirred at 70°C for overnight. The solution was evaporated to gain crude, which then redissolved in water (15 mL). After addition of approximately 20 g of ice, the aqueous solution residue was acidified by 0.1 M HCl for the precipitation and kept in refrigerator for overnight. The precipitate was filtered to afford compound **2b** as a brown solid (90 mg, 20% yield); ^{1}H NMR (400 MHz, CD_3OD): δ_H (ppm) 7.48 (2H, s, NC*H*=C), 7.12 (2H, d, J 8.0 Hz, Ar*H*), 6.84 (2H, d, J 8.0 Hz, Ar*H*), 4.16 (1H, t, C*H*CH_2CO_2H), 2.52 (2H, d, CH_2CO_2H; ^{13}C NMR (100 MHz, $CDCl_3$) δ_C (ppm) 175.7, 170.4, 157.7, 140.5, 137.1, 124.2, 117.3, 108.1, 41.2, 30.8.

2.3.3 General synthesis and characterization of oligoethylene glycol ditosylate (3a-d)

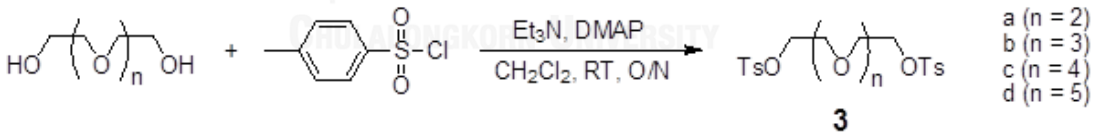

3

Oligoethylene glycol (1 equiv) and triethylamine (Et_3N, 3 equiv) were mixed in CH_2Cl_2 (750 mM) on ice bath. The mixture was stirred for 10 min and then slowly added CH_2Cl_2-soluble 4-Toluenesulfonyl chloride solution (TsCl, 4 equiv). After that the mixture was added 4-dimethyl amino pyridine (DMAP, 0.01 equiv) and stirred at room temperature for 3 days. For extraction, the mixture was added deionized water (25 mL) and extracted with CH_2Cl_2 (3×25 mL). The organic portions were combined, dried over $MgSO_4$. After the filtration and evaporation, the crude product was purified by column chromatography (EtOAc/hexane) to provide the corresponding oligoethylene glycol ditosylate (**3a-d**).

Triethylene glycol ditosylate (3a)

According to above general procedure, **3A** was synthesized from triethylene glycol (1.0 mL, 7.50 mmol). The crude product was purified by column chromatography (EtOAc/Hexane = 20:80 to 50:50) to provide **3a** as a white solid (2.71 g, 79% yield): R_f (50% EtOAc/hexane) 0.35; ^{1}H NMR (400 MHz, $CDCl_3$): δ_H (ppm) 7.78 (2H, d, J 8.0 Hz, Ar*H*), 7.33 (2H, d, J 8.0 Hz, Ar*H*), 4.13 (2H, t, $CH_2CH_2OSO_2$), 3.65 (2H, t, CH_2CH_2O), 3.52 (2H, s, CH_2O), 2.44 (3H, s, CH_3Ar). HRMS (ESI): $[M+Na]^+$, found 481.1105 $C_{20}H_{26}NaO_8S_2^+$ requires 481.0967.

Tetraethylene glycol ditosylate (3b)

According to above general procedure, **3b** was synthesized from tetraethylene glycol (1.0 mL, 5.79 mmol). The crude product was purified by column chromatography (EtOAc/Hexane 20:80 to 50:50) to provide **3b** as a pale yellow oil (1.48 g, 51% yield): R_f (50% EtOAc/hexane) 0.35; ^{1}H NMR (400 MHz, $CDCl_3$): δ_H (ppm) 7.72 (2H, d, J 8.0 Hz, Ar*H*), 7.27 (2H, d, J 8.0 Hz, Ar*H*), 4.08 (2H, t, $CH_2CH_2OSO_2$), 3.61 (2H, t, CH_2CH_2O), 3.49 (4H, m, OCH_2CH_2O), 2.37 (3H, s, CH_3Ar). HRMS (ESI): $[M+Na]^+$, found 525.1325 $C_{22}H_{30}NaO_9S_2^+$ requires 525.1229.

Pentaethylene glycol ditosylate (3c)

According to above general procedure, **3c** was synthesized from pentaethylene glycol (1.0 mL, 4.72 mmol). The crude product was purified by column chromatography (EtOAc/Hexane 20:80 to 80:20) to provide **3c** as a pale yellow oil (1.93 g, 75% yield): R_f (50% EtOAc/hexane) 0.10; ^{1}H NMR (400 MHz, $CDCl_3$): δ_H (ppm) 7.79 (2H, d, J 8.0 Hz, Ar*H*), 7.34 (2H, d, J 8.0 Hz, Ar*H*), 4.15 (2H, t, $CH_2CH_2OSO_2$), 3.68 (2H, t, CH_2CH_2O), 3.59 (6H, m, OCH_2CH_2O), 2.44 (3H, s, CH_3Ar). HRMS (ESI): $[M+Na]^+$, found 569.1596 $C_{24}H_{34}NaO_{10}S_2^+$ requires 569.1491.

Hexaethylene glycol ditosylate (3d)

According to above general procedure, **3d** was synthesized from hexaethylene glycol (2.0 mL, 7.97 mmol). The crude product was purified by column chromatography (EtOAc/Hexane 50:50 to 100:0) to provide **3d** as a pale yellow oil (1.93 g, 75% yield): R_f (80% EtOAc/hexane) 0.22; ^{1}H NMR (400 MHz, $CDCl_3$): δ_H (ppm) 7.79 (2H, d, J 8.0 Hz, Ar*H*), 7.34 (2H, d, J 8.0 Hz, Ar*H*), 4.15 (2H, t, $CH_2CH_2OSO_2$), 3.68 (2H, t, CH_2CH_2O), 3.61, 3.57 (8H, m, OCH_2CH_2O), 2.44 (3H, s, CH_3Ar). HRMS (ESI): $[M+Na]^+$, found 613.1860 $C_{26}H_{38}NaO_{11}S_2^+$ requires 613.1754.

2.3.4 Synthesis and characterization of Tetraethylene glycol dihalide (4a and 4b)

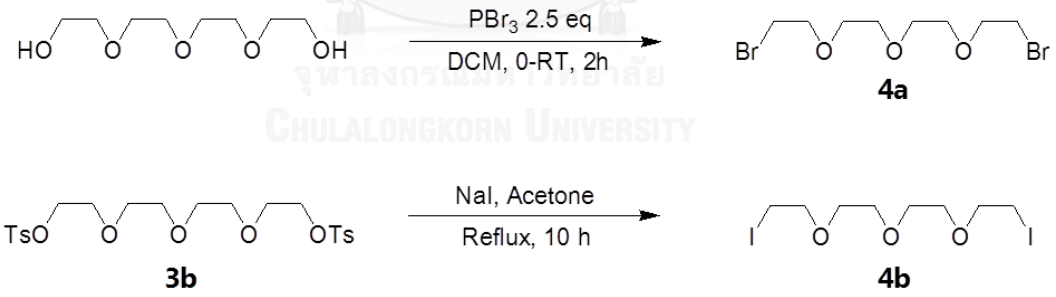

Tetraethylene glycol dibromide (4a)

Tetraethylene glycol (1mL, 5.79 mmol) in CH_2Cl_2 was stirred at 0°C on ice bath. After that Phosphorus tribromide (PBr_3) (1.37 mL, 14.48 mmol) was added and the mixture was stirred at room temperature for 3 hours. The solution was quenched with $NaHCO_3$ solution and extracted with CH_2Cl_2 (3×25 mL). The organic portions were combined, wash by H_2O. The mixture was dried over $MgSO_4$ and evaporated

under reduced pressure. The crude obtained product was purified by column chromatography (MeOH/EtOAc = 50:50) to provide the corresponding dibromide (**4a**) as a pale yellow oil (1.10 g, 92% yield): R_f (50% EtOAc/hexane) 0.35**;** ^{1}H NMR (400 MHz, $CDCl_3$): δ_H (ppm) 3.81 (2H, t, CH_2CH_2Br), 3.66 (4H, s, CH_2CH_2O), 3.46 (2H, t, CH_2CH_2Br).

Tetraethylene glycol diiodide (4b)

Tetraethylene glycol ditosylate (**3b**, 0.4 g, 0.80 mmol) and NaI (4.0 equiv.) were disperse in acetone (20 mL) and stirred at reflux temperature for 6 hours. The solution was quenched with DI water and extracted with CH_2Cl_2 (3×25 mL). The organic portions were combined and wash by H_2O. The mixture was dried over $MgSO_4$ and evaporated under reduced pressure. The crude obtained product was purified by column chromatography (MeOH/EtOAc = 50:50) to provide the corresponding diiodide (**4b**) as a pale yellow oil (0.314 g, 95% yield): R_f (50% EtOAc/hexane) 0.35**;** ^{1}H NMR (400 MHz, $CDCl_3$): δ_H (ppm) 3.77 (2H, t, CH_2CH_2I), 3.68 (4H, s, CH_2CH_2O), 3.27 (4H, m, CH_2CH_2I).

2.3.5 General synthesis and characterization of bis DHPs (5a-d)

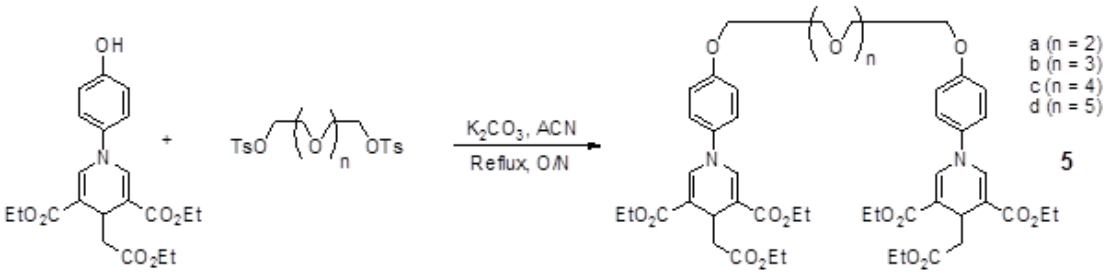

DHP(Et)-4AP (2.2 equiv) in ACN (23 mmol) and potassium carbonate (K_2CO_3, 6.0 equiv) were dispersed and the reaction was stirred at ambient temperature for

1h under nitrogen atmosphere. The reaction mixture was then added ACN-soluble oligoethylene glycol ditosylate solution (1.0 equiv) and refluxed overnight and filtered. The solvent was evaporated and the residue was added deionized water (25 mL), extracted with CH_2Cl_2 (3×25 mL). The organic portions were combined, dried over $MgSO_4$, and evaporated under reduced pressure. The crude obtained product was purified by column chromatography (EtOAc/hexane) to provide the corresponding bis DHPs (**5a-d**)

bis DHP-3 (5a)

According to above general procedure, **5a** was synthesized from triethylene glycol ditosylate (105 mg, 0.23 mmol). The crude product was purified by column chromatography (EtOAc/Hexane 50:50) to provide **5a** as a pale yellow oil (131 mg, 62% yield): R_f (50% EtOAc/hexane) 0.12; ^{1}H NMR (400 MHz, $CDCl_3$): δ_H 7.46 (2H, s, NC*H*=C), 7.14 (2H, d, *J* 8.7 Hz, Ar*H*), 6.93 (2H, d, *J* 8.7 Hz, Ar*H*) 4.25-4.21 (4H, m, DHP-$CO_2CH_2CH_3$), 4.14-4.09 (3H, m, OCH_2 and $CHCH_2CO_2Et$), 4.04-4.00 (2H, q, *J* 7.0 Hz, $CH_2CO_2CH_2CH_3$), 3.87 (2H, t, OCH_2), 3.76 (2H, s, OCH_2), 2.56 (2H, d, *J* 4.6 Hz, CH_2CO_2Et), 1.26 (6H, t, *J* 7.0 Hz, DHP-$CO_2CH_2CH_3$), 1.16 (3H, t, *J* 7.0 Hz, $CH_2CO_2CH_2CH_3$); ^{13}C NMR (100 MHz, $CDCl_3$) δ_C 171.8, 166.8, 157.4, 138.2, 136.8, 122.9, 115.7, 107.6, 70.9, 69.7, 67.9, 60.2, 60.0, 40.6, 29.7, 21.0, 14.4; HRMS (ESI): $[M+Na]^+$, found 943.3807. $C_{50}H_{64}N_2NaO_{17}^+$ requires 943.3943.

bis DHP-4 (5b)

According to above general procedure, **5b** was synthesized from tetraethylene glycol ditosylate (116 mg, 0.23 mmol). The crude product was purified by column chromatography (EtOAc/Hexane 50:50) to provide **5b** as a pale yellow oil (178 mg, 80% yield): R_f (80% EtOAc/hexane) 0.40; ^{1}H NMR (400 MHz, $CDCl_3$): δ_H 7.46 (2H, s, NC*H*=C), 7.13 (2H, d, *J* 8.7 Hz, Ar*H*), 6.93 (2H, d, *J* 8.7 Hz, Ar*H*) 4.24-4.19 (5H, m, DHP-$CO_2CH_2CH_3$ and $CHCH_2CO_2Et$), 4.12 (2H, t, OCH_2), 4.03 (2H, q, *J* 7.0 Hz, $CH_2CO_2CH_2CH_3$), 3.86 (2H, t, OCH_2), 3.76-3.66 (4H, m, OCH_2), 2.56 (2H, d, *J* 4.6 Hz,

C*H*$_2$CO$_2$Et), 1.29 (6H, t, *J* 7.0 Hz, DHP-CO$_2$CH$_2$C*H*$_3$), 1.17 (3H, t, *J* 7.0 Hz, CH$_2$CO$_2$CH$_2$C*H*$_3$); ^{13}C NMR (100 MHz, CDCl$_3$) δ_C 171.7, 166.8, 157.4, 138.3, 136.8, 122.8, 115.7, 107.6, 70.9, 70.7, 69.7, 67.9, 60.2, 60.0, 40.7, 29.6, 14.4, 14.2; HRMS (ESI): $[M+Na]^+$, found 987.4149. $C_{50}H_{64}N_2NaO_{17}^+$ requires 987.4205.

bis DHP-5 (5c)

According to above general procedure, **5c** was synthesized from penaethylene glycol ditosylate (123 mg, 0.23 mmol). The crude product was purified by column chromatography (EtOAc/Hexane 80:20) to provide **5c** as a pale yellow oil (131 mg, 57% yield): R_f (80% EtOAc/hexane) 0.30; ^{1}H NMR (400M Hz, CDCl$_3$): δ_H 7.46 (2H, s, NC*H*=C), 7.13 (2H, d, *J* 8.7 Hz, Ar*H*), 6.93 (2H, d, *J* 8.7 Hz, Ar*H*) 4.26-4.20 (5H, m, DHP-CO$_2$C*H*$_2$CH$_3$ and C*H*CH$_2$CO$_2$Et), 4.12 (2H, t, OC*H*$_2$), 4.03 (2H, q, *J* 7.0 Hz, CH$_2$CO$_2$C*H*$_2$CH$_3$), 3.86 (2H, t, OC*H*$_2$), 3.73-3.67 (6H, m, OC*H*$_2$), 2.57 (2H, d, *J* 4.6 Hz, C*H*$_2$CO$_2$Et), 1.28 (6H, t, *J* 7.0 Hz, DHP-CO$_2$CH$_2$C*H*$_3$), 1.18 (3H, t, *J* 7.0 Hz, CH$_2$CO$_2$CH$_2$C*H*$_3$); ^{13}C NMR (100 MHz, CDCl$_3$) δ_C 171.7, 166.8, 157.4, 138.3, 136.8, 122.8, 115.7, 107.6, 70.9, 70.7, 69.7, 67.9, 60.2, 60.0, 40.7, 29.6, 14.4, 14.2.

bis DHP-6 (5d)

According to above general procedure, **5d** was synthesized from hexaethylene glycol ditosylate (136 mg, 0.23 mmol). The crude product was purified by column chromatography (EtOAc/Hexane 100:0) to provide **5d** as a pale yellow oil (100 mg, 41% yield): R_f (100% EtOAc) 0.30; ^{1}H NMR (400 MHz, CDCl$_3$): δ_H 7.44 (2H, s, NC*H*=C), 7.11 (2H, d, *J* 8.7 Hz, Ar*H*), 6.92 (2H, d, *J* 8.7 Hz, Ar*H*) 4.25-4.18 (5H, m, DHP-CO$_2$C*H*$_2$CH$_3$ and C*H*CH$_2$CO$_2$Et), 4.11 (2H, t, OC*H*$_2$), 4.02 (2H, q, *J* 7.0 Hz, CH$_2$CO$_2$C*H*$_2$CH$_3$), 3.84 (2H, t, OC*H*$_2$), 3.72-3.65 (8H, m, OC*H*$_2$), 2.56 (2H, d, *J* 4.6 Hz, C*H*$_2$CO$_2$Et), 1.26 (6H, t, *J* 7.0 Hz, DHP-CO$_2$CH$_2$C*H*$_3$), 1.16 (3H, t, *J* 7.0 Hz, CH$_2$CO$_2$CH$_2$C*H*$_3$); ^{13}C NMR (100 MHz, CDCl$_3$) δ_C 171.6, 166.8, 157.4, 138.3, 122.8, 115.7, 107.6, 70.6, 60.2, 60.0, 40.6, 29.7, 14.4; HRMS (ESI): $[M+Na]^+$, found 1075.4626. $C_{50}H_{64}N_2NaO_{17}^+$ requires 1075.4627.

2.3.6 General synthesis and characterization of mono DHP form DHP-4AP compounds (6a-e)

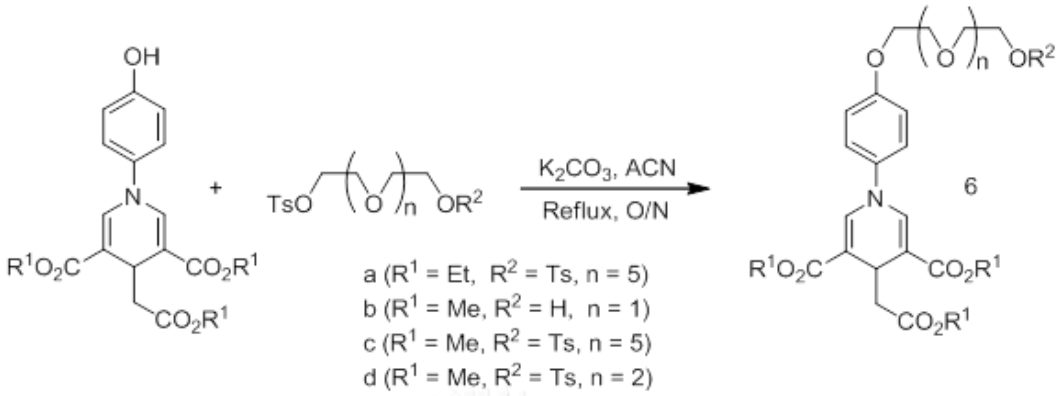

In the case of ethylene glycol monotosylate, monotosylate (0.8 equiv) in ACN (77 mM) and potassium carbonate (K_2CO_3, 6.0 equiv) were dispersed and the reaction was stirred at ambient temperature for 1h under nitrogen atmosphere. The reaction mixture was then added ACN-soluble DHP solution (1.0 equiv), refluxed overnight and filtered. The solvent was evaporated and the residue was added deionized water (25 mL), extracted with CH_2Cl_2 (3×25 mL). The organic portions were combined, dried over $MgSO_4$, and evaporated under reduced pressure. For ethylene glycol ditosylate, ditosylate (1.5 equiv) in ACN and potassium carbonate (K_2CO_3, 6.0 equiv) were dispersed and synthesized according to above general procedure. The crude obtained product was purified by column chromatography (EtOAc/CH_2Cl_2) to provide the corresponding mono DHP (**6a-e**)

mono DHP(Et)-6-OTs (6a)

According to above general procedure, **6a** was synthesized from **1c** (500 mg, 1.42 mmol) and hexaethylene glycol ditosylate (1.10 g, 1.86 mmol). The crude product was purified by column chromatography (EtOAc/CH_2Cl_2 10:90 to 50:50) to provide **6b** as a pale yellow oil (510 mg, 50% yield): R_f (50% EtOAc/CH_2Cl_2) 0.35; ^{1}H NMR (400M Hz, $CDCl_3$): δ_H 7.78 (2H, d, *J* 8.7 Hz, Ar*H*), 7.45 (2H, s, NC*H*=C), 7.32 (2H, d, *J* 8.7 Hz, Ar*H*), 7.12 (2H, d, *J* 8.7 Hz, Ar*H*), 6.92 (2H, d, *J* 8.7 Hz, Ar*H*) 4.24-4.18 (5H, m, DHP-$CO_2CH_2CH_3$ and $CHCH_2CO_2Et$), 4.15-4.10 (4H, m, OCH_2), 4.02 (2H, q, *J* 7.0 Hz,

$CH_2CO_2CH_2CH_3$), 3.84 (2H, m, OCH_2), 3.71-3.56 (18H, m, OCH_2), 2.55 (2H, d, *J* 4.6 Hz, CH_2CO_2Et), 2.43 (3H, s, $ArCH_3$), 1.26 (6H, t, *J* 7.0 Hz, DHP-$CO_2CH_2CH_3$), 1.16 (3H, t, *J* 7.0 Hz, $CH_2CO_2CH_2CH_3$); ^{13}C NMR (100 MHz, $CDCl_3$) δ_C 171.6, 166.8, 157.4, 138.3, 136.8, 129.8, 128.2, 122.8, 115.7, 107.6, 70.8-67.9, 60.2, 60.0, 40.6, 29.7, 14.4, 14.2; HRMS (ESI): $[M+Na]^+$, found 844.3232. $C_{40}H_{55}NNaO_{15}S^+$ requires 844.3190.

mono DHP(Me)-2-OH (6b)

According to above general procedure, **6b** was synthesized from **1d** (333 mg, 0.92 mmol) and diethylene glycol ditosylate (200 mg, 0.77 mmol). The crude product was purified by column chromatography (EtOAc/CH_2Cl_2 20:80) to provide **6c** as a pale yellow oil (64 mg, 18% yield): R_f (20% EtOAc/CH_2Cl_2) 0.12; ^1H NMR (400 MHz, $CDCl_3$): δ_H 7.48 (2H, s, NC*H*=C), 7.14 (2H, d, *J* 8.7 Hz, Ar*H*), 6.94 (2H, d, *J* 8.7 Hz, Ar*H*) 4.24 (1H, t, C*H*CH_2CO_2Me), 4.14 (2H, m, OCH_2), 3.88 (2H, m, OCH_2), 3.78-3.75 (8H, m, OCH_2 and DHP-CO_2CH_3), 3.67 (2H, m, OCH_2), 3.59 (3H, m, DHP-CO_2Me), 2.57 (2H, d, *J* 4.6 Hz, CH_2CO_2Me; ^{13}C NMR (100 MHz, $CDCl_3$) δ_C 171.6, 166.8, 157.4, 138.3, 136.8, 129.8, 128.2, 122.8, 115.7, 107.6, 70.8-67.9, 60.2, 60.0, 40.6, 29.7, 14.4, 14.2; MALDI-TOF: $[M]^+$, found 447.231. $C_{40}H_{55}NNaO_{15}S^+$ requires 449.1686.

mono DHP(Me)-6-OTs (6c)

According to above general procedure, **6c** was synthesized from **1d** (500 mg, 1.38 mmol) and hexaethylene glycol ditosylate (1226 mg, 2.07 mmol). The crude product was purified by column chromatography (EtOAc/CH_2Cl_2 20:80) to provide **6d** as a pale yellow oil (624 mg, 58% yield): R_f (50% EtOAc/CH_2Cl_2) 0.37 and get bis DHP-6 as by-product (183 mg, 11% yield): R_f (50% EtOAc/CH_2Cl_2) 0.22; ^1H NMR (400 MHz, $CDCl_3$): δ_H 7.78 (2H, d, *J* 8.7 Hz, Ar*H*), 7.47 (2H, s, NC*H*=C), 7.33 (2H, d, *J* 8.7 Hz, Ar*H*), 7.12 (2H, d, *J* 8.7 Hz, Ar*H*), 6.92 (2H, d, *J* 8.7 Hz, Ar*H*) 4.23 (1H, t, C*H*CH_2CO_2Me), 4.15-4.10 (4H, m, OCH_2), 3.85 (2H, m, OCH_2), 3.74-3.57 (27H, m, OCH_2), 2.56 (2H, d, *J* 4.6 Hz, CH_2CO_2Et), 2.43 (3H, s, $ArCH_3$); ^{13}C NMR (100 MHz, $CDCl_3$) δ_C 171.9, 167.1, 157.5,

144.7, 138.5, 136.6, 129.8, 127.9, 122.8, 115.7, 107.2, 70.8-67.9, 51.4, 51.3, 40.6, 29.6, 29.5, 21.6; HRMS (ESI): $[M+Na]^+$, found 802.2815. $C_{37}H_{49}NNaO_{15}S^+$ requires 802.2721.

mono DHP(Me)-3-OTs (6d)

According to above general procedure, **6d** was synthesized from **1d** (500 mg, 1.38 mmol) and triethylene glycol ditosylate (949 mg, 2.07 mmol). The crude product was purified by column chromatography (EtOAc/CH_2Cl_2 10:90) to provide **6e** as a pale yellow oil (536 mg, 60% yield): R_f (50% EtOAc/hexane) 0.15 and get bis DHP(Me)-3 as the by product (134 mg, 15% yield): R_f (80% EtOAc/hexane) 0.50; ^{1}H NMR (400 MHz, $CDCl_3$): δ_H 7.79 (2H, d, *J* 8.7 Hz, Ar*H*), 7.48 (2H, s, NC*H*=C), 7.33 (2H, d, *J* 8.7 Hz, Ar*H*), 7.13 (2H, d, *J* 8.7 Hz, Ar*H*), 6.93 (2H, d, *J* 8.7 Hz, Ar*H*) 4.23 (1H, t, C*H*CH_2CO_2Me), 4.16 (2H, m, OCH_2), 4.11 (2H, m, OCH_2) 3.88 (2H, m, OCH_2), 3.77-3.51 (15H, m, OCH_2), 2.57 (2H, d, *J* 4.6 Hz, CH_2CO_2Me), 2.43 (3H, s, ArCH_3); ^{13}C NMR (100 MHz, $CDCl_3$) δ_C 171.9, 167.1, 157.5, 144.7, 138.5, 136.6, 129.8, 127.9, 122.8, 115.7, 107.2, 70.8-67.9, 51.4, 51.3, 40.6, 29.6, 29.5, 21.6; HRMS (ESI): $[M+Na]^+$, found 670.1962. C31H37NNaO12S$^+$ requires 670.1934.

2.3.7 Synthesis and characterization of mono DHP(Me)-6-OMe (7)

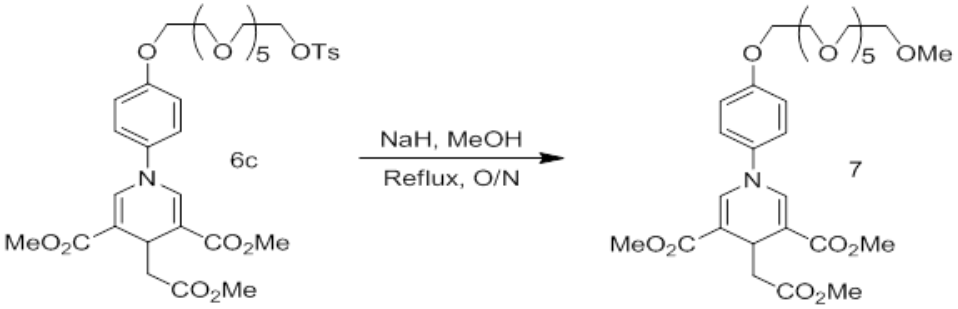

Excess MeOH (20 mL) was added as the coupling reagent and solvent into the reaction flask contained NaH (6.0 equiv) on an ice bath. The mixture was stirred and then added dropwise **6c** (200mg, 0.24 mmol), heated at reflux overnight. After the

solution was quenched with Brine solution and filtered. The solvent was evaporated and the residue was added deionized water (25 mL), extracted with CH_2Cl_2 (3×25 mL). The organic portions were combined and neutralized by 0.1 M HCl, dried over $MgSO_4$, and evaporated under reduced pressure. The crude obtained product was purified by column chromatography (MeOH/EtOAc = 2:98) to provide mono DHP derivative (**7**) as a pale yellow oil (103 mg, 63% yield): R_f (50% EtOAc/ CH_2Cl_2) 0.15; ^{1}H NMR (400 MHz, $CDCl_3$): δ_H 7.79 (2H, d, *J* 8.7 Hz, Ar*H*), 7.48 (2H, s, NC*H*=C), 7.33 (2H, d, *J* 8.7 Hz, Ar*H*), 7.13 (2H, d, *J* 8.7 Hz, Ar*H*), 6.93 (2H, d, *J* 8.7 Hz, Ar*H*) 4.23 (1H, t, C*H*CH_2CO_2Me), 4.16 (2H, m, OCH_2), 4.11 (2H, m, OCH_2) 3.88 (2H, m, OCH_2), 3.77-3.51 (15H, m, OCH_2), 2.57 (2H, d, *J* 4.6 Hz, CH_2CO_2Me), 2.43 (3H, s, ArCH_3);

2.3.8 Synthesis and characterization of mono DHP(Et)-6-OH (8)

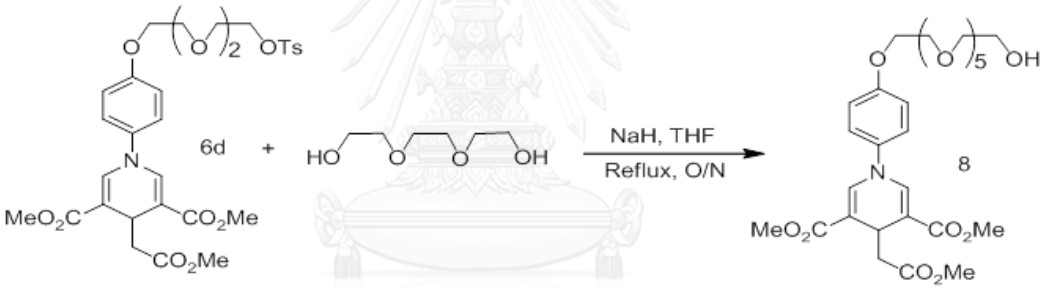

6.0 equiv of NaH in farafin oil was added into the reaction mixture containing 3.0 equiv of triethylene glycol in THF (10 mL). The mixture was stirred at 60°C for 1h and then, added **6d** (200 mg, 0.31 mmol) which diluted in 5 mL THF drop wise by auto syringe. After 10 hours under 60°C, the solvent was evaporated and the residue was quenched by brine solution (20 mL). Then, the mixture was extracted with DCM (3×25 mL) and checked pH of organic fraction. This fraction was neutralized by 0.1 M HCl and extract again with DCM, organic fraction was dried over $MgSO_4$, and evaporated under reduced pressure. The crude obtained product was purified by column chromatography (MeOH/EtOAc = 2:98) to provide mono **8** as a pale yellow oil (79 mg, 65% yield): R_f (100% EtOAc) 0.22;

2.4 Analytical experiment

The photophysical properties study, metal sensing and surfactant sensing were achieved in milliQ water and MeOH. Oxidative sensing, pH sensing were achieved in milliQ water and Britton-Robinson Buffer (BR buffer) pH 6-12. Protein sensing attained in phosphate buffer saline PBS pH 7.4

2.4.1 Photophysical properties study

The stock solution of all target molecules was prepared by dissolving each compound in MeOH and dileted it to get the concentration of 200 μM stock solutions (100 mL).

i) UV-Visible spectroscopy

The UV-Visible absorption spectra of the stock solutions of fluorophores were recorded from 200 nm to 500 nm at ambient temperature.

ii) Fluorescence spectroscopy

The stock solutions of fluorophores were diluted into the concentration of 1 μM with MeOH (100% MeOH, v/v) and mill Q water (99.5% aq, v/v). The emission spectra of fluorophores were recorded from 380 nm to 700 nm at ambient temperature using an excitation wavelength at 366 nm for all sensors.

iii) Molar extinction coefficient (ε)

The molar extinction coefficient (ε) of all compounds were calculated from the UV-Visible absorption spectra in aqueous solution and organic solution (MeOH) of analytical samples at varied concentrations were recorded. The maximum absorbance of all samples should never exceed 1. Graphs of absorption maximum wavelength (λ_{max}) of each compound were plotted against the concentration at the respective excitation wavelengths. Each plot should be a straight line with 0 interceptions. The molar extinction coefficient (ε) can also be calculated from

plotting of absorption maximum (A) *vs* concentration (C) represented into the following equation:

$$A = \varepsilon bC$$

iV) Fluorescence quantum yield (Φ_F)

The fluorescence quantum yield of all compounds were performed in aqueous solution (milliQ water) and organic solution (MeOH) by using Quinine sulfate in 0.1 M H_2SO_4 (Φ=0.54) as a reference. The UV-Visible absorption spectra of analytical samples and reference samples at varied concentrations were recorded. The maximum absorbance of all samples should never exceed 0.1. The fluorescence emission spectra of the same solutions using appropriate excitation wavelengths selected were recorded based on the absorption maximum wavelength (λ_{max}) of each compound. Graphs of integrated fluorescence intensities were plotted against the absorbance at the respective excitation wavelengths. Each plot should be a straight line with 0 interception and gradient *m*.

In addition, the fluorescence quantum yield (Φ_F) was obtained from plotting of integrated fluorescence intensity *vs* absorbance represented into the following equation:

$$\Phi_X = \Phi_{ST}\left(\frac{Grad_X}{Grad_{ST}}\right)\left(\frac{\eta_X^2}{\eta_{ST}^2}\right)$$

The subscripts Φ_{ST} denote the fluorescence quantum yield of a standard reference which used quinine sulfate in 0.1 M H_2SO_4 (Φ=0.54) and Φ_X is the fluorescence quantum yield of sample and η is the refractive index of the solvent.

2.4.2 Metal ion sensor

Stock solution for each metal ion was prepared in MilliQ water by using metal acetate except ferric nitrate (Fe^{3+}), ferrous sulfate (Fe^{2+}) and cadmium sulfate (Cd^{2+}) into a concentration of 2 mM. For allosteric experiment, stock solutions of metal ion

(IA, IIA) soluble in water such as those where the counter ion is perchlorate ion (ClO_4^-) or hexafluoro phosphate ion (PF_6^-) was prepared in acetonitrile.

i) Selectivity study

To attained the fluorescence quenching profile, All probes and metal solution were mixed into tip and diluted with MilliQ water or MeOH depending on requirements, in order to obtain a final concentration of 1 μM and 100 μM for probe and metal ion, respectively. The mixture allowed to stand at room temperature for 30 min and recorded spectra from 380 nm to 700 nm at ambient temperature by fluorescence spectrophotometer. Increasing the concentration of fluorophore and metal ions to 10 μM and 1000 μM (about 10 times of the spectrophotometer), in order to achieve the visible fluorescence response and photograph under black light.

ii) Time-dependent quenching study

The fluorescent quenching by Au^{3+} proceed gradually, consequently, the fluorescent signal was investigated for 60 minutes. By assignment the concentration ratio of probe:Au^{3+} at 1:100 μM, the mixture was allowed to stand at ambient temperature for 0 to 60 minutes. The spectra were reported by using fluorescent spectrometer. Time-dependent quenching of all compounds toward Au^{3+} were shown by plotting between I_0/I and time

iii) Fluorescent and UV-vis titration

To reach the fluorescence titration spectra, the mixtures of fluorophore/metal were prepared by the ratio of 1/0-100 and allowed to stand at room temperature for 30 min and 15 min for Au^{3+} and Fe^{2+} titration, respectively. Then the spectra were recorded by fluorescent spectrometer. UV–vis metal binding titration was prepared as same as fluorescence titration but increasing the concentration of fluorophore to about 10-100 μM, recorded spectra by UV-vis spectrophotometer.

iv) Interference study

The mixture of fluorophore/Au^{3+}/others metal ions and fluorophore/Fe^{2+}/others metal ions with ratio of 1/100/100 were used to investigated competitive experiments of bis DHP probe for Au^{3+} sensing and Fe^{2+} sensing, respectively. Other substances tested the same experiment, used the same method as shown in the above.

v) Limit of detection (LOD)

LOD is the lowest quantity of a substance that can be detected, but not necessarily quantitated as an exact value. LOD is estimated from:

$$LOD = 3\frac{\sigma}{K_{sv}}$$

Where;

σ is the standard deviation of the response deriving from the maximum intensity of fluorophore at 1 μM of 9 samples.

K_{sv} is the slope of the calibration curve obtained from fluorescent titration spectra of probe, plotting between I_0/I and molar concentration of expletive analyte.

2.4.3 Surfactant sensor

The stock solution of **1d** was diluted to 1 μM in milliQ water were prepared. The emission spectrum of **2a** was recorded from 380 nm to 700 nm at ambient temperature using an excitation wavelength at 366 nm and the photophysical properties were studied three types surfactant; anionic surfactant, cationic surfactant and non-ionic surfactants. The stock surfactants were prepared in milliQ water. Concentrations of all stock surfactants were adjusted to 1000 mM and were added to the fluorophore solutions. The final volumes of the mixtures were adjusted to 1400 μL and detected real-time and after 1 hour

2.4.4 Protein sensor

Stock solution for each protein was prepared in phosphate buffer saline (PBS) pH= 7.4 to get the absorbance at 280 nm (A_{280}) to be 1.0. To study effect of protein, the **1d** was added into tip and oxidizing agent was mixed. The mixture was diluted with PBS, in order to obtain a final concentration of 1d is 1 and A_{280} of protein is 0.1. The mixture was excited at wavelength of 366 nm and recorded fluorescence spectra from 380 nm to 700 nm at ambient temperature by fluorescence spectrophotometer.

2.4.5 Oxidative sensor

Stock solution for each oxidizing agent was prepared in MilliQ water to get a concentration of 10 mM. To attain the fluorescence behavior, the **1d** and oxidizing agent were mixed into tip and diluted with MQ, in order to obtain a final concentration of 1d and analytes are 1 μM and 100 μM, respectively. The mixture was allowed to stand at room temperature for 60 min, measured, fluorescence spectra with an excitation wavelength of 362 nm and recorded spectra from 380 nm to 700 nm at ambient temperature by fluorescence spectrophotometer. Real-time experiment used the same condition to study as well.

2.4.6 pH sensor

Stock buffer solution for pH range 2-12 was prepared by Britton-Robinson method. Britton-Robinson universal buffer solutions (BR buffer) pH = 2-12 were prepared by mixing appropriate volumes of acids and basic buffer components. The acidic buffer component comprises 0.04 M phosphoric acid, 0.04 M boric acid, and 0.04 M acetic acid. Various Buffer Solutions were titrated using 0.2 M sodium hydroxide. Basic sample stock solutions were prepared by dilution of 0.2 M sodium hydroxide with mill-Q water.

To attain the fluorescence profile, the final volume of the mixtures was adjusted to 1 mL to afford the final concentration of 100 μM for the fluorophore and

diluted with BR buffer. After the solution was mixed, fluorescence spectra were measured with an excitation wavelength of 366 nm at room temperature. Fluorescence spectra were recorded from 380 to 700 nm by fluorescence spectrophotometer. This concentration used to get the visible fluorescence response and photograph under black light. The determination of pK_a was assessed using the Henderson–Hasselbalch equation:

$$log[(I_{max} - I)/I - I_{min}] = pH - pK_a$$

Where I is the observed fluorescence intensity, I_{max} and I_{min} are the corresponding maximum and minimum, respectively. The mixture of fluorophore/disrupting chemicals with ratio 1/100 in BR buffer was use to investigated competitive experiments in the pH system.

CHAPTER III

RESULTS AND DISCUSSION

3.1 Systhesis and characterization of fluorophores

3.1.1 Synthesis of bis(1,4-dihydropyridine) derivatives from DHP-OH (1a)

Initially, we have designed a structure of 1,4-dihydropyridine derivatives (bis DHP-OH) containing two DHP units of **1a** linked with oligoethylene glycol chains (n=2-5) by using the synthetic route below (**Scheme 3.1**). In this conceptual design, DHP is selected as fluorophore unit, and oligoethylene glycol as linker between DHP moiety and also may act as a metal ion receptor unit as well as increase water solubility.

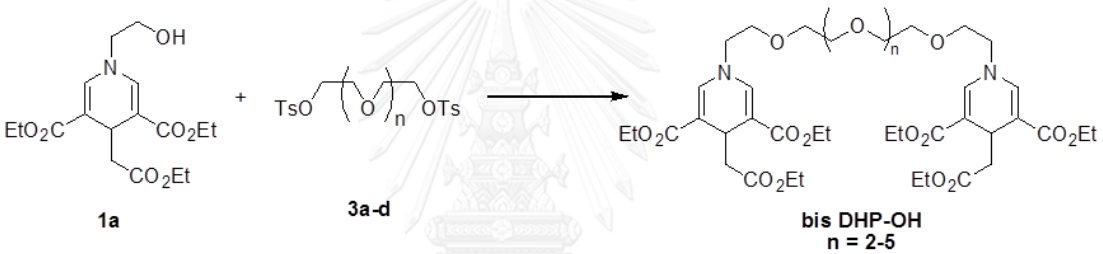

Scheme 3.1 Synthetic route of bis DHP-OH

The first step, we have synthesized DHP-OH (**1a**) from the reaction between ethyl propiolate and ethanolamine in DCM at room temperature for 5 hours (**Scheme 3.2**) to give the corresponding β-amino acrylate (**1a'**). The treatment of the crude **1a'** with $TiCl_4$ (Lewis acid) for overnight produced DHP-OH in excellent yield (84%) via cyclotrimerization reaction based on our recently reported method [19] and the characterization data such as ^{1}H NMR, ^{13}C NMR and Mass spectroscopy also agreed with the corresponding structures.

.

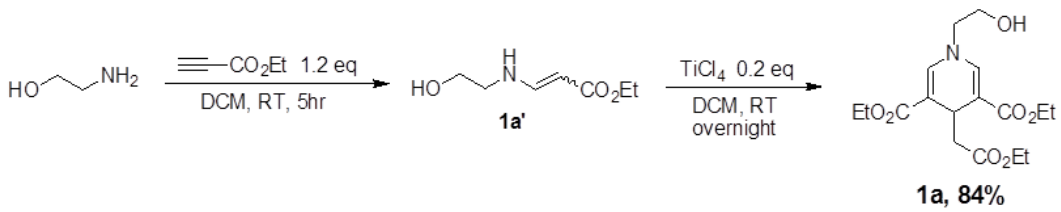

Scheme 3.2 preparation of DHP-OH (**1a**)

Next step, oligoethylene glycol ditosylates (**3a-d**) were prepared by tosylation reaction of ethylene glycol (**Scheme 3.3**). Initially, tosyl chloride dissolved in DCM solution and 4-dimethylaminopyridine (DMAP) as catalyst was added into the DCM solution of ethylene glycol. The reaction mixture was stirred for 3 days to gain ditosylate compound as a major product (3a-d) in moderate to good yields (50-75%). The ditosylate products were difficult to be isolated by a column chromatography because of their high polarity resulting in strongly adsorbed on the silica gel stationary phase.

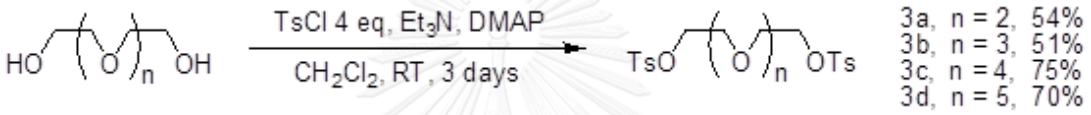

Scheme 3.3 Preparation of oligoethylene glycol ditosylate (**3a-d**)

^{1}H NMR spectra of **3a-d** in $CDCl_3$ were shown in **Figure 3.1**. The twin doublet peaks in aromatic region around 7.33 and 7.78 ppm were assigned to the phenyl ring protons and singlet peak at 2.44 ppm for the protons of methyl group in tosylate unit. The glycol chain appeared as three to four multiplet peaks in a range of 4.17-3.52 ppm that their integrated values were in accordance to the length of its glycol.

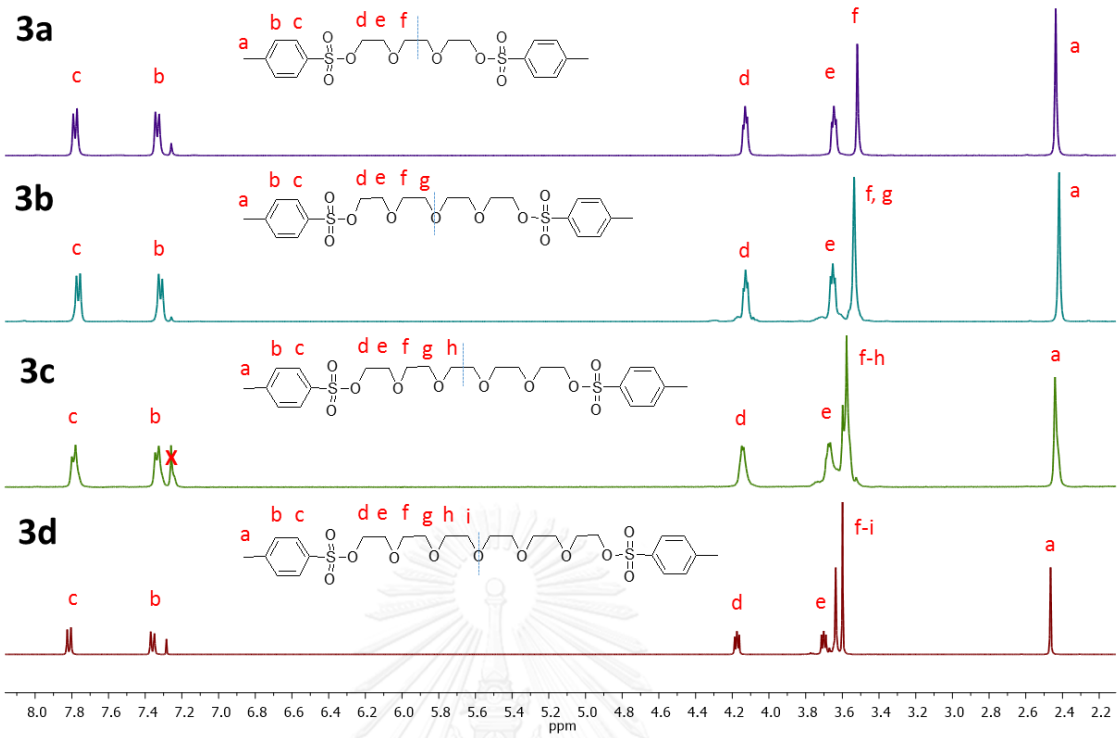

Figure 3.1 ^{1}H NMR spectra (400 MHz) of **3a-d** in $CDCl_3$

The target bis DHP-OH was obtained by reacting **1a** with **3b** via S_N2 reaction as shown in **Scheme 3.4**. The reaction conditions were varied in order to optimize the yield of the expected product (**Table 3.1**). However, there were no satisfied results observed.

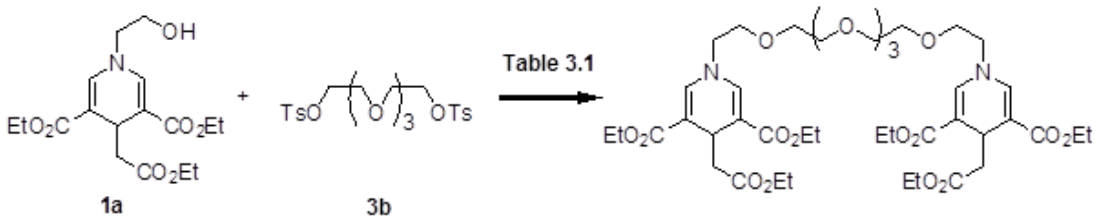

Scheme 3.4 Preparation of bis DHP-OH from ditosylate substrate

For the reaction conditions 1 and 2, K_2CO_3 was used as a base in ACN and DMF solution under N_2 atmosphere for 3 days, respectively, but there was no reaction occurred. NaH, which is a stronger base was used in the subsequent experiments (entry 3-8) in various solvents such as acetone, ACN and DMF. Each

condition was monitored from 1 to 3 days. According to the results of TLC, many fluorescent spots without the major ones were observed implying the disorganized reaction. The attempt to separate the crude mixture by a column chromatography was not successful.

Table 3.1 Synthetic condition for preparation of bis DHP-OH from DHP-OH (**1a**) for 1 to 3 days under reflux temperature.

Entry	Substrate	Base	Solvent	%Yield
1	**3b**	K_2CO_3	ACN	N/A
2	**3b**	K_2CO_4	DMF	N/A
3	**3b**	NaH	Acetone	
4	**3b**	NaH	ACN	
5	**3b**	NaH	DMF	**Mixture impossible to isolate**
6	**4a**	NaH	Acetone	
7	**4a**	NaH	ACN	
8	**4a**	NaH	DMF	
9	**4b**	NaH	Acetone	
10	**4b**	NaH	ACN	

As we were encountering a problem with ditosylate method, tetraethylene dihalide (**4a-b**) was simultaneously synthesized from the method [48-50] shown in **Scheme 3.5**. The dibromide **4a**, obtained from bromination reaction by using phosphorus tribromide (PBr_3) as brominating agent, and The diiodide **4b**, derived from iodination by using NaI, were both separated as pale yellow oil in excellent yields (92%) and (95%), respectively. Both ^{1}H NMR spectra of compounds **4a** and **4b** are displayed in **Figure 3.2**.

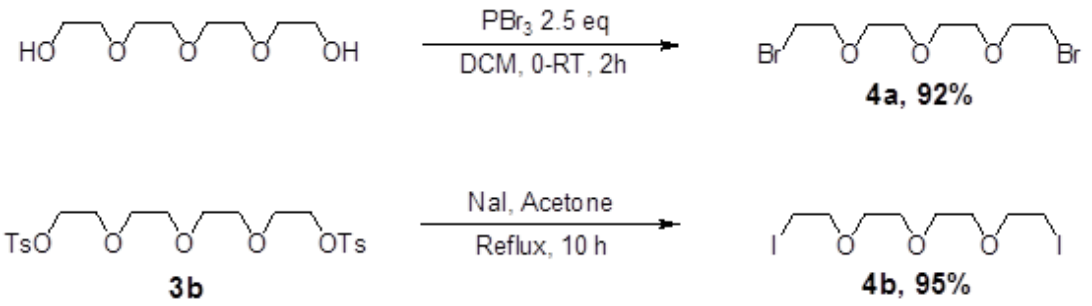

Scheme 3.5 Preparation of tetraethylene glycol dibromide (**4a**) and diiodide (**4b**).

Bromide or iodide atom is known as a less moisture sensitive leaving group than tosylate group. Hopefully, they could be used to optimize this type of coupling reaction and provide the desired product without any by-products for the easier purification.

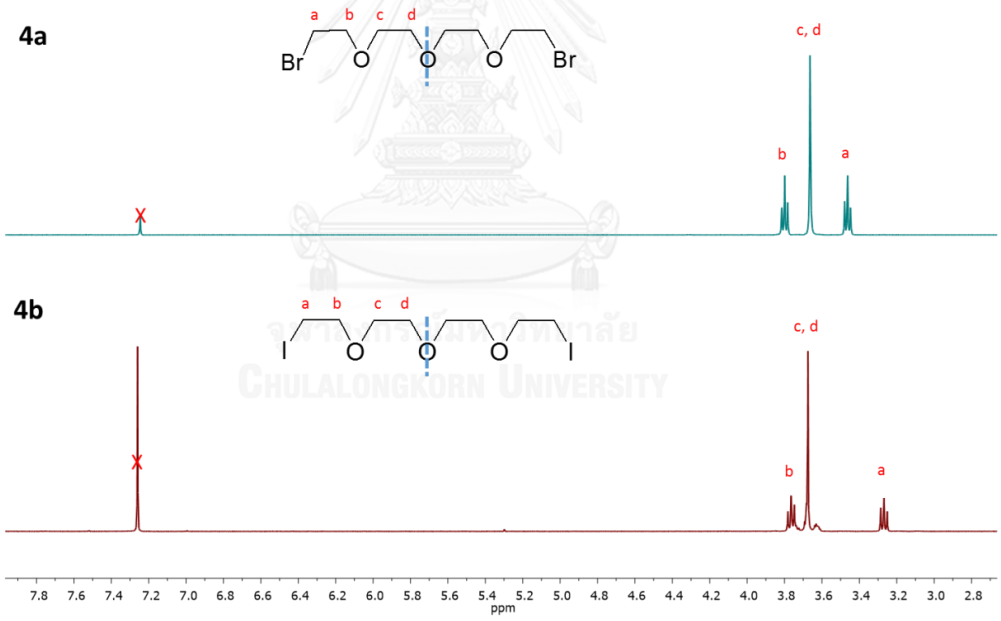

Figure 3.2 ^{1}H NMR spectra (400 MHz) of **4a** and **4b** in $CDCl_3$

4a and **4b** were then used to synthesize bis DHP-OH from coupling reaction with **1a** under the reaction conditions shown in table 3.1 (**Scheme 3.6**). Unfortunately, the results were also unsuccessful because the reaction produced many fluorescent spots in TLC and difficult to separate as same as the earlier reactions.

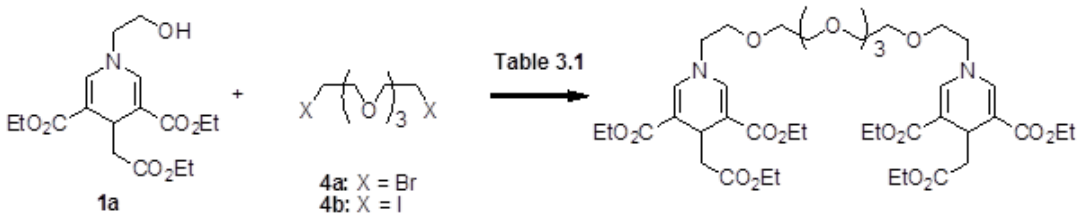

Scheme 3.6 Preparation of bis DHP-OH from dibromide substrate

3.1.2 Synthesis of novel 1,4-dihydropyridine derivatives (1c-d)

Since bis DHP-OH could not be synthesized from **1a**, we then looked for new target DHP derivatives. From recent literatures concerning to the substitution reaction by using the ditosylate substrates, most of them used more acidic phenol as nucleophilic moiety (the example shown in the **Figure 1.17** and **1.18**) [39, 40, 51-54]. Therefore, novel DHP derivatives containing phenolic unit were designed and synthesized from 3-aminophenol (3AP) and 4-aminophenol (4AP) with copper(I) iodide (CuI) as catalyst followed by Sirijindalert's method (**Scheme 3.7**).

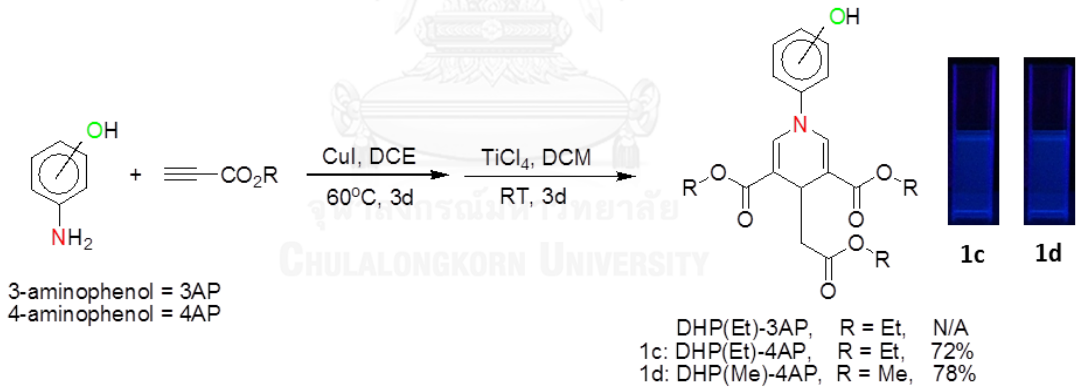

Scheme 3.7 Preparation of novel DHP derivatives (**1c** and **1d**) and their appearances in MeOH under black light

Though DHP(Et) derived from 3AP cannot be isolated or identified, as there are several products shown in TLC, may be due to less reactivity of the starting material, 3AP. DHP(Et) (**1c**) derived from 4AP was purified much easily because of its complete and clean reaction. Compound **1c** was isolated as a yellow oil in good yield (72%) by column chromatography. **1c** exhibits blue color in MeOH media under black light. The reason that reaction of 4AP was better, because probably the para

position of OH-group makes its aniline moiety more nucleophilic hence resulting in the complete cyclotrimerization reaction (**Figure 3.3**). Moreover, methyl propiolate was also used to obtain **1d** in good yield (78%) also as a pale yellow oil. It is expected that the bis DHP structure from **1d** will be formed much easily due to its smaller size.

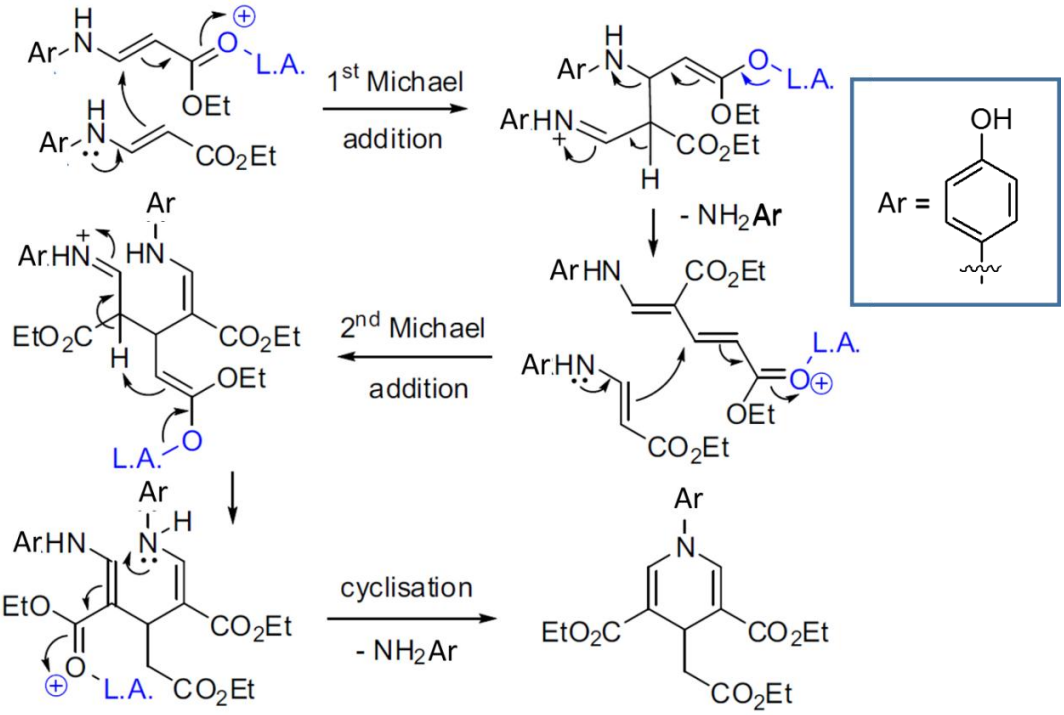

Figure 3.3 Purposed cyclotrimerization mechanism of DHP(Et)-4AP **1c** formation.

According to the ^{1}H NMR spectrum of **1c** in $CDCl_3$ as shown in **Figure 3.4**, a characteristic singlet peak of two alkene protons in DHP ring displayed at around 7.41 ppm and a doublet of methylene proton attached at 4-position of the DHP ring appeared around 2.60 ppm. Other important peaks of the twin aromatic proton peaks are shown at 6.93 and 6.83 corresponding to the proton of 4AP substrate. There are also other peaks such as two types of ethyl ester peaks of 6 protons around 4.23 and 4.06 ppm and 9 protons as triplet peaks at 1.30 and 1.21 ppm, and a methyne proton inserted at about 4.24 ppm. In case of **1d**, ^{1}H NMR spectrum could be interpreted much easily than that of **1c** due to less remaining alkyl ester peaks at 3.74 and 3.60 ppm as two singlet peaks of methyl ester protons.

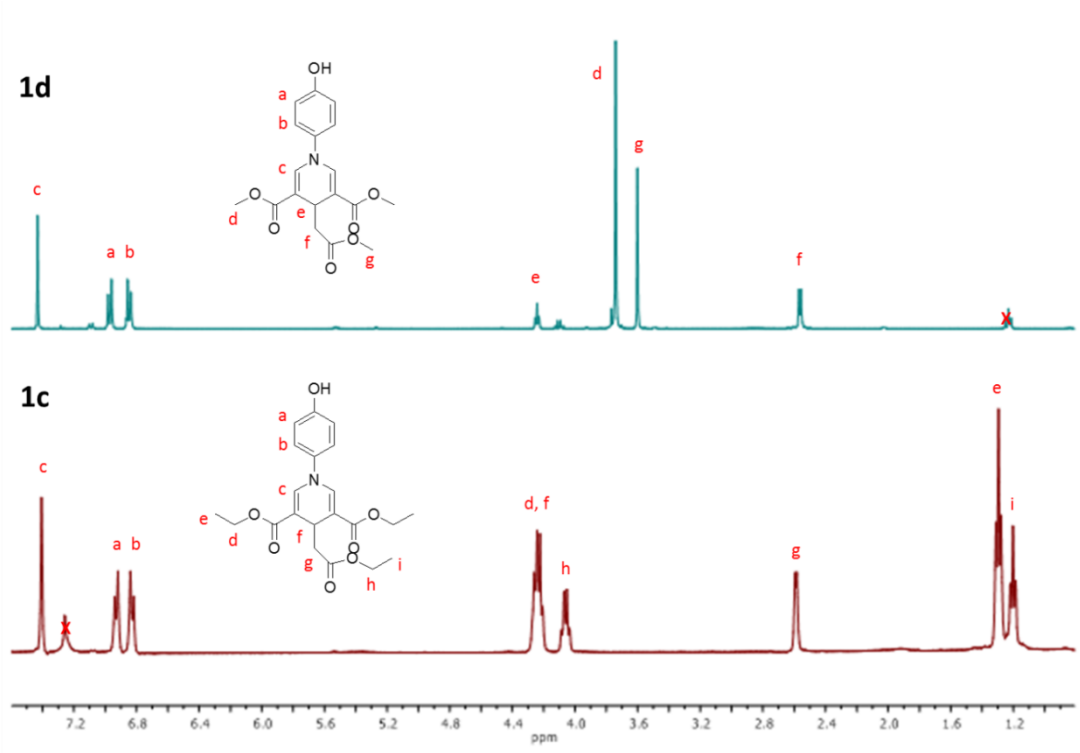

Figure 3.4 ^{1}H NMR spectra (400 MHz) of **1c** and **1d** in $CDCl_3$

3.1.3 Synthesis of bis(1,4-dihydropyridine) derivatives (5a-d) from DHP(Et)-4AP

The synthesis of bis DHP derivatives (**5a-d**) from DHP(Et) (**1c**) were made by S_N2 coupling reaction between **1c** and **3a-d** (**Scheme 3.8**) (conditions: K_2CO_3 as base in ACN solution under nitrogen atmosphere at ambient temperature for 1h) to provide the corresponding product **5a-d** in moderate to excellent yields (41-80 %) as pale yellow oils with blue color in methanol under black light. Percent yields of **5a-d** also depend on the purification step by column chromatography due to the high polarity of the glycol moiety. Longer glycol chains are likely to have lower yield also from the difficult separation step as described. Another effect for bad yield is possibly due to the incomplete S_N2 reaction that formed mono coupling by-product. In the case of **5b**, the percent yield was successfully improved by increasing reaction temperature and time. All compounds were characterized by ^{1}H NMR spectroscopy, ^{13}C NMR spectroscopy and Mass spectroscopy.

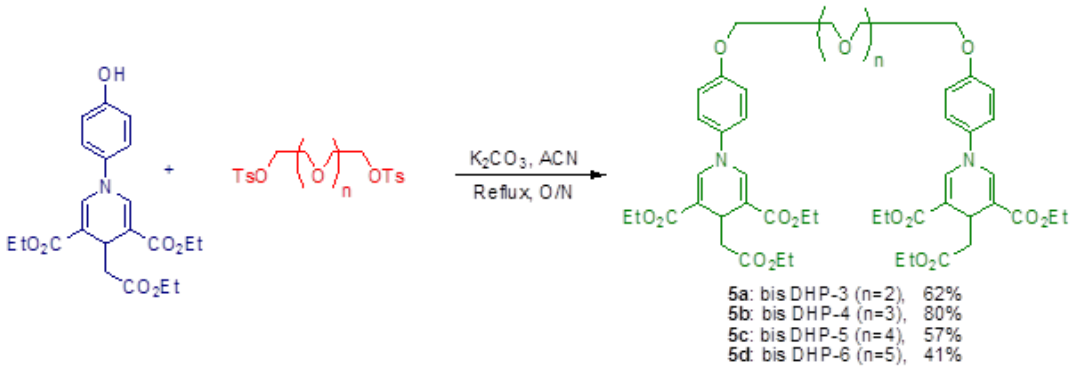

Scheme 3.8 Preparation of bis DHPs (**5a-d**) under mild condition.

For ^{1}H NMR (**Figure 3.5),** the **5a-d** consist of two parts which are DHP moiety and glycol chain. Being symmetrical structures also makes the target molecules to have symmetrical appearances in NMR spectra. All molecules comprise of major characteristic peaks of the DHP ring, singlet peak of two alkene protons in DHP ring appeared around 7.41 ppm, doublet of methylene protons appeared around 2.60 ppm, the twin aromatic two protons at 6.93 and 6.83 ppm as doublet peaks, ethyl ester peaks of 12 protons around 4.23 and 4.06 ppm and 18 protons as triplet peaks at 1.30 and 1.21 ppm and two methylene protons inserted at 4.24 ppm as a triplet peak. There are also methylene protons in triplet appeared around 4.12 and 3.85 ppm and multiplet peaks with the corresponding integration depending on the length of glycol chain appeared around 3.70-3.72 ppm. The integration values are between 2 to 8 for **5a-d**.

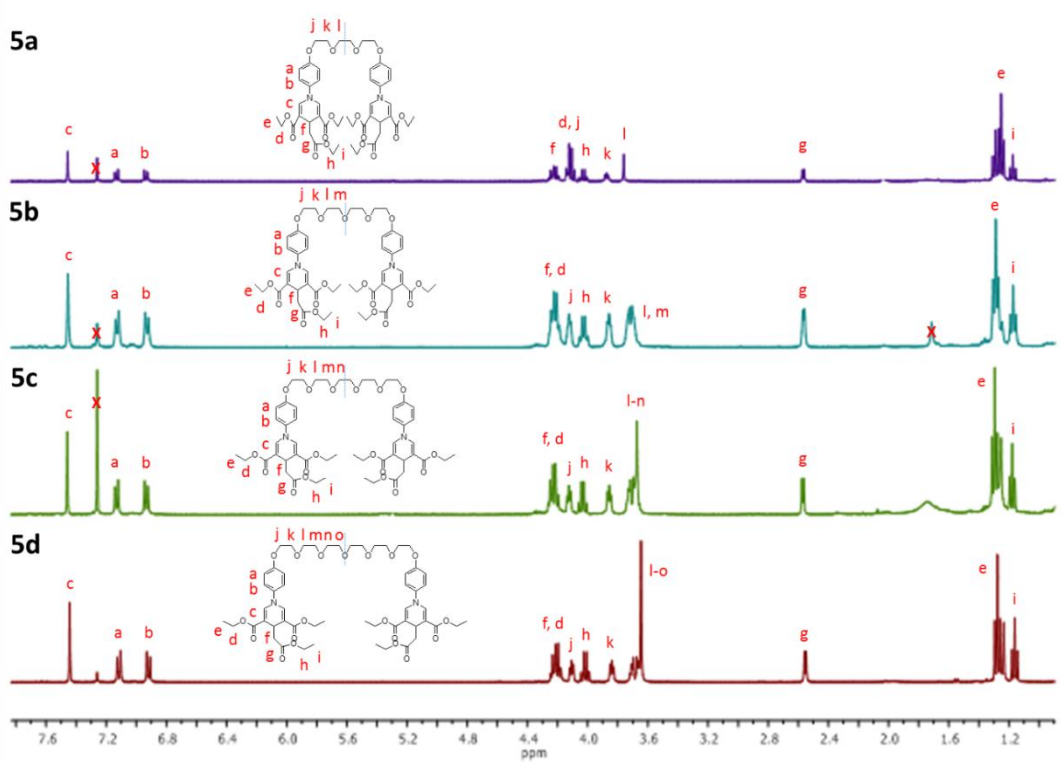

Figure 3.5 ^{1}H NMR stack of bis DHPs (**5a-d**) in $CDCl_3$

3.1.4 Synthesis of mono(1,4-dihydropyridine) derivatives from DHP(Me) (6c, 7, 8)

Initially, the researchers intended to synthesize **5a-d** for the study of allosteric property. According to the concept, glycol chain not only enhances the solubility in water but also improves its ability to bind with metal ion such as alkali and alkaline earth. However, the binding experiment found no selectivity at all (It will be described in more details in the section 3.3 and 3.4). It is considered that since the terminal DHP moieties are too large, it is impossible for such big molecules to form the pseudo crown conformation. For this reason, we have solved the problem by switching the target molecule to mono DHP instead of the bis DHP. The molecule has a free end that might be easy to bind with the target compound. Therefore, new mono DHPs were synthesized (**6c**, **7** and **8**) to compare the sensing properties with those of the bis DHPs (**Scheme 3.9**).

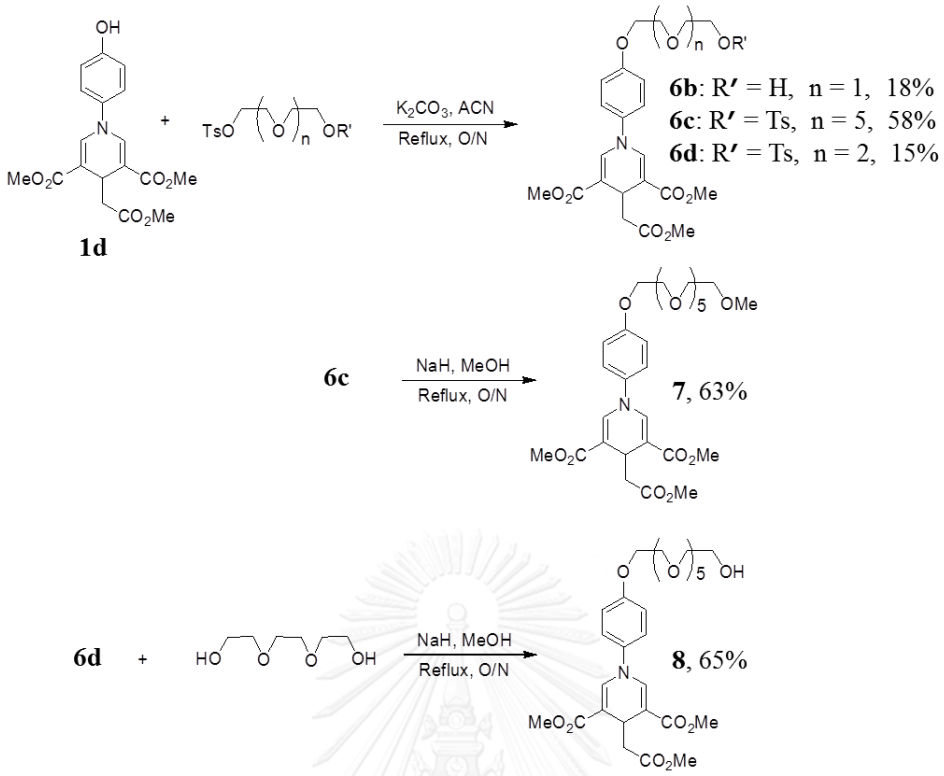

Scheme 3.9 Synthesis of mono DHP derivatives (**6c**, **7** and **8**)

Compound **6b** was synthesized by coupling **1d** with diethylene glycol mono tosylate under mild condition in 18% yield. The target molecule **7** was also synthesized under mild condition from **1d** and hexaethylene glycol ditosylate (**3d**) to gain **6c**, followed by the reaction using NaH as base in MeOH to achieve the corresponding **7** in moderate yield (63%). For the synthesis of compound **8**, the reaction started by coupling reaction of **1d** and triethylene glycol ditosylate (**3a**) to obtain **6d** and then **6d** was reacted with triethylene glycol to gain **8** in good yield (65%). All compounds, obtained in poor to moderate yield as yellow oil, emit blue color under blacklight in MeOH. These compounds were characterized by ^{1}H NMR spectroscopy, ^{13}C NMR spectroscopy and Mass spectroscopy. ^{1}H NMR spectra in **Figure 3.6** showed the same characteristic peaks at 7.47 and 2.56 ppm from DHP moiety. The methoxy-end of **7** appears at 3.37 ppm.

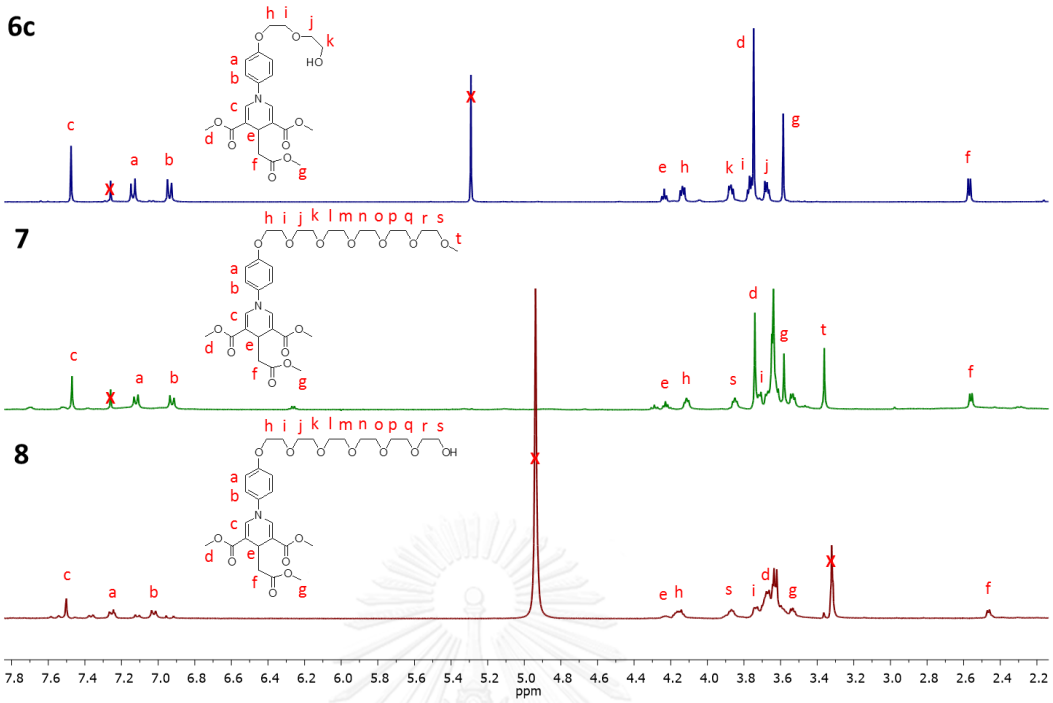

Figure 3.6 ^{1}H NMR stack of mono DHP (**6c**, **7** and **8**) in $CDCl_3$

These compounds have a huge problem in extraction and purification because they are relatively soluble in water and this high polarity makes the separation by column chromatography extremely difficult resulting in low yields.

3.2 Photophysical properties

3.2.1 Photophysical properties

Photophysical properties of all target molecules were studied at concentration of 50 μM in MeOH. By possessing the identical fluorofhore, all compounds illustrated the similar absorption (360–368 nm) and emission (454-466 nm) peaks. The maximum absorption (λ_{ab}) of all compounds were recorded by UV-vis spectrometer in range of 200-500 nm. Most absorption maxima were observed at about 360-368 nm corresponding to the characteristic **π**-**π*** transition of the DHP ring[11, 12, 14]. The molar extinction coefficients (**ε**) of these bands were measured and calculated to be about 6.3 × 10^3 M^{-1} cm^{-1} and 5.9 × 10^3 M^{-1} cm^{-1} for DHP(Et)-4AP (**1c**) and mono DHP-6-OMe (**7**), respectively. And these data for bis DHPs (**5b**-**d**) are

the range of $1.6 \times 10^4 - 1.5 \times 10^4$ M^{-1} cm^{-1}. Moreover, we also found peaks at 274 nm that is *N*-substituted aryl moiety of DHP. All absorption parameters were summarized in **Table 3.2**. Interestingly, **ε** of most bis DHPs are approximately twice higher than that of DHP-4AP because of the increasing number of DHP unit.

Table 3.2 Photophysical properties of all compounds in MeOH.

Compounds	Absorption		Emission	
	λ_{ab} (nm)	ε (M^{-1} cm^{-1})	λ_{em} (nm)	Φ_f^{α}
DHP(Et)-4AP	368	6,292	466	0.69
DHP(Me)-4AP	368	-	462	-
bis DHP-3	364	-	454	-
bis DHP-4	365	15,965	454	-
bis DHP-5	366	14,832	454	-
bis DHP-6	366	14,784	454	0.74
mono DHP-2-OH	364	-	454	-
mono DHP-6-OMe	360	5,894	454	0.32

$^{\alpha}$ Quinine sulfate in 0.1 M H_2SO_4 (Φ_f = 0.54) was the reference.

The maximum emissions (λ_{em}) of all compounds were recorded by Fluorescent spectrometer in range of 380-680 nm (λ_{ex} = 366). The emission maxima were observed at 466 and 462 nm for **1c** and **1d**, respectively. These data for bis DHPs (**5b-d**) and mono sub compounds (**7** and **8**) are 454 nm. The data showed that the structure containing the maximum emission of glycol chain blue shifted around 8-12 nm. The fluorescence quantum efficiencies (Φ_f) were investigated for only 3 target molecules which have different structures (**1c**, **5d** and **7**) (**Table 3.2**). Mono-sub compound was found to have the lowest Φ_f (0.32) in MeOH when compare to its values of **1c** and **5d** (0.69 and 0.74, respectively).

3.3.2 Solvent effect

From the **Table 3.3**, the solvent polarity does not affect significantly to the measured absorption data. Unlike the results from the absorption experiments, the emission maxima of these three substances were red shifted in aqueous solvent around 9-15 nm. The fluorescence quantum efficiencies (Φ_f) in milliQ water for **1c** and **5d** are 0.08 and 0.09, respectively. This huge difference between the quantum yields in H_2O and MeOH probably comes from two possible reasons; better solubility in MeOH and the stabilization of DHP excited state in more polar H_2O. Hence, the less stabilized excited state in organic solvent can lead to a much better fluorescent emission which in turn gives the higher quantum efficiency. Interestingly, compound **7** showed Φ_f at around 0.32 in aqueous solution because its water solubility was better than those of the other two DHP derivatives.

Table 3.3 Comperative photophysical properties of **1c**, **5d** and **7** in milliQ water and MeOH

Compounds	Solvents	Absorption		Emission	
		λ_{ab} (nm)	ε (M^{-1} cm^{-1})	λ_{em} (nm)	Φ_f^{α}
DHP(Et)-4AP (1c)	MeOH	368	6.3×10^3	466	0.69
	H_2O	368	6.3×10^3	475	0.08
bis DHP-6 (5d)	MeOH	366	1.5×10^4	454	0.74
	H_2O	366	1.5×10^4	469	0.09
mono DHP-6-OMe (7)	MeOH	360	5.9×10^3	454	0.30
	H_2O	365	2.0×10^3	465	0.32

$^{\alpha}$ Quinine sulfate in 0.1 M H_2SO_4 (Φ_f = 0.54) was the reference.

3.3 Metal ion sensor

3.3.1 Metal selectivity of all target molecules in organic and aqueous systems

Metal selectivity of all target molecules (**1c**, **1d**, **5a-d**, **6c**, **7**, **8**) were studied over standard set of 24 metal ions (Li^{+}, Na^{+}, K^{+}, Mg^{2+}, Ca^{2+}, Sr^{2+}, Ba^{2+}, Pb^{2+}, Al^{3+}, Ga^{3+}, Bi^{3+} Ag^{+}, Hg^{+}, Mn^{2}, Fe^{2+}, Co^{2+}, Ni^{2+}, Cu^{2+}, Zn^{2+}, Cd^{2+}, Hg^{2+}, Cr^{3+}, Fe^{3+} and Au^{3+}) at the concentration of sensor:ion = 1:100 μM in organic (95% MeOH/H_2O) and aqueous (0.5% MeOH/H_2O) media. All experiments were excited at λ_{max} = 366 nm and detected in range of 380-680 nm after 30 minutes for reaction mode. The trials showed that all compounds only selected to be quenched by gold(III) ion (Au^{3+}) in aqueous conditions while these in organic solvent did not show any metal selectivity. The representatives of metal selectivity are shown in **Figure 3.7** and **3.8**.

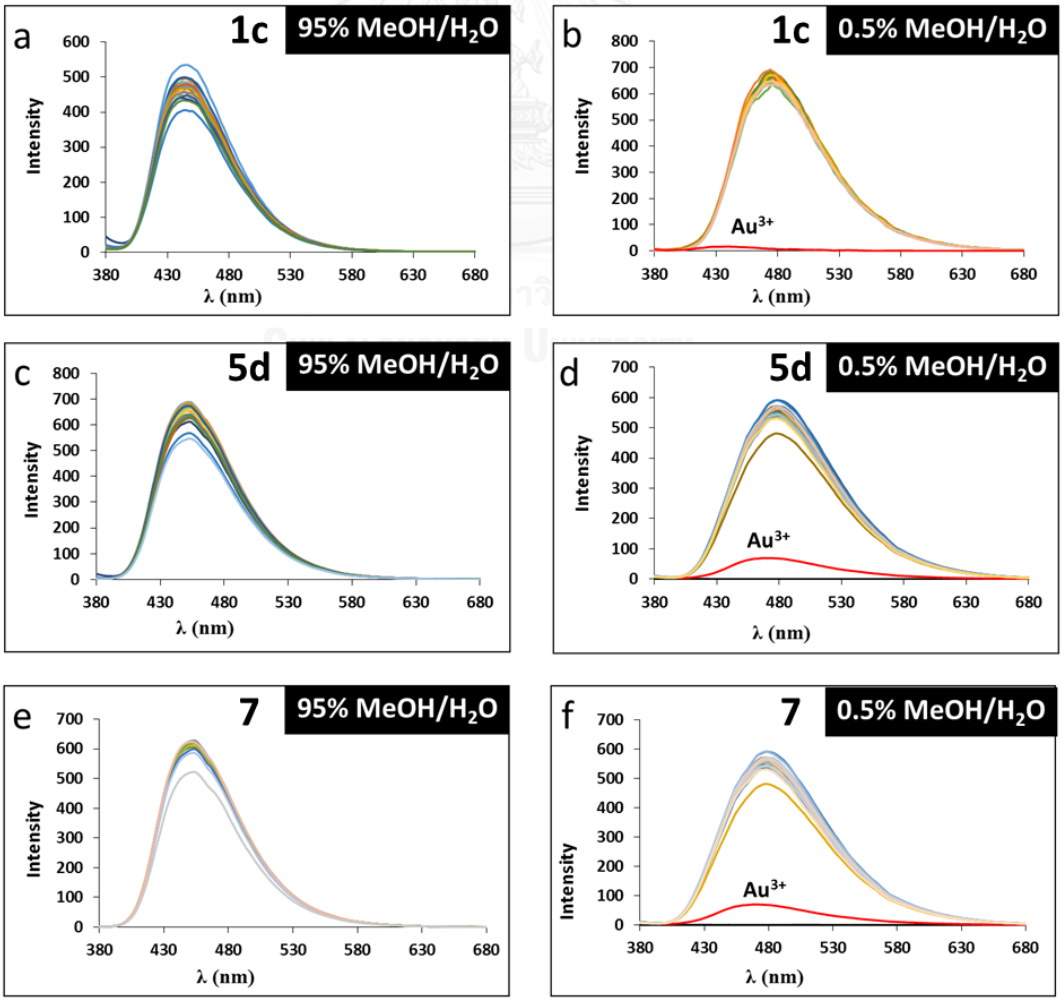

Figure 3.7 Metal selectivity of 3 representative molecules (1 μM): **1c**, **5d** and **7** toward standard set of metal ions (100 μM) in 2 different solvent systems (95% MeOH/H_2O and 0.5% MeOH/H_2O).

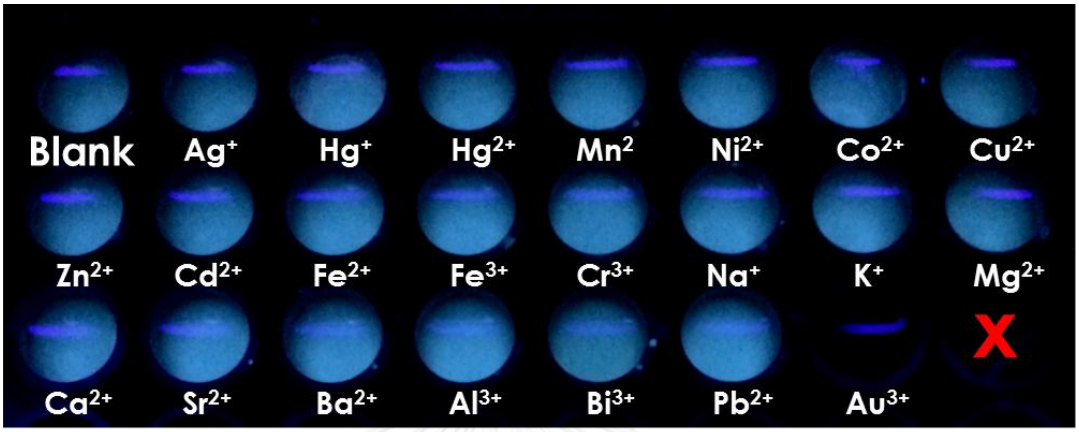

Figure 3.8 Metal selectivity in well-plate of **5d** (10 μM) over 22 types of metal ions (100 μM) in aqueous solution under black light.

3.3.2 Time-dependent quenching of all fluorescent sensors in aqueous system

The time-dependent quenching experiments between DHP derivative sensors (**1c**, **5b**, **5c**, **5d** and **7**) and Au^{3+} were investigated at the concentration of sensor:Au^{3+} = 1:100 μM in aqueous solution and detected every 5 minutes for 12 times (**Figure 3.9**). The results revealed that all compounds reacted with Au^{3+} readily in the first 30 minutes and then the fluorescent intensity decreased gradually until the reaction completed.

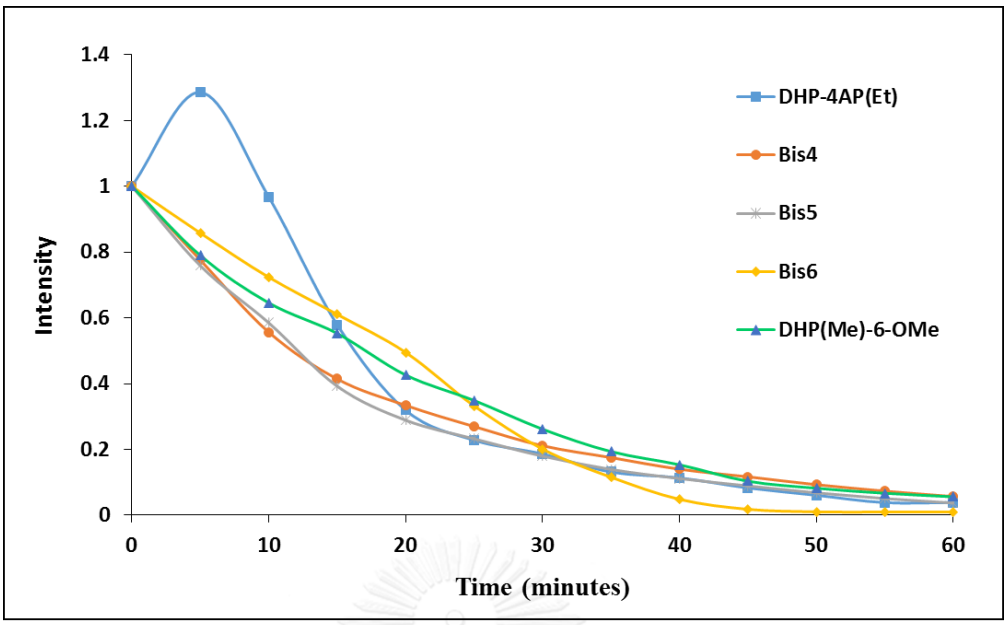

Figure 3.9 Time-dependent reaction between 1 μM sensors and 100 μM Au^{3+} in aqueous solution for 60 minutes.

The fluorescent change of DHP(Et)-4AP (**1c**) is different from those of other sensors. **Figure 3.10** illustrated the comparative fluorescent behavior between **1c** and **5d**. In case of **1c**, the fluorescent signal was enhanced in the first 10 minutes and then quenched continuously over 20 minutes-time by 30-40 nm blue-shift. Unlike **1c**, compound **5d** quenched the fluorescent signal from the beginning without any signal shift. Such fluorescent changes could not be explained explicitly. However, the glycol chain in molecule obviously plays an important role to affect the reaction with Au^{3+} the different manner.

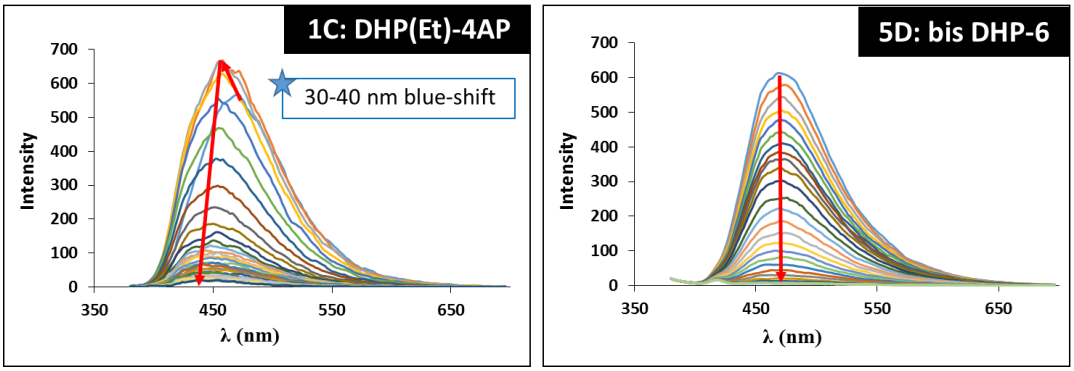

Figure 3.10 Comparison of time-dependent fluorescent behavior between **1c** and **5d** (1 μM) over Au^{3+} (100 μM) in aqueous solution.

In theory, compound containing **π**-bond conjugation would have lower energy gap according to increase conjugated **π**-bond. If this conjugated molecule was disturbed, its energy band gab would be changed. For **1c**, the electron density in DHP ring would be withdrawn by Au^{3+} binding to the phenolic moiety. This decreasing electron density affected to **π**-electron inside the conjugation and its band gap then was increased to higher wavelength (blue-shift) during the fluorescent quenching.

3.3.3 Time-dependent quenching of DHP(Et)-4AP (1c) in aqueous system by UV-vis spectrometry technique

Once more information to confirm the quenching mechanism is time-dependent absorption signal change detected by UV-vis spectrometer. Because all quenching behaviors were similar, the fluorophore **1c** was chosen for the quenching mode study with Au^{3+}. This experiment was examined at the concentration of **1c**:Au^{3+} = 50:500 μM in aqueous solution and detected every 5 minutes for 8 times (**Figure 3.11**). The absorption peak of **1c** (λ_{max} = 377 nm) was progressively decreased upon addition of Au^{3+}, which was accompanied with a new band at about 355 nm (22 nm blue-shift) confirming the possibility of structural change in the DHP ring. This hypsochromic shift is probably caused by the aromatization of the DHP ring to a pyridine ring, as the new band appears in the same area as the characteristic band of a pyridinium ring (around 325-342 nm) [55-57].

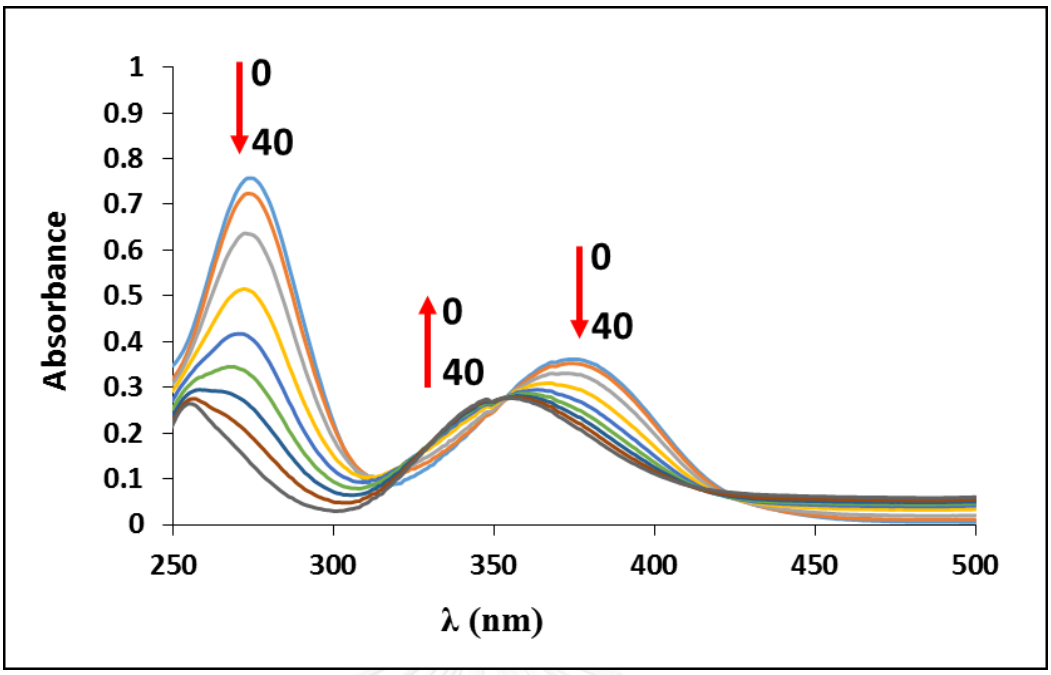

Figure 3.11 Time-dependent absorption of **1c** (10 μM) with Au^{3+} (100 μM) in aqueous solution for 40 minutes.

3.3.4 Effect of aqueous media in Au^{3+} sensing

From previous experiments, the metal sensing were studied in both MeOH and H_2O which most fluorophores selected with Au^{3+} in only aqueous condition. For more information, we studied effect of mixed solvent between MeOH, ACN and THF with MillQ water in various ratios to explore the quenching mechanism of this reaction. Bis DHP-4 (**5b**) was chosen to represent all substances. All solvent ratios were investigated at the concentration of **5b**:Au^{3+} = 1:100 μM and detected after 30 minutes (**Figure 3.12**). From this figure, the proportion of water in the mixed solvent has a direct effect on the reaction referring to the (I_0/I)-1 value (I_0 = intensity at λ_{max} of **5b** and I = intensity at λ_{max} of **5b** with Au^{3+}). In other words, the reaction better occurs when the water ratio is higher. Conclusively, 100% aqueous solution is an ideal condition for the investigation of Au^{3+} sensing properties of DHP derivative sensors.

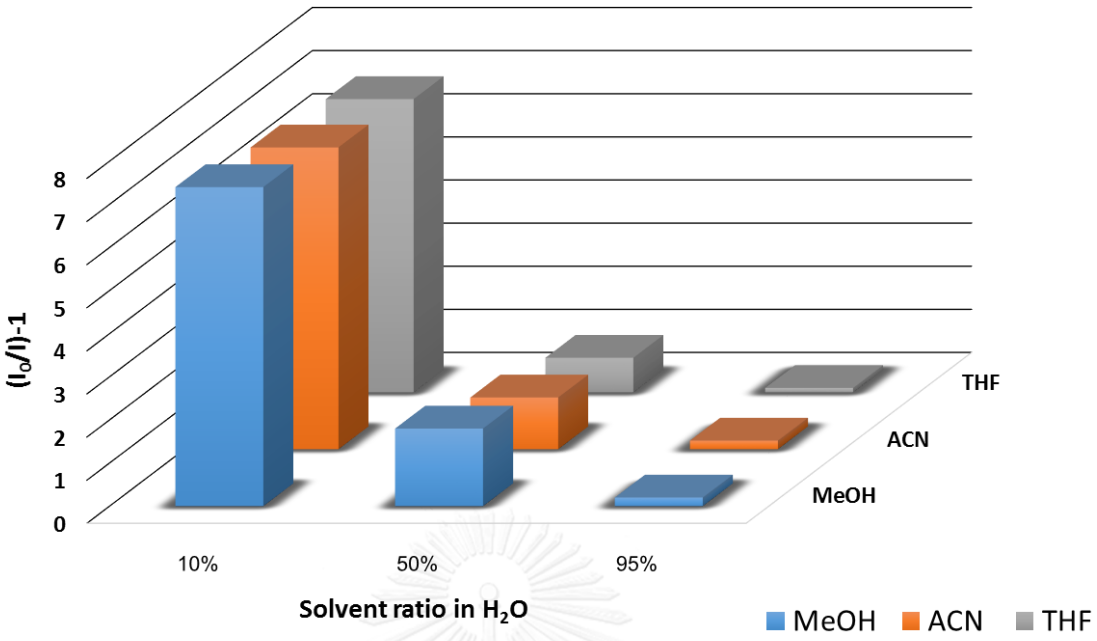

Figure 3.12 Solvent effect for quenching reaction of **5b** (1 μM) with Au^{3+} (100 μM).

3.3.5 Fluorescent titration of bis DHP-6 toward Au^{3+} (Stern-Volmer plot)

The fluorescent titration of 1μM bis DHP-6 (**5d**) in aqueous solution toward Au^{3+} ion was carried out at excitation wavelength of 366 nm and detected after 15 minutes. Upon addition of increasing amounts of Au^{3+} (1 μM to 100 μM) to the solution of **5d** in aqueous media, the quenching fluorescent signal increased with Au^{3+} concentration (**Figure 3.13**). The long time of gold-induced fluorescent quenching of **5d** was probably from the structure change via oxidation reaction in DHP moiety.

The fluorescent quenching efficiency can be represented with the Stern-Volmer constant (K_{SV}) according to the following equation:

$$\frac{I_0}{I} - 1 = K_{SV}[analyte]$$

A linear plot (inset of **Figure 3.13**) gave the K_{SV} of 0.0163 μM^{-1} with the limit of detection (LOD) of 2.65 μM Au^{3+} (522 ppb).

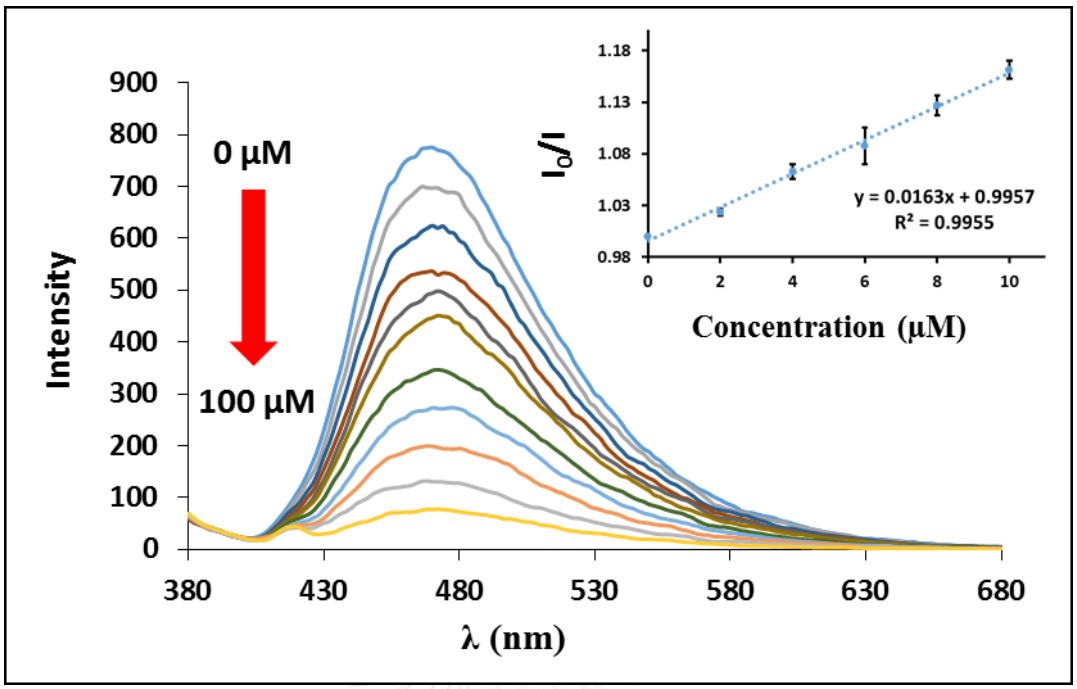

Figure 3.13 Fluorescent quenching responses of **5d** (1 µM) with the addition of Au^{3+} (0 to 100 µM.) in aqueous solution. The inset at the top right shows the Stern-Volmer plot in the Au^{3+} concentration of 0-10 µM.

3.3.6 Competitive experiment over other metal ions

In order to further evaluate the selectivity of DHP sensors for Au^{3+} detection, competitive experiments were studied over other metal cations. The fluorescent response of **5d** to Au^{3+} in milliQ water in the presence of 100 equiv. of various cations was presented in **Figure 3.14**. The interference can be determined in bar diagram from plotting of $(I_0-I_X)/(I_0-I_{Au})$ and types of competing metal ions. Where I_0 = maximum fluorescent intensity of **5d** without metal ion, I_X = maximum fluorescent intensity of **5d** with Au^{3+} and another metal ion, I_{Au} = maximum fluorescent intensity of **5d** with Au^{3+}. Therefore, without the interference from other metal ions, the value for y axis is equal to 1. The fluorescent response of **5d** with Au^{3+} were slightly affected in the presence of Mn^{2+}, Na^{+} and Cr^{3+}, probably influenced by the disturbance to the oxidation reaction with Au^{3+} from these three ions.

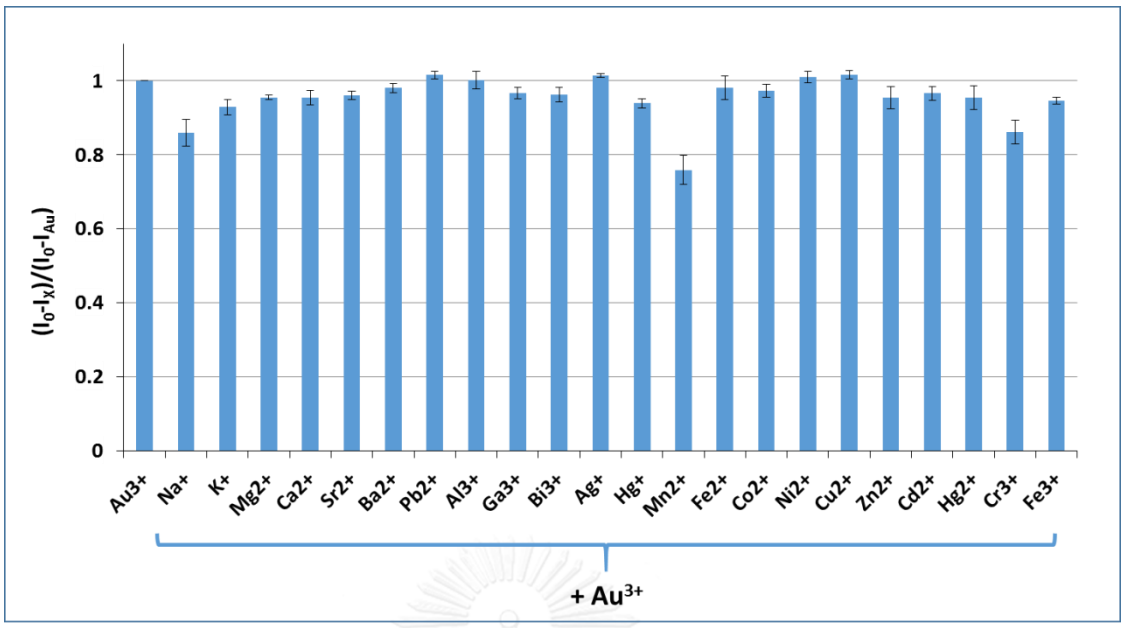

Figure 3.14 Competitive experiment in the **5d**·Au^{3+} system with interfering metal ions. [**5d**] = 1 μM, [Au^{3+}] = 100 μM and [M^{n+}] = 100 μM in aqueous solution.

The result of **7** was also investigated as same as the above experiment which some metal ions (Cu^{2+}, Mg^{2+}, Fe^{3+} and Cr^{3+}) could slightly interfere the Au^{3+}-induced quenching response of **7** (**Figure 3.15**)

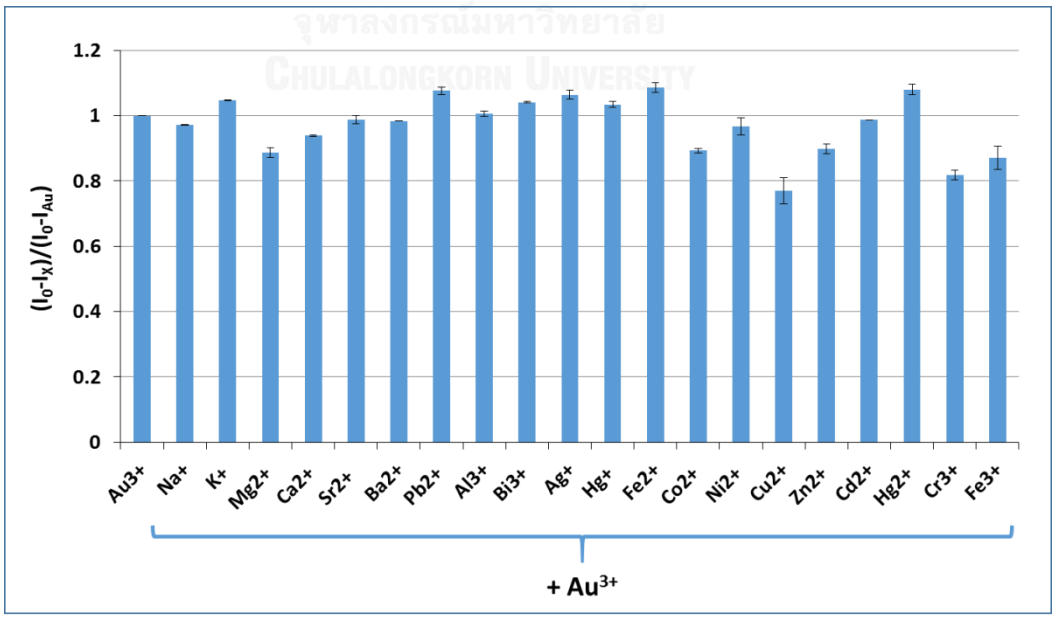

Figure 3.15 Competitive experiment in the **7**·Au^{3+} system with interfering metal ions. [**7**] = 1 μM, [Au^{3+}] = 100 μM and [M^{n+}] = 100 μM in aqueous solution.

3.3.7 ^{1}H NMR experiments for study the sensing mechanism of bis DHP-6 against Au^{3+}

^{1}H NMR experiment was conducted to seek more evidence to support the reaction mechanism between DHP probe and Au^{3+} by oxidative reaction of pyridine ring converted to pyridinium ring. Due to the less solubility of DHP in D_2O and this requirement of this interaction under aqueous media, we hence mocked the experiment followed by the fluorescent condition of DHP over metal ions ([DHP]:[M^{+}] = 1:100 μM in ≈ 95.5% milliQ/MeOH) for excess reaction time.

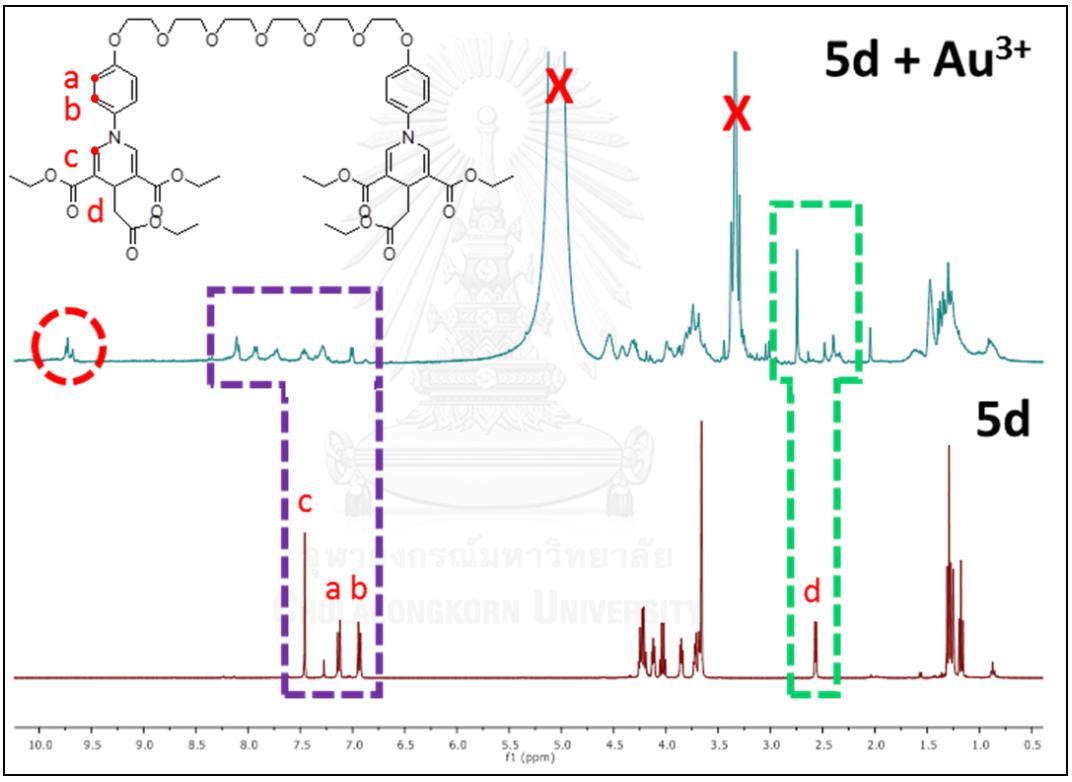

Figure 3.16 ^{1}H NMR experiments of **5d** against Au^{3+}

From the ^{1}H NMR spectra of **5d** below (**Figure 3.16**), there were many peaks of new possible substances appeared in range of 8.5–10.0 ppm. We assumed that these ones were not peak of previous DHP because of its complete reaction. There were the significant change of olefinic protons, especially in the peak around 9.5-10.0 ppm which confirmed the existence of methine proton in pyridinium ring, converted

from former dihydropyridine ring. These results were consistent with antecedent reports which proposed all possible products from oxidation reaction of DHP derivative (product 1) and its continuous reaction such as hydrolysis, second oxidation and protonation-induced rearomatization (product 2, 3 and 4, respectively) (**Figure 3.17**) [20].

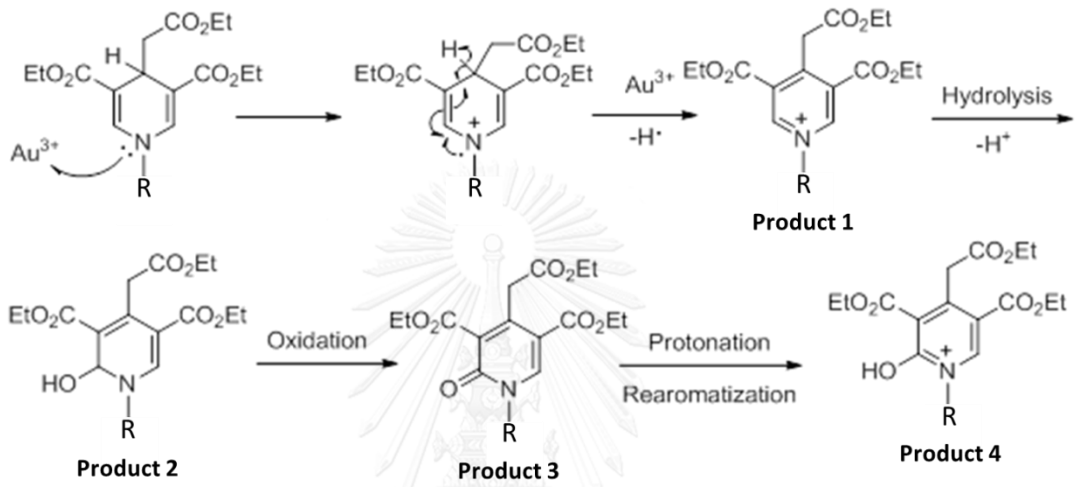

Figure 3.17 Proposed mechanism of Au^{3+} ion-induced oxidation reaction for 1,4-dihydropyridine derivative.

Moreover, doublet peak of methylene at 2.5 ppm had disappeared but there were new singlet peaks occur around 2.0-3.0 ppm which also supported the fact that DHP ring was truly oxidized by Au^{3+}. Mechanism of Au^{3+} ion-induced oxidation reaction of **5d** was demonstrated in **Figure 3.18**.

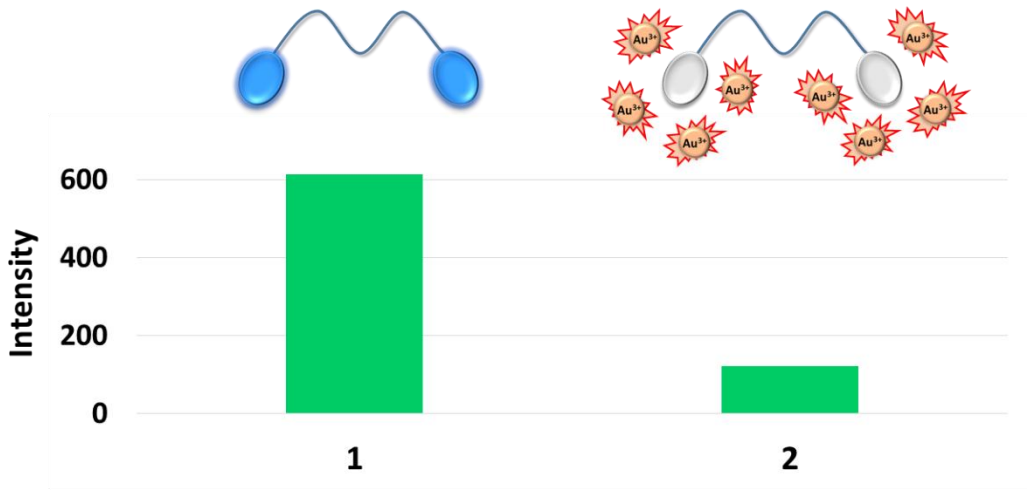

Figure 3.18 Sensing behavior of **5d** against Au^{3+} in aqueous solution.

3.4 Allosteric experiment

The key of this study is to synthesize compounds containing two receptor units in molecule, in which the binding to substances in the first receptor can result in the property change in the binding with analyte in the second one. This work, we have synthesized bis DHP derivatives (**5a**-**d**) having DHP moiety and glycol chain as the receptor unit. In theory, polyethylene glycol can arrange itself to be pseudo crown in organic media, which can potentially bind with alkali and alkaline earth metal [22, 51, 58, 59] (**Figure 3.19**). However, the previous selectivity studies do not show the selectivity against metal ions in various organic conditions (ACN, THF, MeOH, DMSO and $CHCl_3$). Moreover, even if the pseudo crown was formed but no effect was observed, allosteric experiment by sequence addition of target analyte (alkali and alkaline earth metal) followed by anionic species might be worth trying.

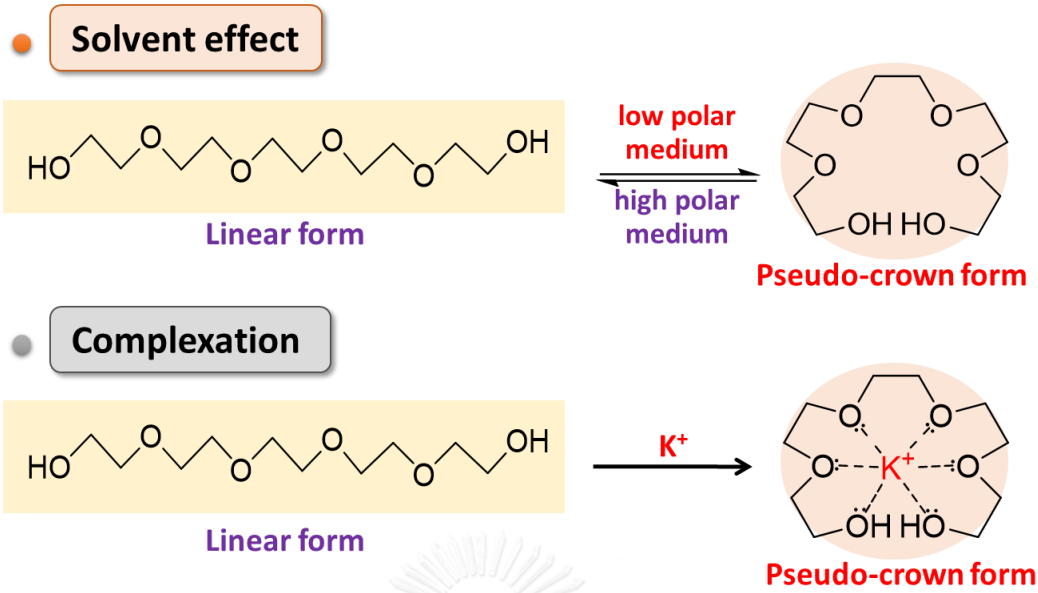

Figure 3.19 Pseudo crown formation of pentaethylene glycol.

5d and **7** were the candidate sensors for additional allosteric study. At the beginning, target effector (Li^+, Na^+ or K^+) was added into the mixture of sensor and the fluorescent signal was detected as initiative signal. It was compared with signal derived from the solution of sensor containing effector and analyte (17 anions and 16 cations). Schematic representation of the experiments was demonstrated in **Figure 3.20**. The mixture sample was prepared in well-plate at concentration of sensor:effector:analyte = 1:100:100 μM in 95.5% ACN/H_2O. Analyte was filled into the mixture after effector was mixed thoroughly for 5 minutes. The fluorescent responses of the final solution was detected and compared with the signal without analyte.

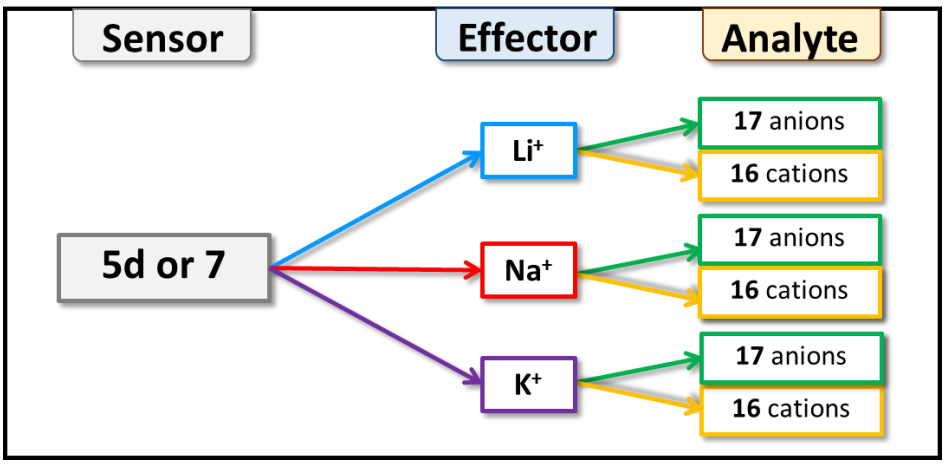

Figure 3.20 Allosteric experiment diagram of **5d** or **7** toward Li^+, Na^+ or K^+ effectors with 16 cation or 17 anion analytes in ACN solution.

These experiments were undertaken in well-plate format, which has the advantage of rapid detection and many samples can be detected at a time by using fluorescent spectrophotometer. Well-plate consists of 8 rows (A-H) and 12 columns of channels which each channel can contain about 300 µL of sample solution (Figure 3.21). The detecting probe of fluorescent spectrophotometer was used to scan the fluorescent response of the fluorescent sensor row by row. Each effector would consume two rows to test one act of analytes. Fluorescent responses of **5d** toward alkali metal ion effector such as Li^+, Na^+ or K^+ were determined. For instance, the data of K^+ mixture were shown in the **Figure 3.22**.

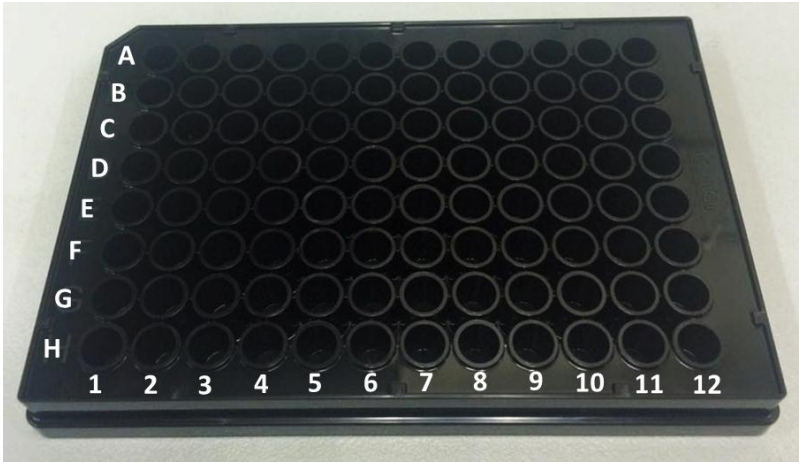

Figure 3.21 Well-plate used in allosteric experiment.

The obtained results were rather varied and had no reproducibility (**Figure 3.22, a** and **b**). Quizzically, this distribution depended on the sequence of measurements as shown in **Figure 3.22**, **c**. In other words, the sample which was detected later gave higher intensity. Therefore, we assumed that ACN solution might be evaporated during the experiment probably by heat of detection to become higher concentration and hence produce the higher fluorescent intensity in the case of later sample. To prove stated assumptions, we executed the backward detection (**Figure 3.22**, **d** and **e**). As expected, the sample containing OH^- as analyte, which formerly had a high intensity, produced lower signal when it was measured as a primal sample (**Figure 3.22**, **f**). This means that obtained fluorescent intensity was not the result from effector or analyte.

Based on the results of allosteric experiments, we concluded that all compounds could not detect in such allosteric characteristics. With the above problems, we therefore looked for new applications to our DHP probes such as surfactant, pH, protein and oxidant sensor.

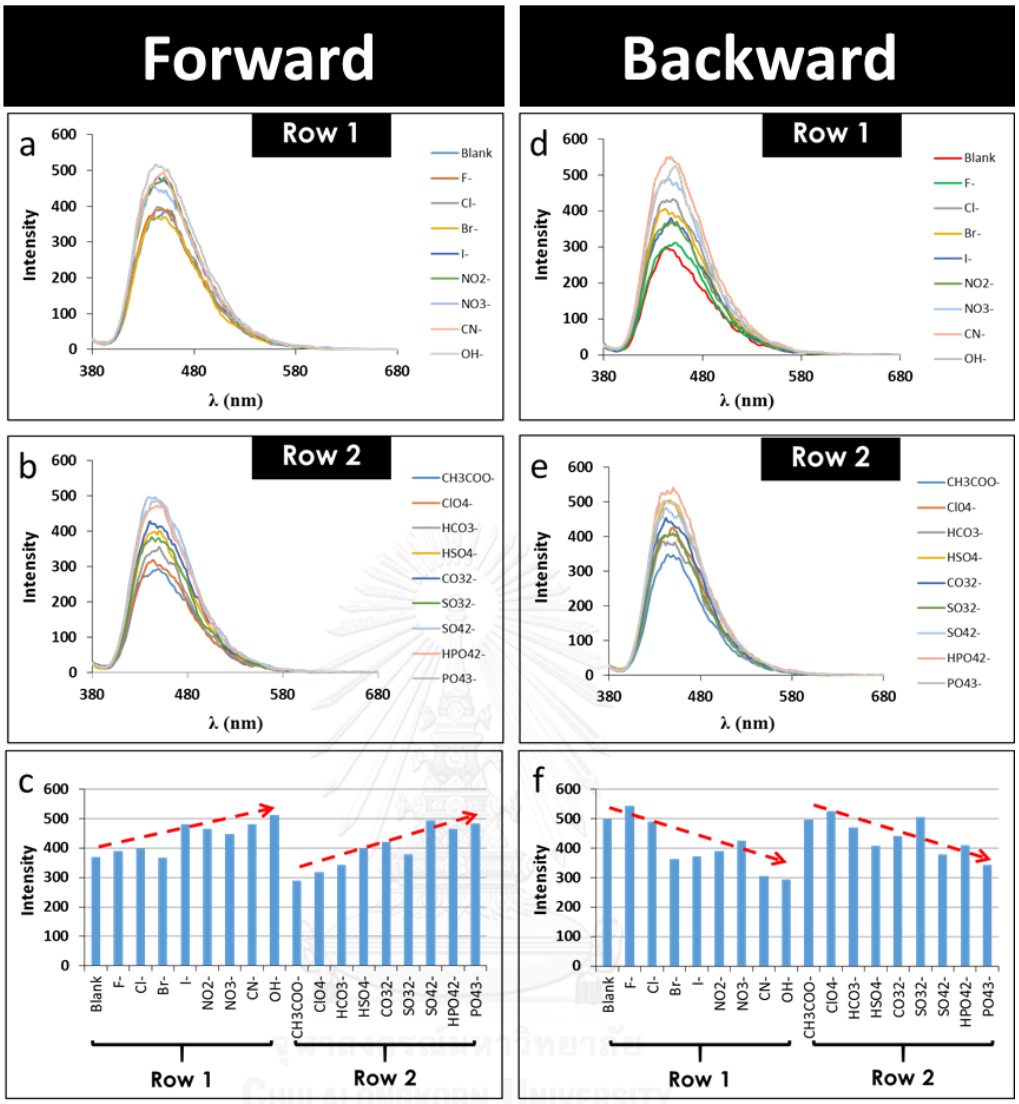

Figure 3.22 Fluorescent responded representation of 1 μM **5d** toward 100 μM K^+ effectors with 100μM of 16 cation analytes in ACN solution (**a**, **b** and **c** for forward detection and **d**, **e** and **f** for backward detection)

3.5 Surfactant experiment

3.5.1 Surfactant selectivity of 3 candidate fluorophores

Several studies have reported that surfactant compound can enhance fluorescent signal that is an additional advantage for the quenching mode of fluorescent chemosensor [60-65]. Therefore, in order to optimize the quenching mode of Au^{3+}-induced reaction, many surfactants were used such as cationic (CTAB, DTAB and TTAB), anionic (SDC, SDS and ALS) and nonionic (Triton X-100 and Tween 20) surfactants. (**Figure 3.23**).

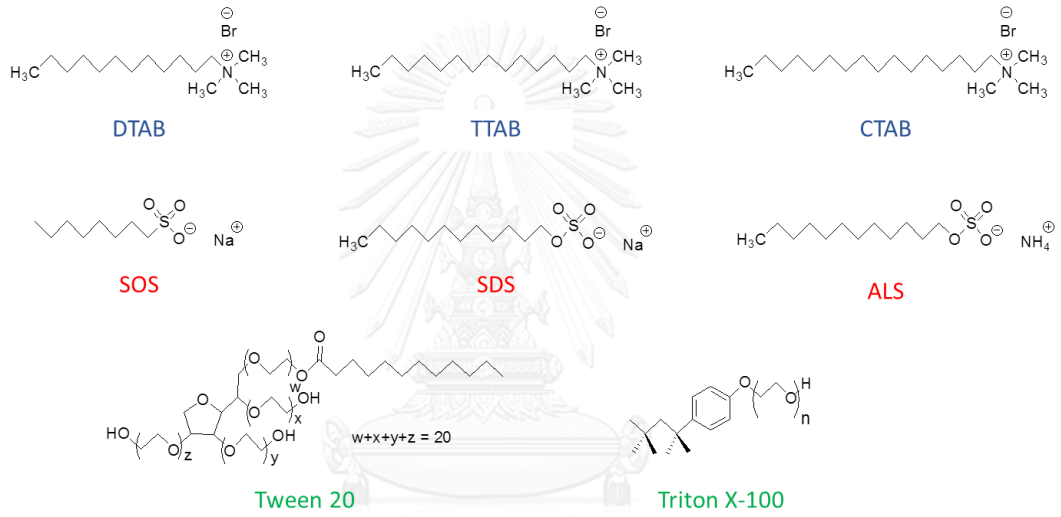

Figure 3.23 Surfactant structure in our experiments.

The fluorescent responses of 3 candidate sensors (**1c**, **5c** and **7**) in the presence of various surfactants (concentration of sensor:surfactant = 1:1000 μM) are shown in **Figure 3.24**. It was found that the initial fluorescent intensity could be enhanced by CTAB and Triton X-100 (TX) for only compound **5c** while **1c** and **7** were not influenced by the addition of these surfactants. It is possible that the signal enhancement may be due to the micellar effect (Critical micelle concentration (CMC) is 220 to 240 μM [66, 67]). Therefore, it is hypothesized that initiative intensity of bis DHP could be enhanced by micellar formation of TX around bis molecule. From this trial, we selected Triton X-100 for further experiments because CTAB has a positive change and might disturb the interaction between sensor and analyte such as anion.

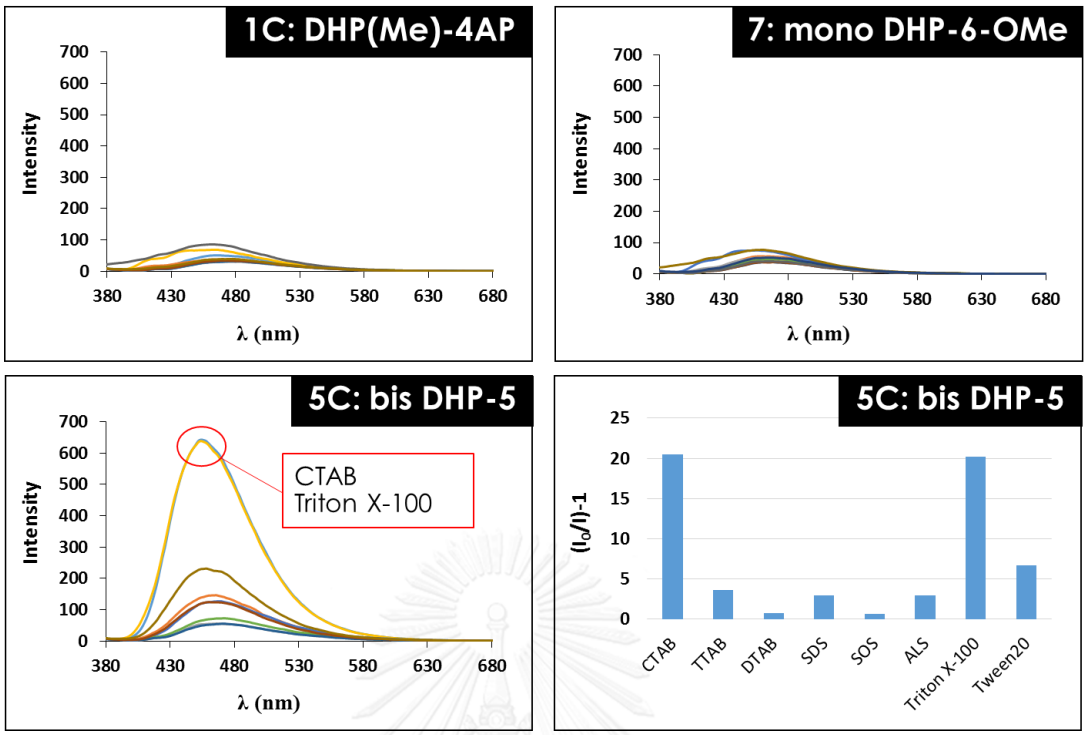

Figure 3.24 Surfactant selectivity of 1 μM DHP sensors (**1c**, **5c** and **7**) toward various 1000 μM surfactants in aqueous system and bar chart showed selectivity of **5c**.

3.5.2 Fluorescent enhancement by Triton X-100 (TX)

From the previous surfactant selectivity test, there was only bis DHP **5c** that increased the signal after addition of TX. All bis DHPs (**5a-d**) were set to be investigated whether their signals can be enhanced by any surfactants. As the results of the experiments shown in **Figure 3.25**, the signal of **5d** bearing longest glycol chain was the most enhanced by the addition of TX around 1.44 times higher than that of **5a**.

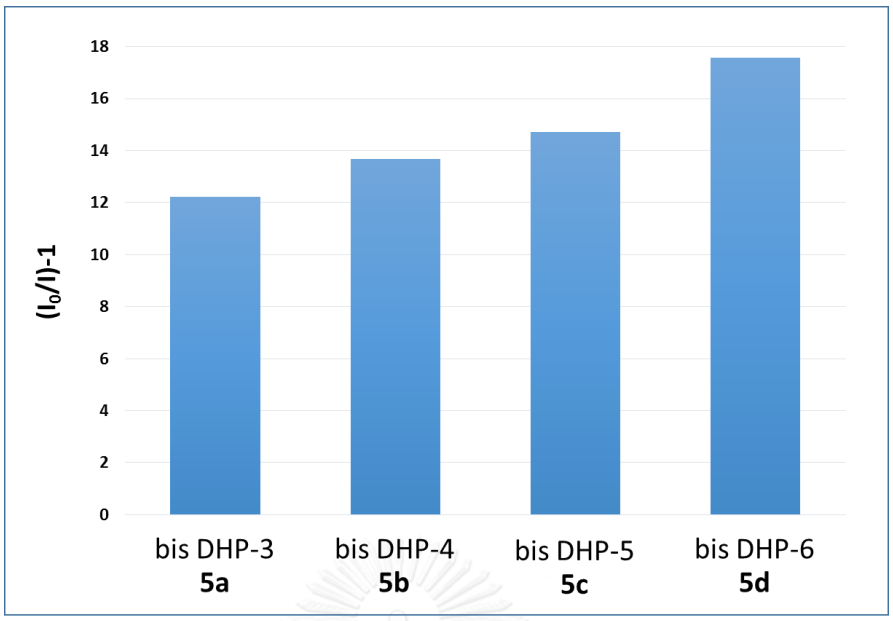

Figure 3.25 Fluorescent enhancement response of **5a-d** (1 μM) toward Triton X-100 (1000 μM) in aqueous solution.

The suitable surfactant concentration in order to study the other properties of **5d** was carried out by varying the concentration of **5d** from 10 μM to 1000 μM (**Figure 3.26**). From bar chart below, the fluorescent intensity was greatly enhanced, when the concentration of TX is greater than 200 μM. That TX concentration was higher than its cmc value thus allowing the stable micellar formatiom, and maintained in the same range of high intensity until 1000 μM. Therefore, the range between the concentrations of 400 – 1000 μM was appropriate for further surfactant experiments.

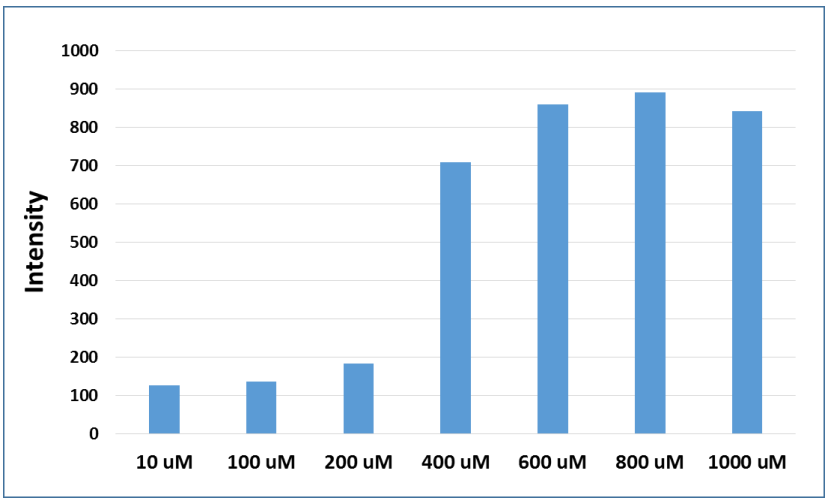

Figure 3.26 Fluorescent enhancement responses of **5d** (1 μM) toward various Triton X-100 concentration (10 - 1000 μM) in aqueous solution.

3.5.3 Metal selectivity

The fact that surfactant assists the lift up of the initial fluorescent intensity of bis DHP sensors (**5a**-**d**) hopefully enable the observation of fluorescent quenching to be much clearly when the probe interacted with target analyte. Based on such assumptions, metal ion selectivity experiments of **5d** (1 μM) toward standard set of metal ions (100 μM) in aqueous mixture with TX (1000 μM) after 30 minutes were undertaken (**Figure 3.27**). Surprisingly, the fluorescent signal when added Fe^{2+} was quenched to about half of the initial signal while addition of Au^{3+} did only slightly quench the fluorescent signal of bis DHP probe in this surfactant system.

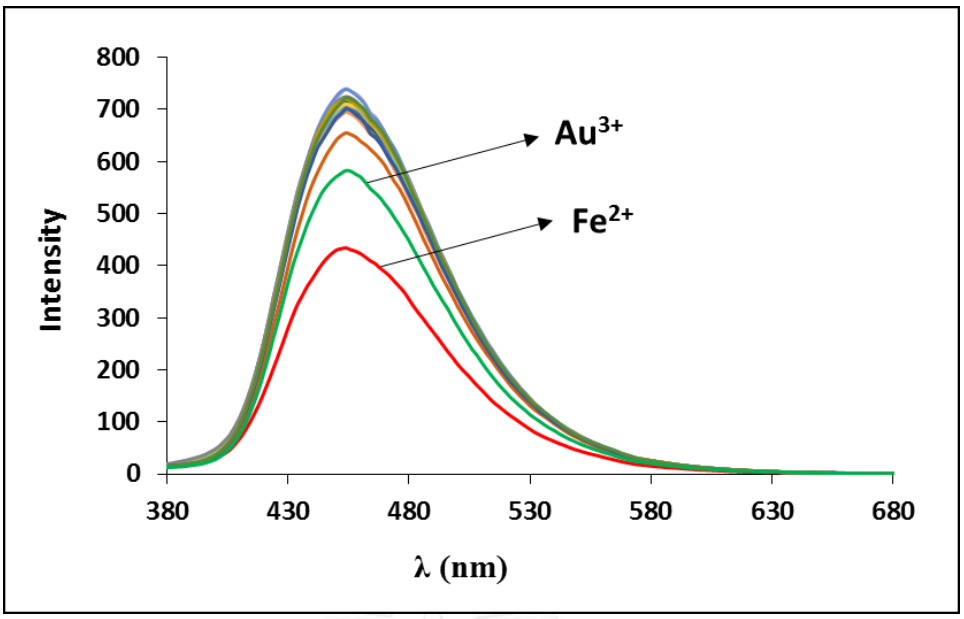

Figure 3.27 Fluorescent response of **5d** (1 μM) toward standard set of metal ions (100 μM) in the solution of triton X-100 (1000 μM).

3.5.4 Time-dependent quenching of Hg^{2+}, Fe^{2+}, Au^{3+}

The time-dependent fluorescent behavior of **5d** (1 μM) toward Hg^{2+}, Fe^{2+} and Au^{3+} cations (100 μM) were investigated in the surfactant-mixed aqueous solution for 30 minutes (**Figure 3.28**). Fluorescent signal unchanged over Hg^{2+} while its signal in the presence of Au^{3+} was enhanced rapidly in the first 5 minutes and then slowly decreased afterwards. In case of Fe^{2+}, the signal was readily quenched in the first 10 minutes and gradually decreased. Therefore, it is still very difficult to conclude that the interaction between Fe^{2+} and bis DHP sensors occurred in reaction mode like its reaction of Au^{3+}. In order to explore the quenching mechanism of this, we intended to study more information such as UV-vis response and time-dependent ^{1}H NMR. This graph illustrates that the reaction time of 10 minutes is the suitable detection time for Fe^{2+} sensing experiment.

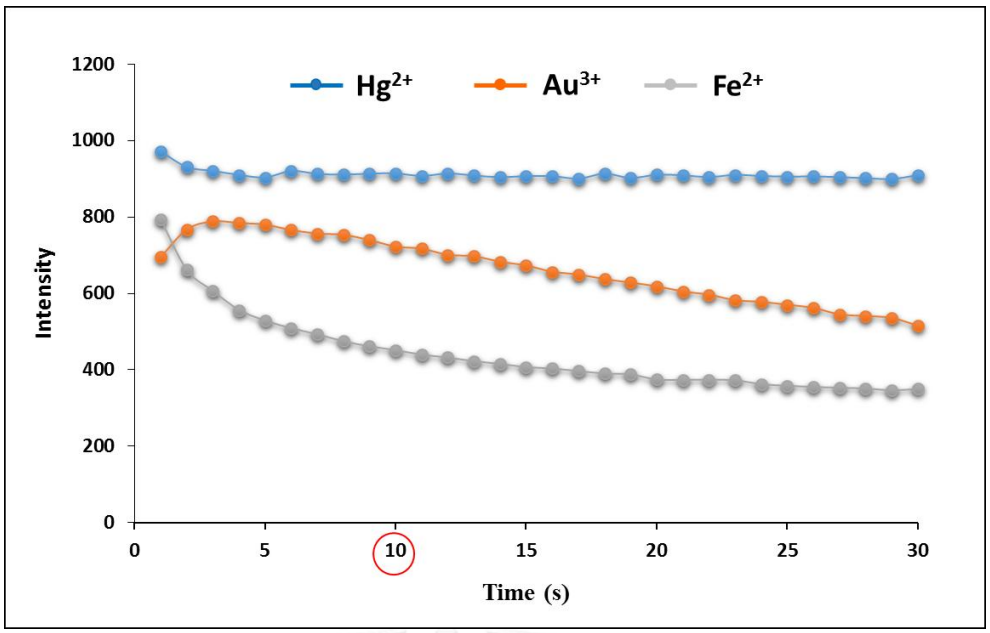

Figure 3.28 Time-dependent fluorescent responses of **5d** (1 μM) against Hg^{2+}, Fe^{2+} and Au^{3+} (100 μM) in the solution of triton X-100 (1000 μM).

3.5.5 Metal selectivity (detect 10 minutes)

Metal selectivity of **5d** were studied over standard set of metal ions at the concentration of sensor:ion = 1:100 μM in the present of 1000 μM TX in aqueous solution. This experiment was achieved with the excitation at λ_{max} = 366 nm and detected in range of 380-680 nm after 10 minutes. The trials showed that only **5d** was selected to Fe(II) ion (Fe^{2+}) while the case of Au^{3+} did not show any signal change (**Figure 3.29**). According to the above results, we could demonstrate the appropriate system for the dual channel probe for the detection of Au^{3+} and Fe^{2+} by addition of TX and adjusting the detection time from 30 to 10 minutes.

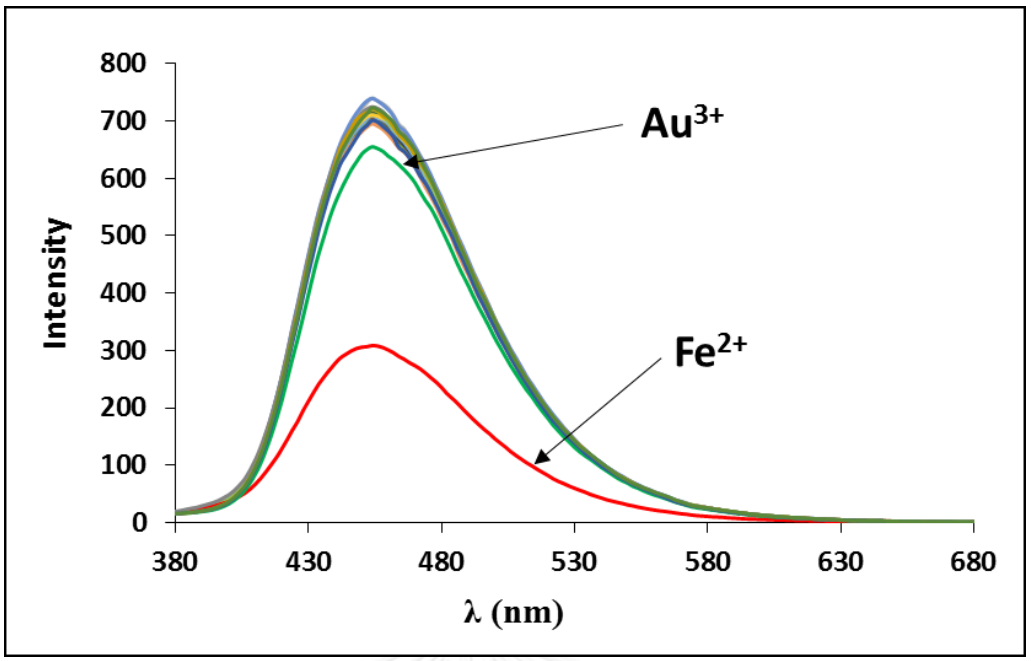

Figure 3.29 Metal selectivity of **5d** (1 μM) over various metal ions (100 μM) in triton X-100 system (1000 μM) and the detection time of 10 minutes.

3.5.6 Fluorescent titration of bis DHP-6+Fe2 (SV-plot) LOD

The fluorescent titration of 1μM bis DHP-6 (**5d**) in triton X-100 mixed-aqueous solution toward Fe^{2+} ion was carried out at excitation wavelength of 366 nm and detected after 15 minutes. Upon addition of increasing amounts of Fe^{2+} (1 μM to 500 μM) to the solution of **5d** in aqueous solution contained triton X-100, the quenching fluorescent signal increased with Fe^{2+} concentration (**Figure 3.30**). The long-time of iron(II)-induced fluorescent quenching of **5d** was probably from the structure change via oxidation reaction in DHP moiety similar to quenching mechanism of Au^{3+}.

The fluorescent quenching efficiency can be represented with the Stern-Volmer constant (K_{SV}) according to the following equation:

$$\frac{I_0}{I} - 1 = K_{SV}[analyte]$$

A linear plot (inset of **Figure 3.30**) gave the K_{SV} of 0.0128 μM^{-1} with the limit of detection (LOD) of 1.69 μM Au^{3+} (≈ 94 ppb).

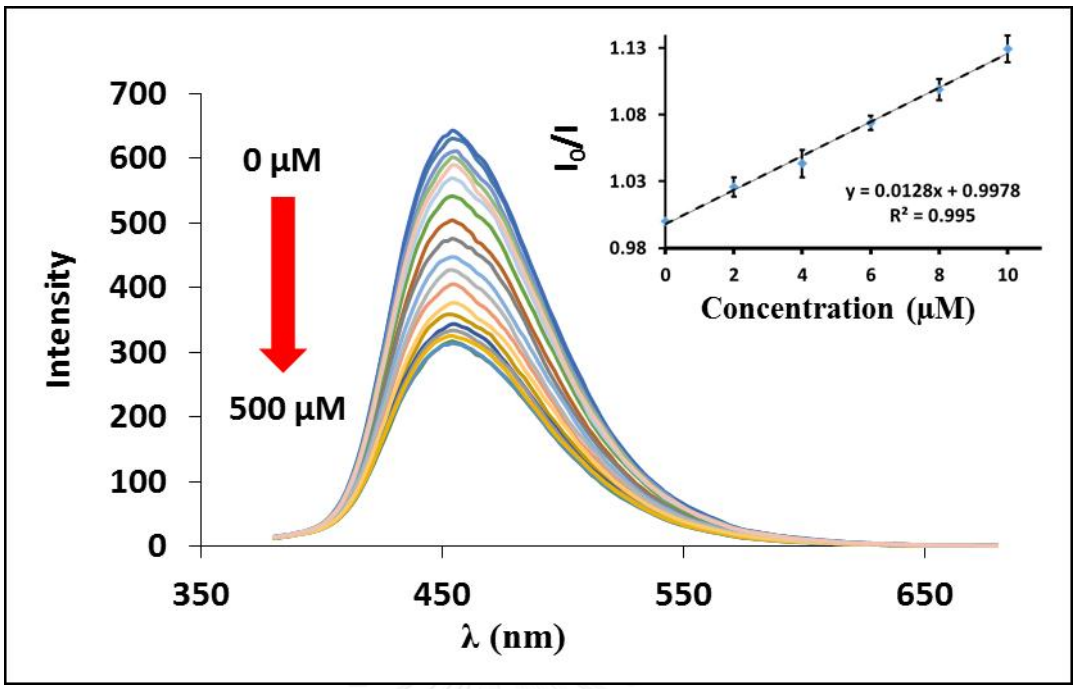

Figure 3.30 Fluorescent titration of **5d** toward Fe^{2+} in Triton X-100 (TX) system in the concentration of 5d:TX:Fe^{2+} = 1:1000:0-500 µM by detected after 15 minutes.

3.5.7 Time-dependent quenching of bis DHP-6 (5d) over Fe^{2+} in surfactant system by UV-vis spectrometry technique

Time-dependent absorption signal change of **5d** was further investigated to acknowledge the quenching behavior by UV-vis spectrometer. This experiment was examined at the concentration of **5d**:TX:Fe^{2+} = 10:1000:1000 µM in aqueous solution and detected every 1 minute for 30 minutes (**Figure 3.31**). Initially, the absorption peak of **5d** belonging to the N-substituted arene (λ_{max} of 277 nm) was enhanced upon addition of TX but when Fe^{2+} was escalated, it split into two bands at about 271 and 281 nm. This aspect of band split by surfactant interaction still has no scientific explanation. However, we surmised that it might be resulted from the micellar formation of TX around DHP moieties. While absorption band at 364 nm as the intensity of the characteristic peak of a DHP ring [11, 12, 14] increased by addition of TX but did not change after the Fe^{2+} addition. This fact explained that there was no oxidative reaction of DHP into pyridinium ring like the quenching case of Au^{3+}.

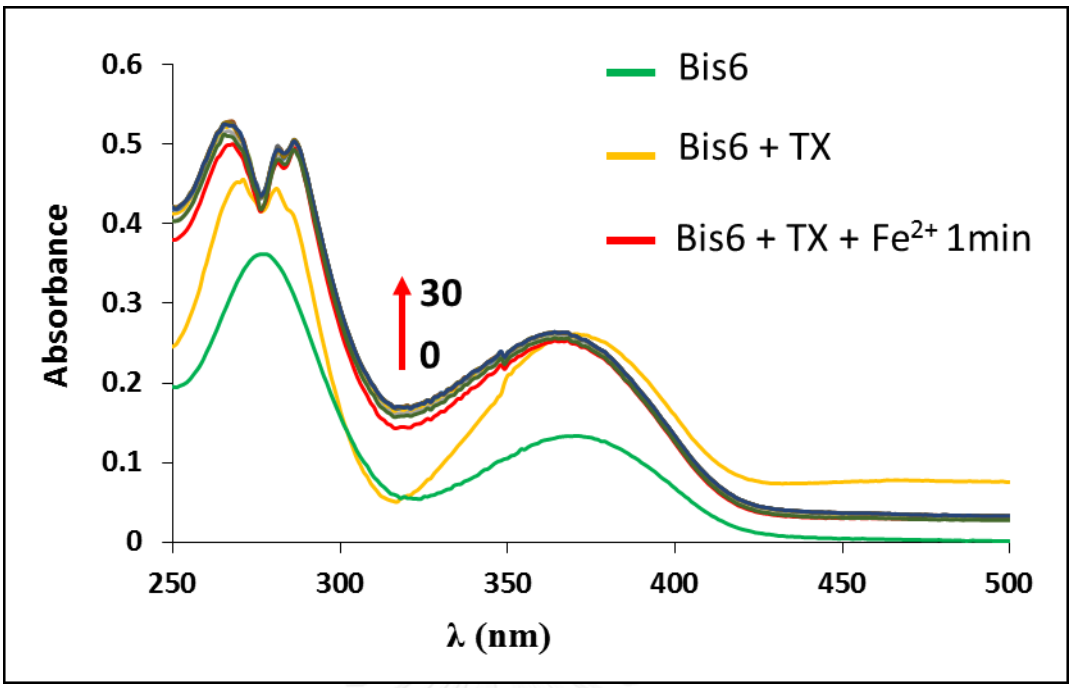

Figure 3.31 Time-dependent absorption signal change of **5d** (10 μM) toward Fe^{2+} (100 μM) in Triton X-100 (1000 μM) aqueous solution for 30 minutes.

3.5.8 Proposed mechanism of bis DHP-6 (5d) based-fluorescent Fe^{2+} ion sensing in surfactant system

As we could prove the absence of the oxidation reaction in **5d** toward Fe^{2+} in TX system, we therefore designed the further experiment to explore the sensing mechanism of **5d** based-fluorescent Fe^{2+} ion sensor. The concept of this experiment is to add Au^{3+} into **5d** contained Fe^{2+} in surfactant mixed-aqueous solution, in order to seek the interaction between TX and Fe^{2+} because the DHP did not involve in the fluorescent intensity decrease as in the results of 3.5.8. we hence studied fluorescent changing behavior of **5d** by sequent addition of analyte to prove that hypothesis. The concentration of **5d**, TX, Fe^{2+} and Au^{3+} in this trial as amount of 1, 1000, 100 and 100, respectively. As illustrated in **Figure 3.32**, in the case entry 2 without surfactant, **5d** could be completely quenched by Au^{3+}. In case of TX system, **5d** was enhanced up to 10 times (entry 3). The fluorescent intensity of this solution was not decreased by filling of Au^{3+} for 15 minutes (entry 4) while addition of Fe^{2+} could decrease its

initial intensity by about 2 fold as was mentioned earlier (entry 5). Interestingly, when Au^{3+} was added into the mixture of **5d** and Fe^{2+} in TX system (entry 6), the fluorescent signal was almost completely quenched in 30 minutes similar to quenching manner in the case without TX (entry 2).

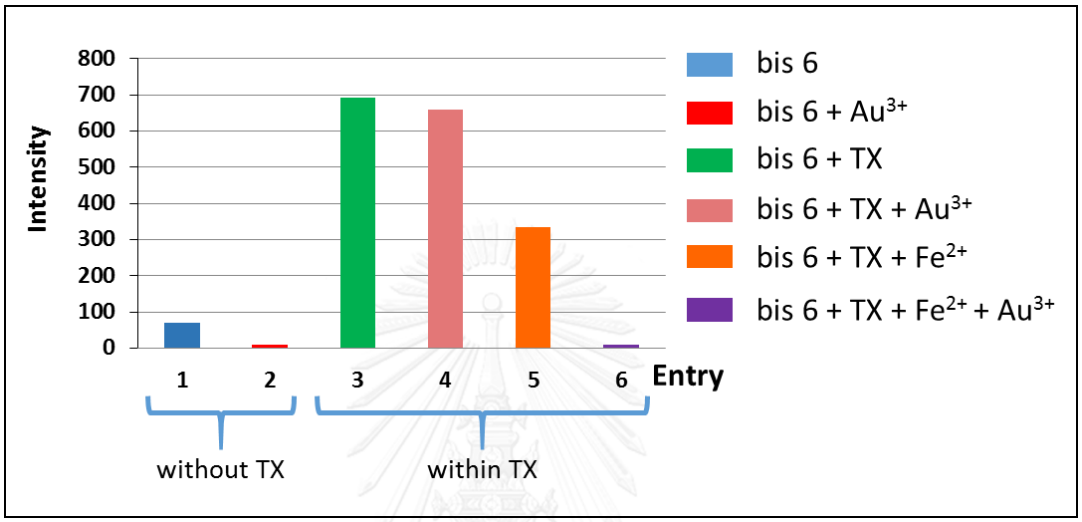

Figure 3.32 Fluorescent response of **5d** toward Au3+ and Fe2+ in the system within and without TX in the concentration of **5d**:TX:Fe^{2+}:Au^{3+} = 1:1000:100:100 μM

It can be hypothesized that the Fe^{2+} ion probably disturb the micellar formation of TX around **5d** and consequently provide some space Au^{3+} to penetrate and oxidized **5d**. The proposed mechanism was demonstrated in the **Figure 3.33**.

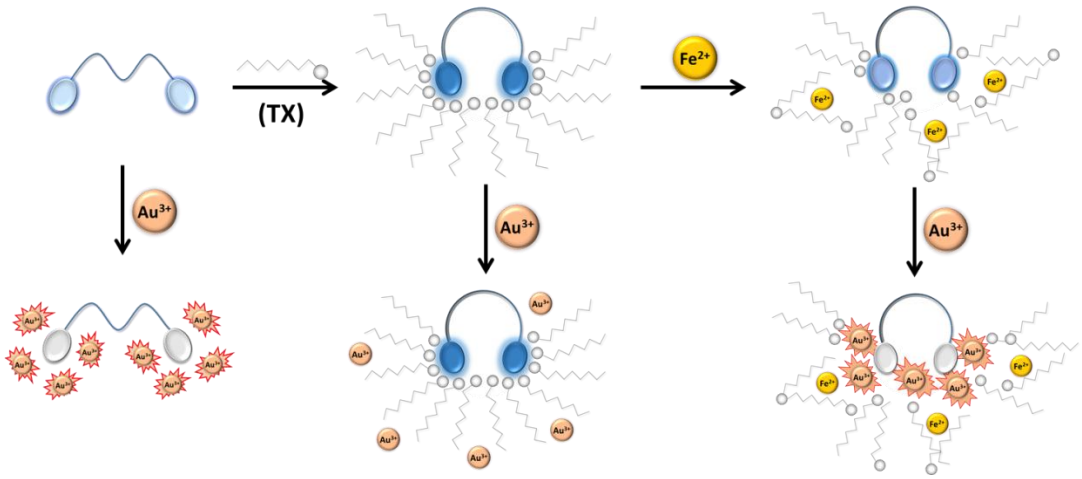

Figure 3.33 Proposed behaviors of 1) **5d**, 2) **5d**•TX 3) **5d**•TX•Au^{3+} 4) **5d**•TX•Fe^{2+} 5) **5d**•TX•Fe^{2+}•Au^{3+} in the concentration of **5d**:TX:Fe^{2+}:Au^{3+}=1:1000:100:100 μM in aqueous media which consistent with their fluorescent intensities.

3.6 pH experiments

3.6.1 pH sensing of candidate fluorophores (1a, 1d and 5d) in buffer solutions.

The effects of pH for metal sensing property of three candidate fluorophores were also investigated. Three candidate DHP derivatives (**1a**, **1d** and **5d**) were chosen as sensors for studying the pH effect as the representatives of the DHP alcohol, DHP phenol and bis DHP, respectively. From the **Figure 3.34**, the conditions of pH effect investigation of these 3 sensors are Britton-Robinson aqueous universal buffer solutions (BR buffer) [68, 69] pH ≈ 4, 7 and 10. The results of the experiments revealed that **1a** and **5d** were not affected by all pH conditions. Only compound **1d** had its fluorescent signal solely quenched toward pH 10. It is possible that phenolic **1d**, which comprise of phenyl group linked to DHP moiety, could be deprotonated under basic condition because its phenolate ring can be stabilized by the electron delocalization. This behavior of electron might result in disturbance to the conjugate system, and hence the fluorescent signal was decreased as mentioned above.

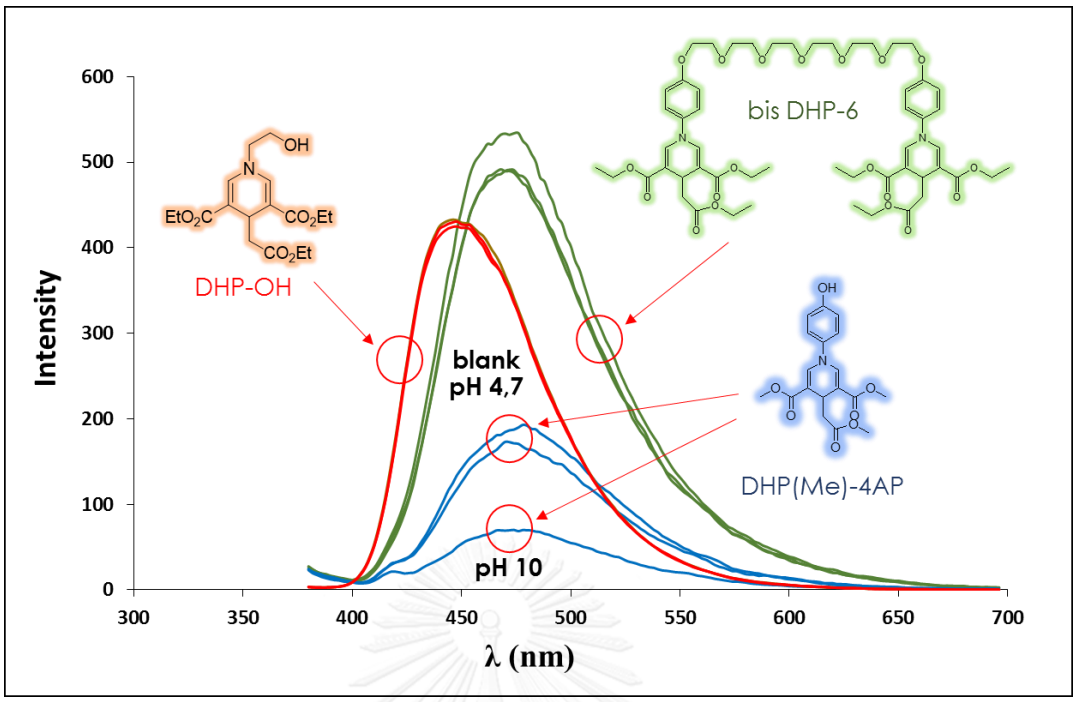

Figure 3.34 pH sensing of **1a**, **1d** and **5d** (100 μM) in BR buffer conditions (pH 4, 7 and 10)

3.6.2 pH-dependent spectral properties

The fluorescent response of the probe **1d** toward BR buffer solution was performed in range of about pH 7 -12 and recorded at excitation wavelength of 366 nm (**Figure 3.35**). Probe **1d** is highly sensitive to the pH adjusted by BR buffer solution. In acidic solution, this probe gave fluorescent signal invariably, but the fluorescent signal was observed to be rapidly decreasing in basic solutions and completely quenched at the pH value of about 11.

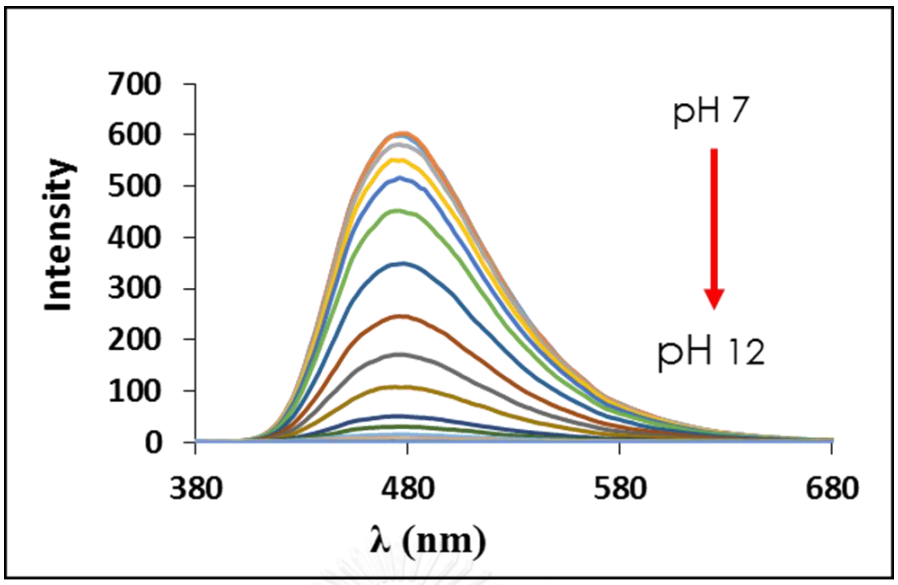

Figure 3.35 pH response of **1d** (100 μM) in the BR buffer pH range of 7 – 12.

The line graph as shown in **Figure 3.36** illustrated a pH range for practical usability (pH ≈ 8.6 – 9.8) which was plotted between fluorescent intensity against pH ($y = -283.69x + 2919.5$; $R^2 = 0.9963$). In addition, we demonstrated the quenching of fluorescence toward various pH controls under black light (pH ≈ 7 – 12) observed by the naked-eye (**Figure 3.37**). These experiments represented that DHP-4AP fluorophores (**1c** and **1d**) were sensitive to pH environment and fast in term of response time, which potentially could be applied to practical applications. This study is considered as the first work among our group that reported about the pH response of DHP derivatives.

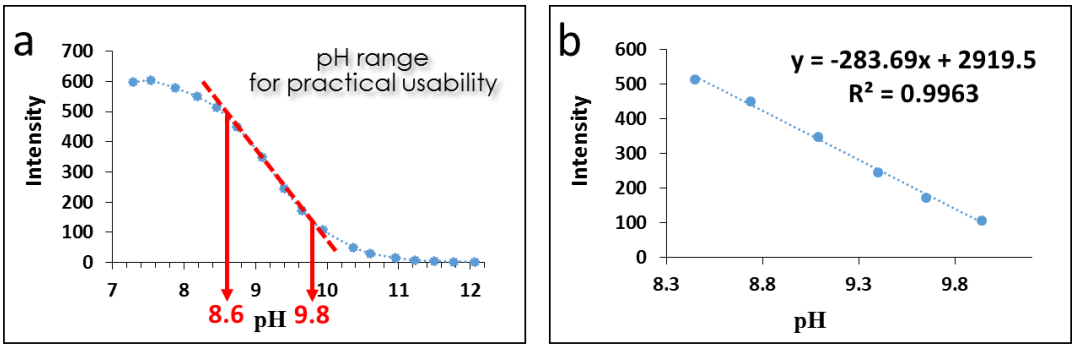

Figure 3.36 (**a**) Line graph of pH response of **1d** (100 μM) in BR buffer pH range of 7 – 12 and (**b**) the linear plot in range of practically usable pH (pH range ≈ 8.5 – 10.0).

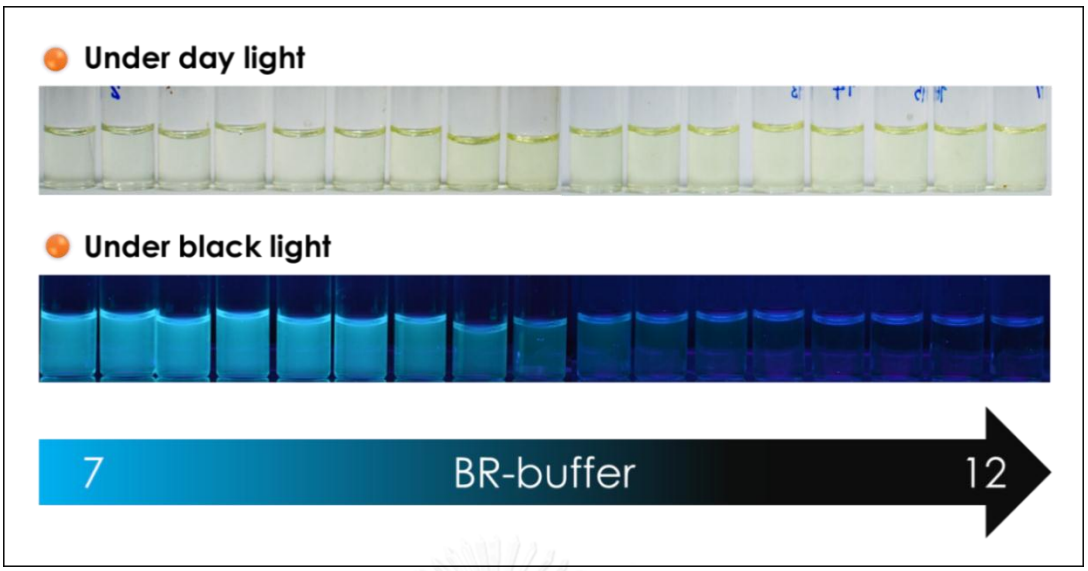

Figure 3.37 Fluorescence quenching of **1d** (100 μM) toward various BR buffer pH controls (pH ≈ 7 – 12)

3.6.3 Determination of pK_a

To get comprehensive data for pH application of DHP-4AP **1d**, pKa of **1d** was determined by using the Henderson-Hasselbalch equation [26-27]: $\log[(I_{max}-I)/(I-I_{min})] = pH-pK_a$, where I is the observed fluorescence intensity, I_{max} and I_{min} are the corresponding maximum and minimum intensity, respectively. This data was investigated to obtain the pK_a value of 9.23 ± 0.03 as shown in **Figure 3.38** which is close to pK_a value of phenol (9.95 in water). Such values Indicate that DHP-4AP probe can be used as base indicator. For commercial pH sensors detected in living cells or sub-cellular structures, pK_a should be inside the critical intracellular pH window (pH ≈ 5-8) [70]. However, probe **1d** has ON–OFF pH sensing properties with "on-state" in the range of 8.6–9.8, which is appropriate for using as neutral and base indicator.

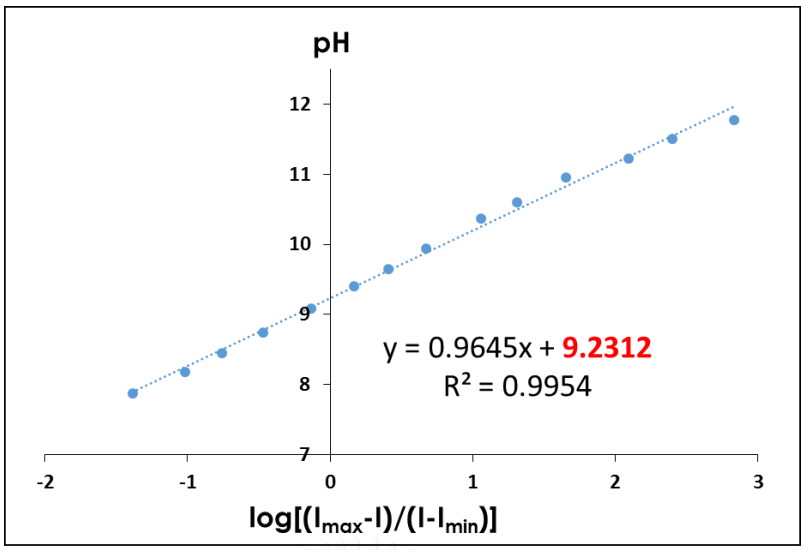

Figure 3.38 pK_a determination of **1d** by using the Henderson-Hasselbalch equation.

3.6.4 Reversibility of DHP(Me)-4AP sensor (1d)

In order to achieve pH-reversibility study of **1d** (**Figure 3.39**), pH value of the aqueous media was altered from pH 7 to pH 11 then back to pH 7 again as one cycle, and this cycle will be repeated 5 times. DHP-4AP probe **1d** was proven to possess high reversibility to pH experiment, demonstrating the resistant property to pH changes in base region. This is also a great advantage for reusable application as pH sensor especially in bioorganic field.

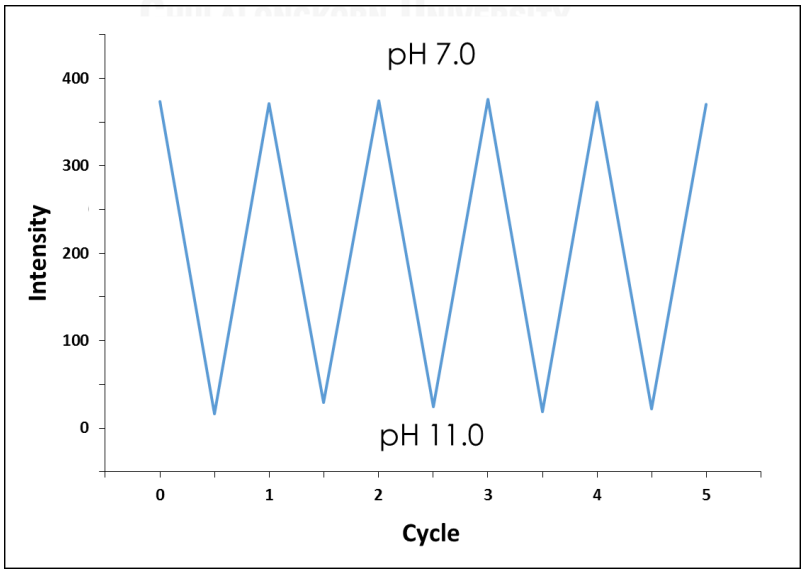

Figure 3.39 pH-reversible study of **1d** in pH of 7.0 and 11.0.

3.6.5 Interference ions

In addition, the high selectivity response to target analyte over interfering species is also important point. Therefore, fluorescent responses of **1d** (1 μM) in two pH conditions (pH 7.44 and 10.51) toward interfering biological species (100 μM) such as cations (Na^{+}, Ca^{2+}, Fe^{2+}, Cu^{2+} and Zn^{2+}) and anions (Cl^{-}, OAc^{-}, NO_3^{-}, CO_3^{2-} and SO_4^{2-}) were examined as shown in **Figure 3.40**. The emission intensities were not gradated by other species in the both two pH systems. These results confirm that DHP-4AP probes exhibit excellent response even in the presence of interfering species.

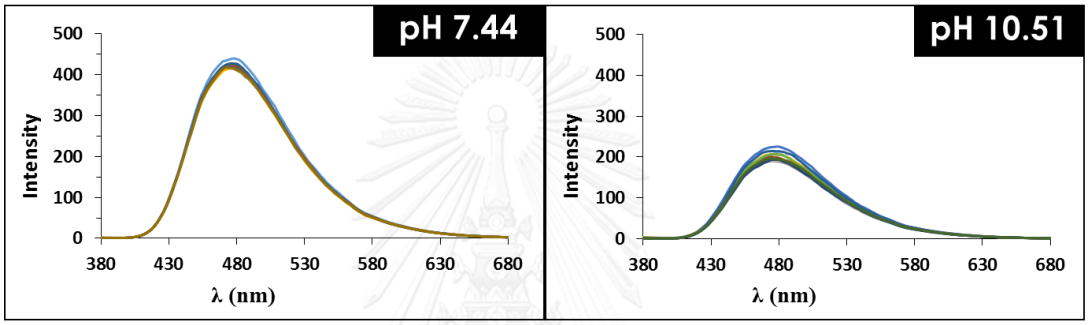

Figure 3.40 Interference of **1d** (1 μM) toward interfering species (100 μM) under two pH conditions.

3.6.6 Practical usability of pH sensor

To evaluate the practical application of the proposed sensor, pH values of different NaOH aqueous samples were tested on the basis of DHP-4AP sensor (**1d**) (**Figure 3.41**). The calculated values, derived from linear equation in base region (pH ≈ 8.5 – 10.5), are pH 8.48 ± 0.17, pH 9.12 ± 0.25, pH 9.52 ± 0.14 and pH 10.10 ± 0.14 for 4 samples while the measured values by pH meter are pH 8.53, pH 9.02, pH 9.52 and pH 10.07, accordingly. The results of the calculated values are very close to the measured values by pH meter implying the potential practical usability of this pH sensor.

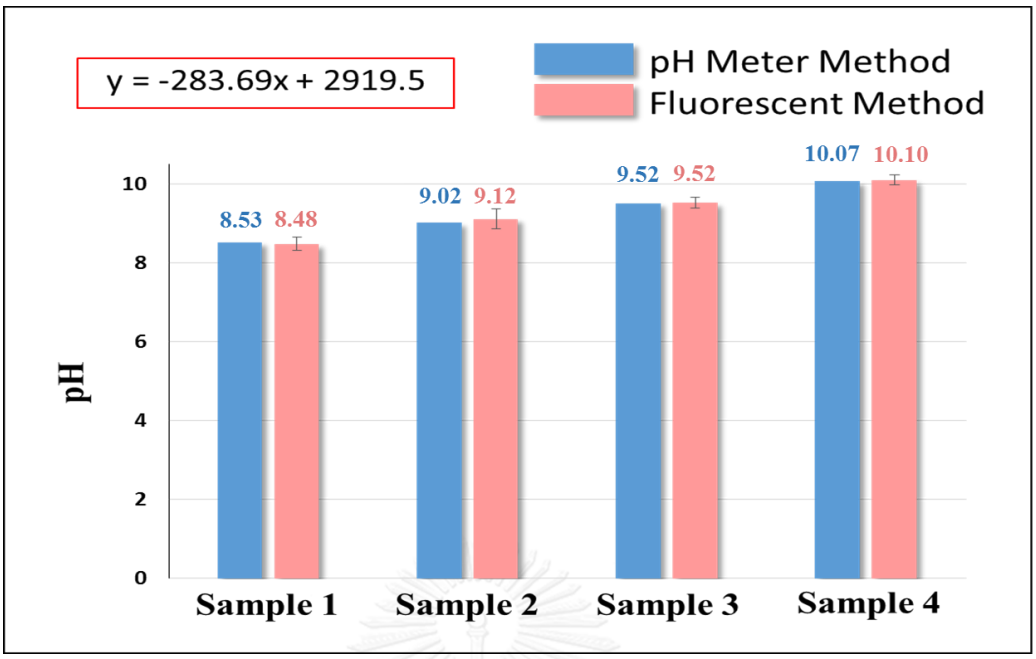

Figure 3.41 pH sensing of different NaOH aqueous samples by using **1d** (1 μM) as pH sensor in base region (pH ≈ 8.5 – 10.5). Blue bar is the measured value from pH meter, pink bar is the calculated pH value according to the developed linearity equation (y = -283.69x + 2919.53).

3.6.7 Metal ion sensing under pH conditions

Metal selectivity of compound **1d** was studied over standard set of 24 metal ions (Li^{+}, Na^{+}, K^{+}, Mg^{2+}, Ca^{2+}, Sr^{2+}, Ba^{2+}, Pb^{2+}, Al^{3+}, Ga^{3+}, Bi^{3+} Ag^{+}, Hg^{+}, Mn^{2}, Fe^{2+}, Co^{2+}, Ni^{2+}, Cu^{2+}, Zn^{2+}, Cd^{2+}, Hg^{2+}, Cr^{3+}, $Fe^{3+}$and Au^{3+}) at the concentration of sensor:ion = 1:100 μM in aqueous (0.5% MeOH/H_2O) solution under pH controls (BR buffers pH 4, 7 and 10). All experiments were excited at λ_{max} = 366 nm and detected in range of 380-680 nm after 30 minutes for reaction mode. According to the results, all pH conditions only selected to gold(III) ion (Au^{3+}) as well as those trials without pH buffer control. However, these fluorescent responses exhibited different behavior as shown in **Figure 3.42**. Gold(III) ion-induced fluorescent signals were observed with 32-38 nm blue-shifts in all pH buffer solutions. In case of pH 4, **1d** intimated the highest fluorescent enhancement of around 5 fold higher than that of the blank one. These experiments demonstrated that the DHP-4AP fluorophores (**1c** and **1d**) are Au^{3+}

selective sensors that can be used on both quenching and enhancing mode depending on the adjustment of the appropriate conditions.

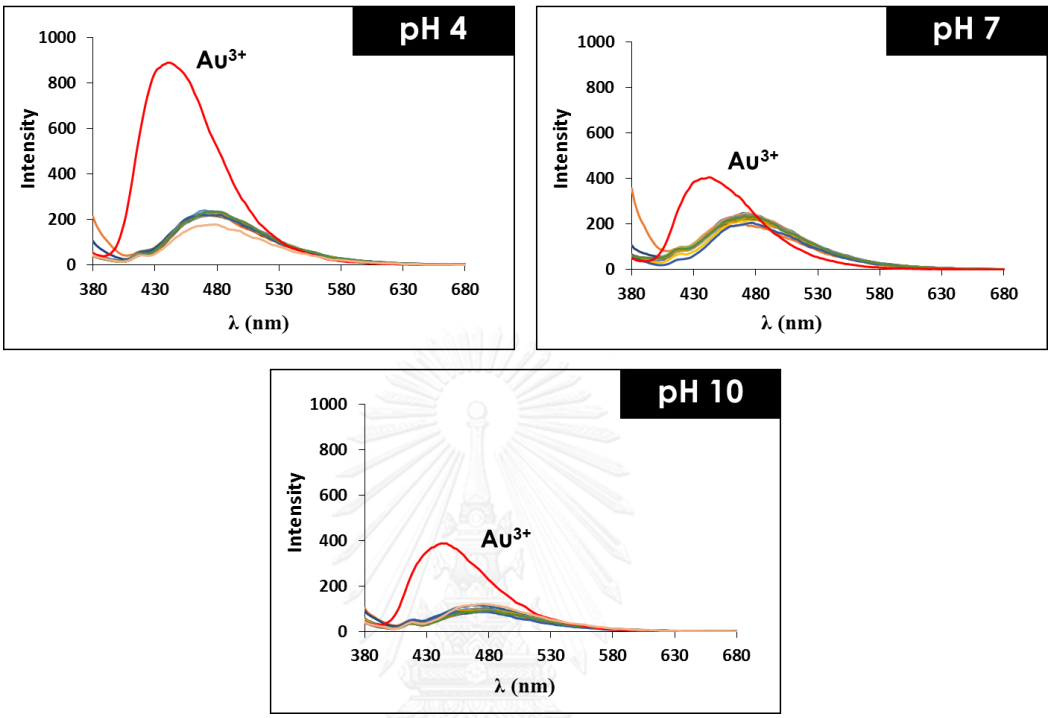

Figure 3.42 Metal selectivity of **1d** (1 μM) over various metal ions (100 μM) in BR Buffers solution pH 4, 7 and 10 in 30 minutes.

3.6.8 Time-dependent fluorescent response in BR buffer solution pH 4

Since the strange behavior was unexplainable, time-dependent fluorescent response toward Au^{3+} in milliQ water and BR buffer solution pH 4 were investigated and detected in every 5 minutes for 2 hours to compare their signal behaviors (**Figure 3.43**). In milliQ water, the signal was increased in first 10 minutes and it was then decreased along the time with blue-shifted about 35 nm at the reaction time of 30 minutes. This result is similar to those of DHP probes examined in aqueous solution. In buffer solution pH 4, its fluorescent intensity was enhanced with 32 nm blue-shift at 30 minutes and then its signal was similarly quenched like the case of uncontrolled pH system. This means that Au^{3+} induced reaction of DHP-4AP in these two conditions probably progress with the same mechanism.

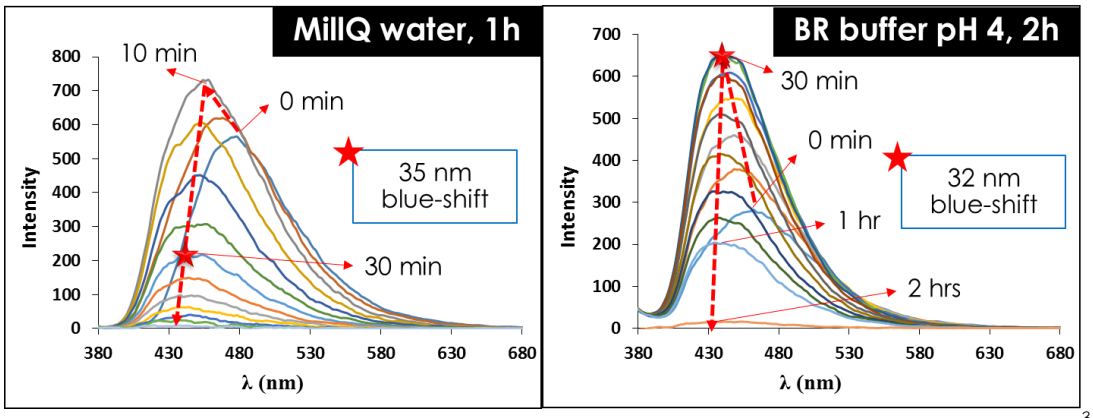

Figure 3.43 Time-dependent fluorescent quenching of **1d** (1 μM) toward Au^{3+} (100 μM) in milliQ water and BR buffer solution pH 4.

3.7 other sensors

3.7.1 Protein sensor (show spectra, bar chart and picture)

According to the previous researches, we have studied usable applications of target molecules such as metal ion sensors, surfactant-tuning metal ion sensors and pH sensors. Moreover, fluorescent bio-sensing properties of DHP probes **1d, 5c** and **7** (1 μM) were also investigated in phosphate buffer saline (PBS) solution pH 7.4 over 14 biological analytes (protein concentrations at A_{280} = 0.1). All proteins consisted of Riboflavin, Risozome, HAS, Papain, bovine serum albumin (BSA), α-Casine, β-Casine, Histone (His), Lipase, α-Lactose, β-Lactose, Albumin, Myoglobin (Myo) and Hemoglobin. **Figure 3.44** (**a**) showed an example measurement of probe **5c** toward BSA in which one detective protein is composed of three lines (sensor, protein and sensor·protein). All proteins were investigated as shown in **Figure 3.44** (**b**).

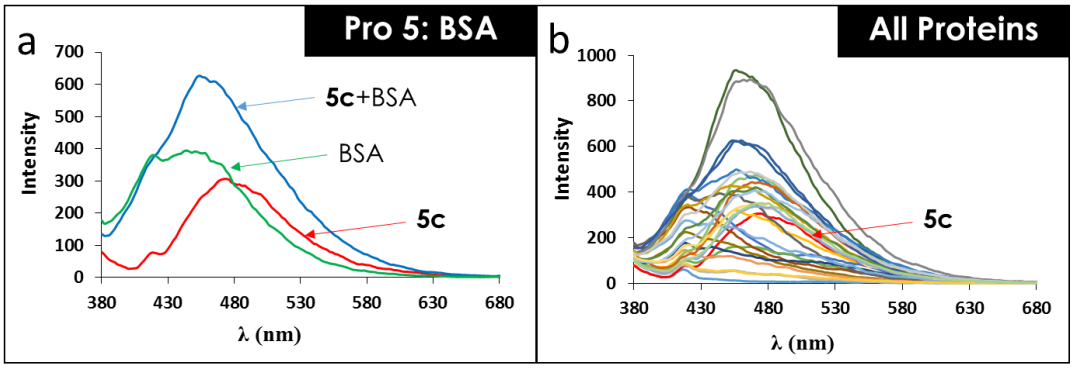

Figure 3.44 Protein Selectivity of **5c** (1 μM) in PBS pH 7.4 toward (**a**) BSA and (**b**) all proteins (protein concentrations at A_{280} = 0.1).

After the consideration of the result, all candidated DHP probes were not selective with most of proteins because the obtained data had no significant changes when compared between integrated values of single sensor combined with single protein and the integration of sensor with protein. Sensing considerations of **5c** toward two proteins (BSA and β-casice) were typically shown in **Figure 3.45**. For protein selectivity of other sensors illustrated the similar results. We would say that all DHP-4AP derivatives are not suitable to be fluorescent proteinsensor.

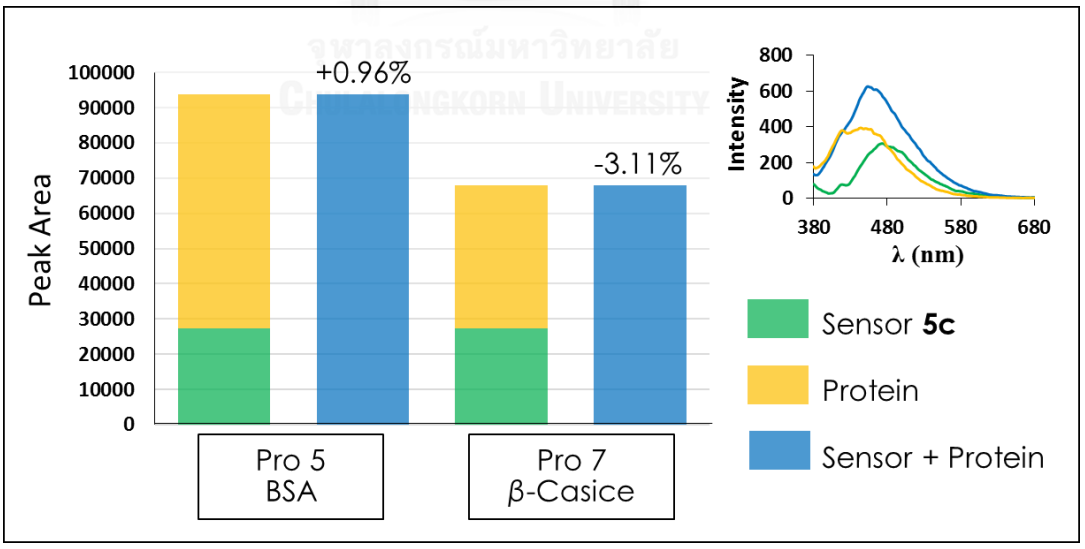

Figure 3.45 Examples of analytical methods for protein-induced fluorescent response.

3.7.2 Oxidative sensor (show spectra detect at 1h and real time) KMnO4 selected

DHP moiety could be oxidized by Au^{3+} in aqueous solution to become the pyridinium ring. Therefore, oxidizing agent-induced oxidative reaction of fluorophore **1d** was studied (concentration of 1d:analyte = 1:100 μM in milliQ water) and detected at the time of 1 hour compared with immediate detection to obtain more information about DHP sensing application. Oxidizing agent in this trial are consisted of NaClO, $NaClO_4$, H_2O_2, Oxone, Tempo, $K_2Cr_2O_7$ and $KMnO_4$. When the fluorescent intensity was detected after the reaction time of 1 hour, its signals were shown in variety behavior but signal was interestingly only quenched by $KMnO_4$ (**Figure 3.46**, **a**). To tune its selectivity, all analytes were immediately detected within 3-5 seconds (**Figure 3.46**, **b**). This trial illustrated excellent selectivity to only $KMnO_4$ with 94.15 % quenching efficiency. This result was consistent with the strong oxidative property of $KMnO_4$.

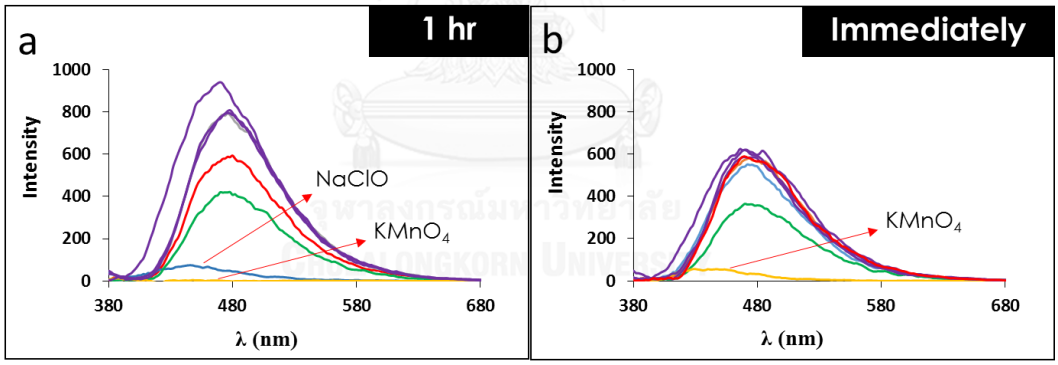

Figure 3.46 Fluorescent response of **1d** (1 μM) over various oxidizing agents (100 μM) with the detection time of (**a**) 1 hour and (**b**) immediate monitoring.

Absorption spectra of 10 μM **5d** toward 1,000 μM $KMnO_4$ in aqueous solution were observed as shown in **Figure 3.47.** Red line showed absorption band of **5d** with $KMnO_4$ which was detected by UV-vis spectrometer while the green line derived from summation of blue and violet line. This investigation intimated that $KMnO_4$ (violet line) was no affect to **5d** by competitive absorption despite the high concentration of $KMnO_4$ (100 equiv.) was used. In addition, the red line exhibited that $KMnO_4$ was also

no oxidation reaction. At this time, we were still wondering how it rapidly inhibited the fluorescent signal of **5d**.

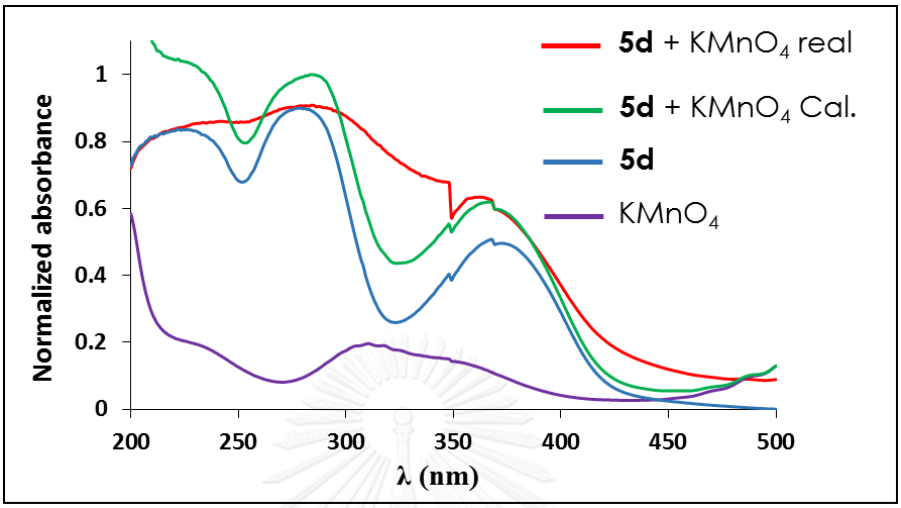

Figure 3.47 Absorption spectra of **5d** toward $KMnO_4$ in aqueous solution.

CHAPTER IV
CONCLUSION

4.1 Conclusion

We have successfully synthesized and developed novel 1,4-dihydropyridine (DHP) derivatives (**1c** and **1d**) as fluorescent chemosensors via the cyclotrimerization of β-amino acrylate by using $TiCl_4$ as Lewis acid at room temperature. The DHP was linked with various chains of oligoethylene glycol for increase water solubility to gained bis DHPs and mono DHPs. According to their photophysical properties in MeOH, all DHP compounds exhibited the maximum absorption wavelength of around 360 to 368 nm and maximum emission at 454 to 466 nm with the florescent quantum efficiencies (Φ_f) of 0.69, 0.74 and 0.32 for **1c**, **5d** and **7**, respectively. For sensing properties, all DHP derivatives selected to gold(III) ion (Au^{3+}) which the fluorescent intensities were time-dependently and proportionally quenched by Au^{3+} concentration. In triton X-100 (TX) system, iron(II) ion (Fe^{2+}) was selected by only bis DHPs group (**5a**-**d**). These interactions between DHP with TX and Fe^{2+} were proposed that TX would form the micelle around DHP to increase fluorescent signal and this molecular assembly could be disturbed by Fe^{2+}, which decreased the fluorescent intensity without reaction unlike the case of Au^{3+}. Compound **5d** exhibited limit of detection (LOD) of 2.65 μM and 1.69 for Au^{3+} and Fe^{2+}, respectively. These results declare that bis DHP sensors can be used as fluorescent chemosensor for Au^{3+} and Fe^{2+} (dual-channel probe). Moreover, fluorophore **1c** and **1d** responded to basic BR buffer solution with the decrease of fluorescent intensity. Probe **1d** revealed the pK_a of about 9.23 followed by The Henderson–Hasselbalch equation. Protein and oxidizing agent selectivity were also examined for the sensing application of DHP derivatives.

4.2 Suggestion for future work

Our group will continue to study the application of DHP derivatives to detect Au^{3+} and Fe^{2+} in living cells, food and drinking water at real-time monitering system. Moreover, we focus to investigate more information for using DHP derivatives as pH sensor.

REFERENCES

[1] Hantzsch, A. Ueber die Synthese pyridinartiger Verbindungen aus Acetessigäther und Aldehydammoniak. Justus Liebigs Annalen der Chemie 215(1) (1882): 1-82.

[2] Fukuzumi, S., Koumitsu, S., Hironaka, K., and Tanaka, T. Energetic comparison between photoinduced electron-transfer reactions from NADH model compounds to organic and inorganic oxidants and hydride-transfer reactions from NADH model compounds to p-benzoquinone derivatives. Journal of the American Chemical Society 109(2) (1987): 305-316.

[3] Yamamoto, T., et al. Asymmetric synthesis and biological evaluations of (+)- and (–)-6-dimethoxymethyl-1,4-dihydropyridine-3-carboxylic acid derivatives blocking N-type calcium channels. Bioorganic & Medicinal Chemistry Letters 21(11) (2011): 3317-3319.

[4] Briede, J., et al. Effects of some 1,4-dihydropyridine Ca antagonists on the blast transformation of rat spleen lymphocytes. Cell Biochemistry and Function 17(2) (1999): 97-105.

[5] Janis, R.A. and Triggle, D.J. New developments in calcium ion channel antagonists. Journal of Medicinal Chemistry 26(6) (1983): 775-785.

[6] Mannhold, R., Jablonka, B., Voigt, W., Schönafinger, K., and Schraven, E. Calcium- and calmodulin-antagonism of elnadipine derivatives: comparative SAR. European Journal of Medicinal Chemistry 27(3) (1992): 229-235.

[7] Striessnig, J., Grabner, M., Mitterdorfer, J., Hering, S., Sinnegger, M.J., and Glossmann, H. Structural basis of drug binding to L Ca2+ channels. Trends in Pharmacological Sciences 19(3) (1998): 108-115.

[8] Mochizuki, A., Fukuoka, T., Kanada, M., Kinjou, N., and Yamamoto, T. Development of Photosensitive Porous Polyimide with Low Dielectric Constant. Journal of Photopolymer Science and Technology 15(2) (2002): 159-165.

[9] Fasani, E., Dondi, D., Ricci, A., and Albini, A. Photochemistry of 4-(2-Nitrophenyl)-1,4-Dihydropyridines. Evidence for Electron Transfer and Formation of an Intermediate†. Photochemistry and Photobiology 82(1) (2006): 225-230.

[10] Fasani, E., Fagnoni, M., Dondi, D., and Albini, A. Intramolecular Electron Transfer in the Photochemistry of Some Nitrophenyldihydropyridines. The Journal of Organic Chemistry 71(5) (2006): 2037-2045.

[11] Jimenez, A.J., Fagnoni, M., Mella, M., and Albini, A. Photoinduced Electron and Energy Transfer in Aryldihydropyridines. The Journal of Organic Chemistry 74(17) (2009): 6615-6622.

[12] Pávez, P. and Encinas, M.V. Photophysics and Photochemical Studies of 1,4-Dihydropyridine Derivatives. Photochemistry and Photobiology 83(3) (2007): 722-729.

[13] Chen, B., Peng, M.-L., Wu, L.-Z., Zhang, L.-P., and Tung, C.-H. Switch between charge transfer and local excited states in 4-aminophenyl-substituted Hantzsch 1,4-dihydropyridine induced by pH change and transition metal ions. Photochemical & Photobiological Sciences 5(10) (2006): 943-947.

[14] Lohani, C.R. and Lee, K.-H. The effect of absorbance of Fe3+ on the detection of Fe3+ by fluorescent chemical sensors. Sensors and Actuators B: Chemical 143(2) (2010): 649-654.

[15] Fang, C., Peng, M., Li, G., Tian, J., and Yin, D. New Functions of Glucosamine as a Scavenger of the Lipid Peroxidation Product Malondialdehyde. Chemical Research in Toxicology 20(6) (2007): 947-953.

[16] Ko, S., Sastry, M.N.V., Lin, C., and Yao, C.-F. Molecular iodine-catalyzed one-pot synthesis of 4-substituted-1,4-dihydropyridine derivatives via Hantzsch reaction. Tetrahedron Letters 46(34) (2005): 5771-5774.

[17] Cheung, L.L.W., Styler, S.A., and Dicks, A.P. Rapid and Convenient Synthesis of the 1,4-Dihydropyridine Privileged Structure. Journal of Chemical Education 87(6) (2010): 628-630.

[18] Sueki, S., Takei, R., Abe, J., and Shimizu, I. Ytterbium-catalyzed synthesis of dihydropyridines. Tetrahedron Letters 52(34) (2011): 4473-4477.

[19] Sirijindalert, T., Hansuthirakul, K., Rashatasakhon, P., Sukwattanasinitt, M., and Ajavakom, A. Novel synthetic route to 1,4-dihydropyridines from β-amino acrylates by using titanium(IV) chloride under facile conditions. Tetrahedron 66(27–28) (2010): 5161-5167.

[20] Homraruen, D., Sirijindalert, T., Dubas, L., Sukwattanasinitt, M., and Ajavakom, A. Selective fluorescent sensor for mercury ions in aqueous media using a 1,4-dihydropyridine derivative. Tetrahedron 69(5) (2013): 1617-1621.

[21] Lakowicz, J.R. Principles of Fluorescence Spectroscopy. in 3rd (ed.). Kluwer John Wiley & Sons inc, 2006.

[22] Kim, S.K., Lee, S.H., Lee, J.Y., Lee, J.Y., Bartsch, R.A., and Kim, J.S. An Excimer-Based, Binuclear, On–Off Switchable Calix[4]crown Chemosensor. Journal of the American Chemical Society 126(50) (2004): 16499-16506.

[23] Yang, Y.-K., Lee, S., and Tae, J. A Gold(III) Ion-Selective Fluorescent Probe and Its Application to Bioimagings. Organic Letters 11(24) (2009): 5610-5613.

[24] Chen, L., et al. Tridentate Lysine-Based Fluorescent Sensor for Hg(II) in Aqueous Solution. Inorganic Chemistry 50(20) (2011): 10028-10032.

[25] Mahapatra, A.K., Hazra, G., Das, N.K., and Goswami, S. A highly selective triphenylamine-based indolylmethane derivatives as colorimetric and turn-off fluorimetric sensor toward Cu2+ detection by deprotonation of secondary amines. Sensors and Actuators B: Chemical 156(1) (2011): 456-462.

[26] Xu, Z., Xiao, Y., Qian, X., Cui, J., and Cui, D. Ratiometric and Selective Fluorescent Sensor for CuII Based on Internal Charge Transfer (ICT). Organic Letters 7(5) (2005): 889-892.

[27] Zhao, Y., Lin, Z., He, C., Wu, H., and Duan, C. A “Turn-On” Fluorescent Sensor for Selective Hg(II) Detection in Aqueous Media Based on Metal-Induced Dye Formation. Inorganic Chemistry 45(25) (2006): 10013-10015.

[28] Chen, X., et al. Hg2+ Selective Fluorescent and Colorimetric Sensor: Its Crystal Structure and Application to Bioimaging. Organic Letters 10(22) (2008): 5235-5238.

[29] Huang, J., Xu, Y., and Qian, X. A Rhodamine-Based Hg2+ Sensor with High Selectivity and Sensitivity in Aqueous Solution: A NS2-Containing Receptor. The Journal of Organic Chemistry 74(5) (2009): 2167-2170.

[30] Kim, J.S., Choi, M.G., Song, K.C., No, K.T., Ahn, S., and Chang, S.-K. Ratiometric Determination of Hg2+ Ions Based on Simple Molecular Motifs of Pyrene and Dioxaoctanediamide. Organic Letters 9(6) (2007): 1129-1132.

[31] Jung, H.S., et al. Coumarin-Derived Cu2+-Selective Fluorescence Sensor: Synthesis, Mechanisms, and Applications in Living Cells. Journal of the American Chemical Society 131(5) (2009): 2008-2012.

[32] Mandal, A.K., Suresh, M., Suresh, E., Mishra, S.K., Mishra, S., and Das, A. A chemosensor for heavy-transition metal ions in mixed aqueous–organic media. Sensors and Actuators B: Chemical 145(1) (2010): 32-38.

[33] Singh, N., Kaur, N., Dunn, J., MacKay, M., and Callan, J.F. A new fluorescent chemosensor for iron(III) based on the β-aminobisulfonate receptor. Tetrahedron Letters 50(8) (2009): 953-956.

[34] Xu, Z., et al. Zn2+-Triggered Amide Tautomerization Produces a Highly Zn2+-Selective, Cell-Permeable, and Ratiometric Fluorescent Sensor. Journal of the American Chemical Society 132(2) (2010): 601-610.

[35] Hsieh, Y.-C., Chir, J.-L., Wu, H.-H., Guo, C.-Q.I., and Wu, A.-T. Synthesis of a sugar-aza-crown ether-based cavitand as a selective fluorescent chemosensor for Cu2+ ion. Tetrahedron Letters 51(1) (2010): 109-111.

[36] Egorova, O.A., Seo, H., Chatterjee, A., and Ahn, K.H. Reaction-Based Fluorescent Sensing of Au(I)/Au(III) Species: Mechanistic Implications on Vinylgold Intermediates. Organic Letters 12(3) (2010): 401-403.

[37] Dong, M., Wang, Y.-W., and Peng, Y. Highly Selective Ratiometric Fluorescent Sensing for Hg2+ and Au3+, Respectively, in Aqueous Media. Organic Letters 12(22) (2010): 5310-5313.

[38] Park, J.E., Choi, M.G., and Chang, S.-K. Colorimetric and Fluorescent Signaling of Au3+ by Desulfurization of Thiocoumarin. Inorganic Chemistry 51(5) (2012): 2880-2884.

[39] Liu, Y., Duan, Z.-Y., Zhang, H.-Y., Jiang, X.-L., and Han, J.-R. Selective Binding and Inverse Fluorescent Behavior of Magnesium Ion by Podand Possessing Plural Imidazo[4,5-f]-1,10-phenanthroline Groups and Its Ru(II) Complex. The Journal of Organic Chemistry 70(4) (2005): 1450-1455.

[40] Ashokkumar, P., Ramakrishnan, V.T., and Ramamurthy, P. Solvent-Controlled Metal Ion Binding Selectivity and Anion Interaction of the Acridinedione-Based Heteroditopic Host. The Journal of Physical Chemistry B 115(1) (2011): 84-92.

[41] Pinrat, O., Boonkitpatarakul, K., Paisuwan, W., Sukwattanasinitt, M., and Ajavakom, A. Glucopyranosyl-1,4-dihydropyridine as a new fluorescent chemosensor for selective detection of 2,4,6-trinitrophenol. Analyst 140(6) (2015): 1886-1893.

[42] Mukherjee, S., Paul, A.K., Krishna Rajak, K., and Stoeckli-Evans, H. ICT based ratiometric fluorescent pH sensing using quinoline hydrazones. Sensors and Actuators B: Chemical 203(0) (2014): 150-156.

[43] Shi, X.-L., et al. Rhodamine-based fluorescent probe for direct bio-imaging of lysosomal pH changes. Talanta 130(0) (2014): 356-362.

[44] Devarayan, K. and Kim, B.-S. Reversible and universal pH sensing cellulose nanofibers for health monitor. Sensors and Actuators B: Chemical 209(0) (2015): 281-286.

[45] Takeuchi, M., Ikeda, M., Sugasaki, A., and Shinkai, S. Molecular Design of Artificial Molecular and Ion Recognition Systems with Allosteric Guest Responses. Accounts of Chemical Research 34(11) (2001): 865-873.

[46] Ikeda, M., Tanida, T., Takeuchi, M., and Shinkai, S. Allosteric Silver(I) Ion Binding with Peripheral **TT** Clefts of a Ce(IV) Double Decker Porphyrin. Organic Letters 2(13) (2000): 1803-1805.

[47] Kumar, M., Kumar, N., and Bhalla, V. Ratiometric nanomolar detection of Cu^{2+} ions in mixed aqueous media: a Cu^{2+}/Li^{+} ions switchable allosteric system based on thiacalix[4]crown. Dalton Transactions 41(34) (2012): 10189-10193.

[48] Vyas, D.J. and Oestreich, M. Expedient access to branched allylic silanes by copper-catalysed allylic substitution of linear allylic halides. Chemical Communications 46(4) (2010): 568-570.

[49] Mundy, B.P. Phosphorus(III) Bromide. in Encyclopedia of Reagents for Organic Synthesis: John Wiley & Sons, Ltd, 2001.

[50] Firouzabadi, H., Iranpoor, N., and Jafarpour, M. A simple, efficient, and highly selective method for the iodination of alcohols using ZrCl4/NaI. Tetrahedron Letters 45(40) (2004): 7451-7454.

[51] Inouye, M., Konishi, T., and Isagawa, K. Artificial allosteric receptors for nucleotide bases and alkali-metal cations. Journal of the American Chemical Society 115(18) (1993): 8091-8095.

[52] Chang, K.-C., Su, I.-H., Senthilvelan, A., and Chung, W.-S. Triazole-Modified Calix[4]crown as a Novel Fluorescent On–Off Switchable Chemosensor. Organic Letters 9(17) (2007): 3363-3366.

[53] Kim, J.S., et al. Metal Ion Sensing Novel Calix[4]crown Fluoroionophore with a Two-Photon Absorption Property. Journal of Organic Chemistry 71(21) (2006): 8016-8022.

[54] Kumar, M., Dhir, A., and Bhalla, V. Regulation of metal ion recognition by allosteric effects in thiacalix[4]crown based receptors. Tetrahedron 65(36) (2009): 7510-7515.

[55] Lin, F., Cheng, S.Z.D., and Harris, F.W. Aromatic poly(pyridinium salt)s. Part 3. Photoreduction in amide solvents. Polymer 43(12) (2002): 3421-3430.

[56] Hapuarachchige, S., et al. Design and Synthesis of a New Class of Membrane-Permeable Triazaborolopyridinium Fluorescent Probes. Journal of the American Chemical Society 133(17) (2011): 6780-6790.

[57] Görner, H. Charge transfer fluorescence of trans-stryrylpyridinium iodides. Journal of Photochemistry and Photobiology A: Chemistry 218(2–3) (2011): 199-203.

[58] Nabeshima, T., Inaba, T., Furukawa, N., Hosoya, T., and Yano, Y. Artificial allosteric ionophore: regulation of ion recognition of polyethers bearing bipyridine moieties by copper(I). Inorganic Chemistry 32(8) (1993): 1407-1416.

[59] Kim, J., Morozumi, T., and Nakamura, H. Discriminating Detection between Mg2+ and Ca2+ by Fluorescent Signal from Anthracene Aromatic Amide Moiety. Organic Letters 9(22) (2007): 4419-4422.

[60] Acharya, S. and Rebery, B. Fluorescence spectrometric study of eosin yellow dye–surfactant interactions. Arabian Journal of Chemistry 2(1) (2009): 7-12.

[61] De, S., Girigoswami, A., and Mandal, S. Enhanced fluorescence of triphenylmethane dyes in aqueous surfactant solutions at supramicellar concentrations—effect of added electrolyte. Spectrochimica Acta Part A: Molecular and Biomolecular Spectroscopy 58(12) (2002): 2547-2555.

[62] Appell, M. and Bosma, W.B. Effect of surfactants on the spectrofluorimetric properties of zearalenone. Journal of Luminescence 131(11) (2011): 2330-2334.

[63] Grases, F., Genestar, C., and Gil, J.J. Effect of surfactants on the fluorescence intensity of organic reagents. Microchemical Journal 31(1) (1985): 44-49.

[64] Osa, M., Itoda, Y., Suzuki, Y., Yumoto, T., and Yoshida, A. A fluorescence probe study on the effects of surfactants on cloud points in aqueous poly(N-isopropylacrylamide) solutions. Polymer Japan 47(1) (2015): 59-65.

[65] Tolosa, J. and H. F. Bunz, U. Water Soluble Cruciforms: Effect of Surfactants on Fluorescence. Chemistry – An Asian Journal 4(2) (2009): 270-276.

[66] Koley, D. and Bard, A.J. Triton X-100 concentration effects on membrane permeability of a single HeLa cell by scanning electrochemical microscopy (SECM). Proceedings of the National Academy of Sciences 107(39) (2010): 16783-16787.

[67] Yu, D., Huang, F., and Xu, H. Determination of critical concentrations by synchronous fluorescence spectrometry. Analytical Methods 4(1) (2012): 47-49.

[68] Britton, H.T.S. and Robinson, R.A. CXCVIII.-Universal buffer solutions and the dissociation constant of veronal. Journal of the Chemical Society (Resumed) (0) (1931): 1456-1462.

[69] Reynolds Iii, J.E., Josowicz, M., Tyler, P., Vegh, R.B., and Solntsev, K.M. Spectral and redox properties of the GFP synthetic chromophores as a function of pH in buffered media. Chemical Communications 49(71) (2013): 7788-7790.

[70] Liu, Q., Hong Su, X., Ying Wang, L., Sun, W., Bo Lei, Y., and Yi Wen, Z. An OFF–ON–OFF type of pH fluorescent sensor: Benzo[c,d]indole-based dimethine

cyanine dye-synthesis, spectral properties and density functional theory studies. Journal of Luminescence 154(0) (2014): 124-130.

APPENDIX

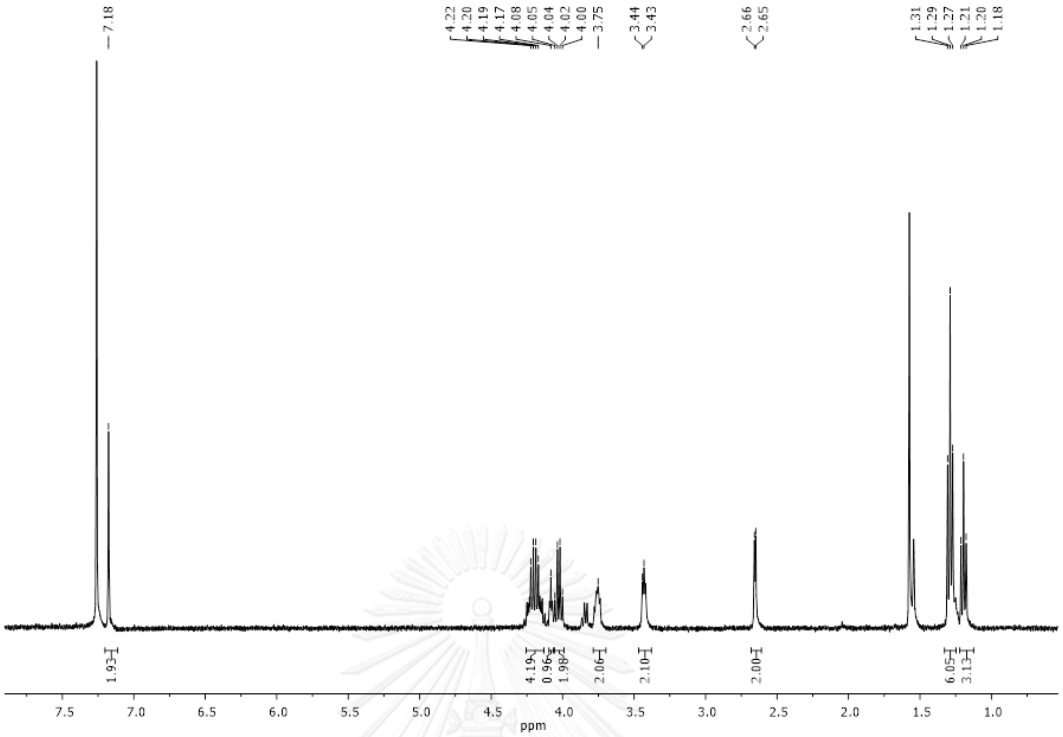

Figure A1 ^{1}H NMR of **1b** in $CDCl_3$

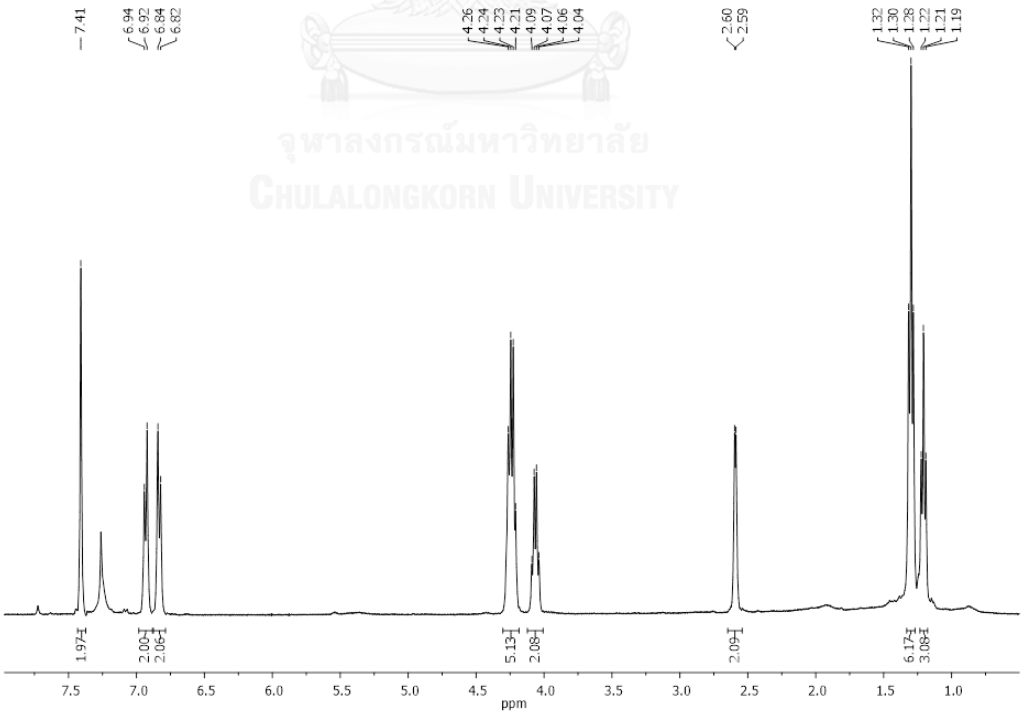

Figure A2 ^{1}H NMR of **1c** in $CDCl_3$

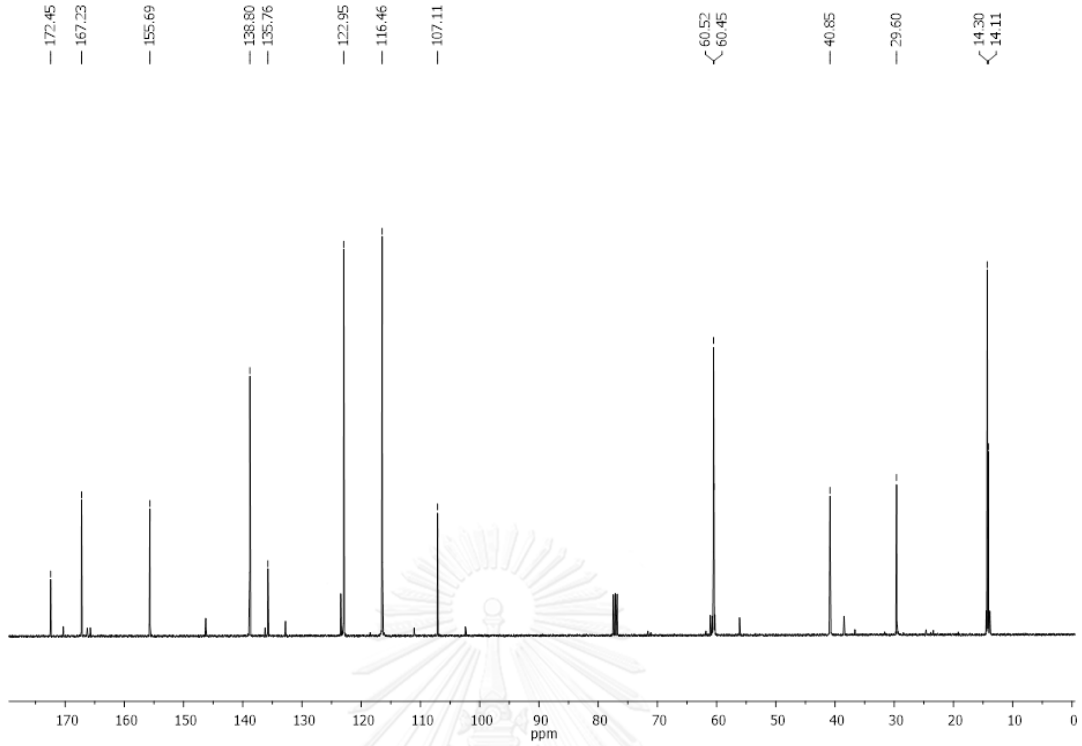

Figure A3 ^{13}C NMR of **1c** in $CDCl_3$

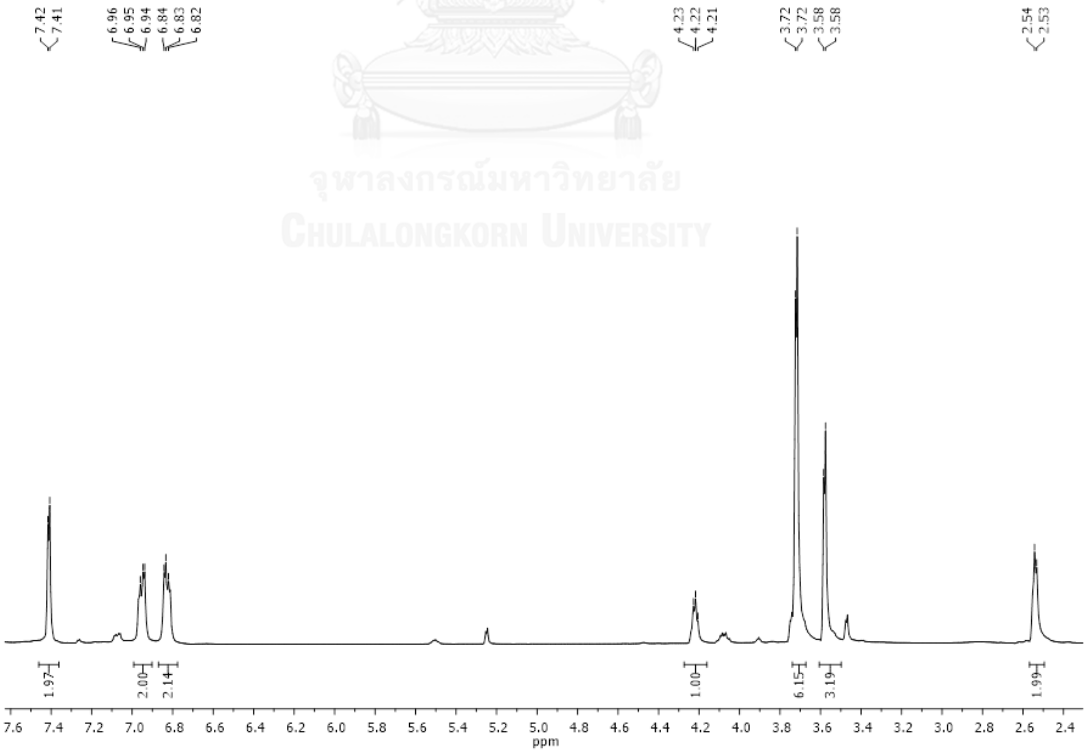

Figure A4 ^{1}H NMR of **1d** in $CDCl_3$

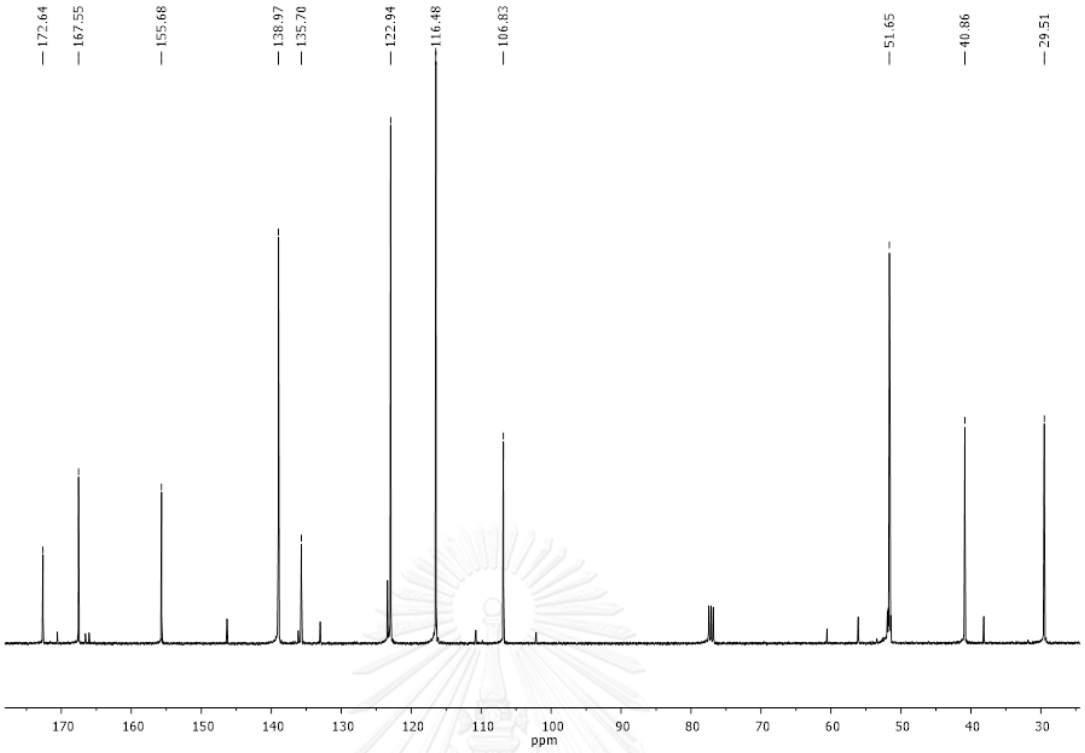

Figure A5 ^{13}C NMR of **1d** in $CDCl_3$

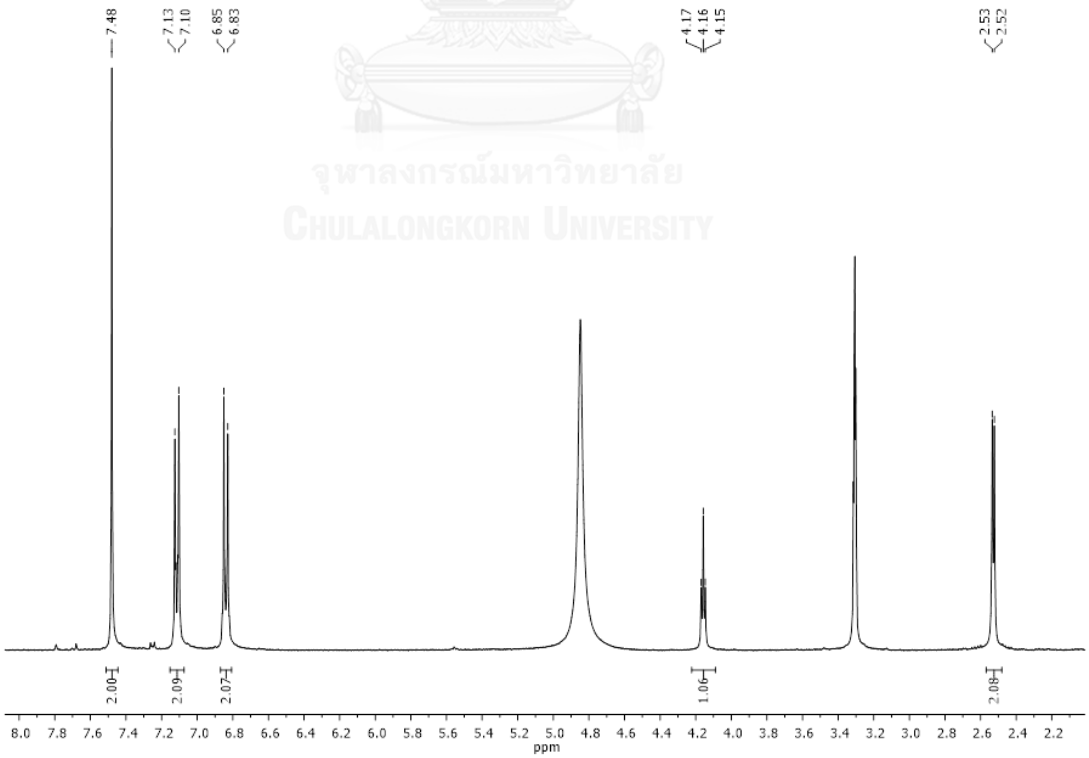

Figure A6 ^{1}H NMR of **2** in $CDCl_3$

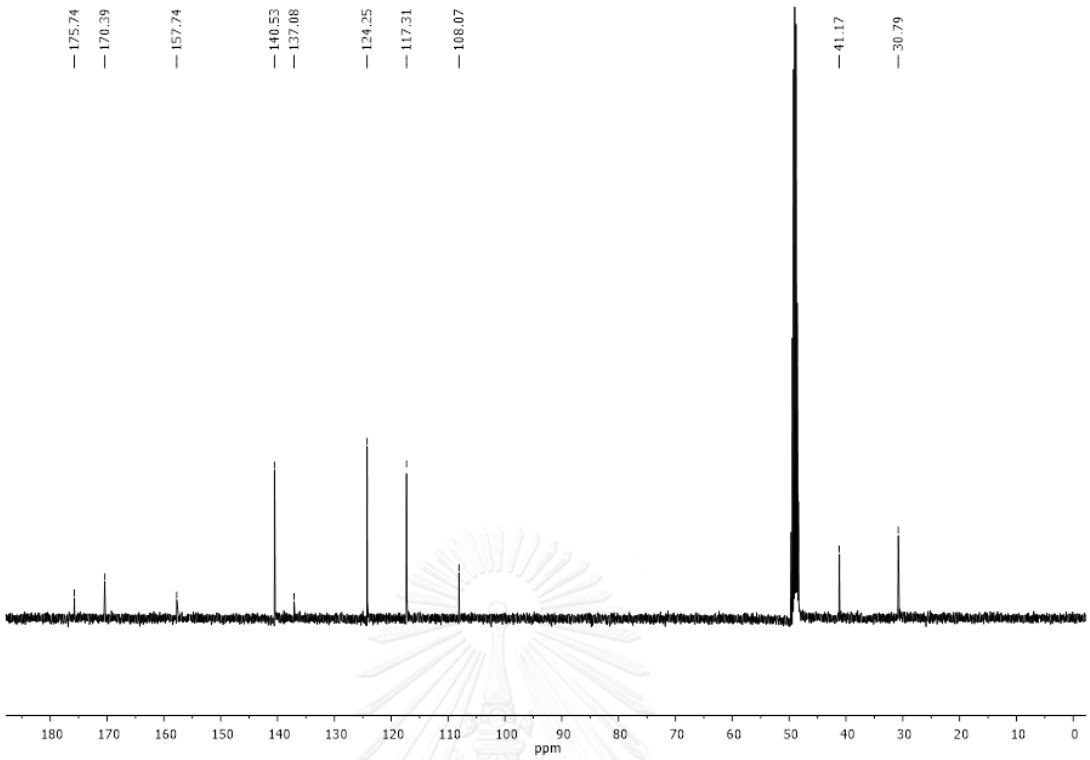

Figure A7 ^{13}C NMR of **2** in $CDCl_3$

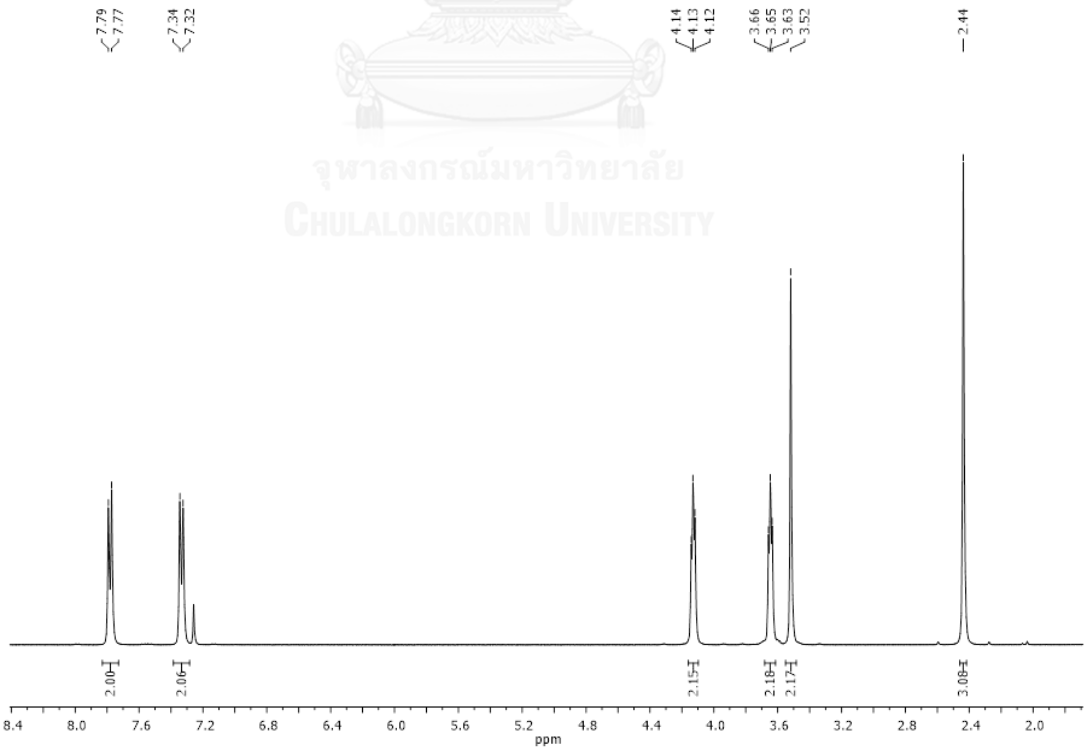

Figure A8 ^{1}H NMR of **3a** in $CDCl_3$

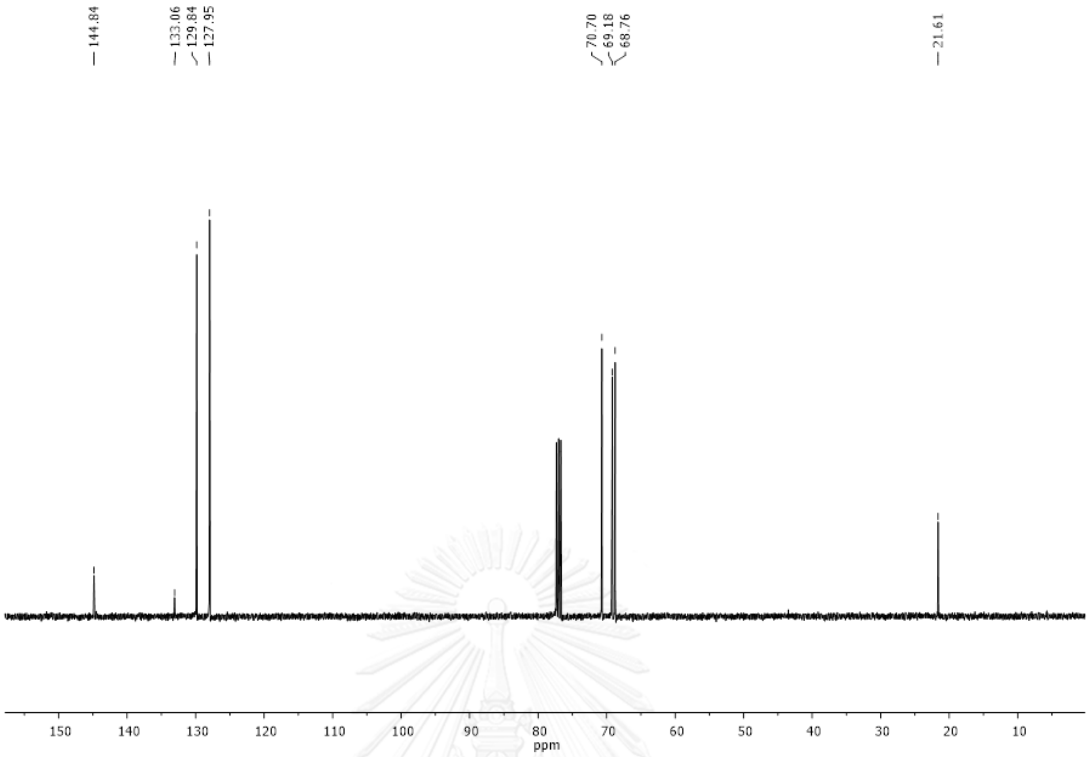

Figure A9 ^{13}C NMR of **3a** in $CDCl_3$

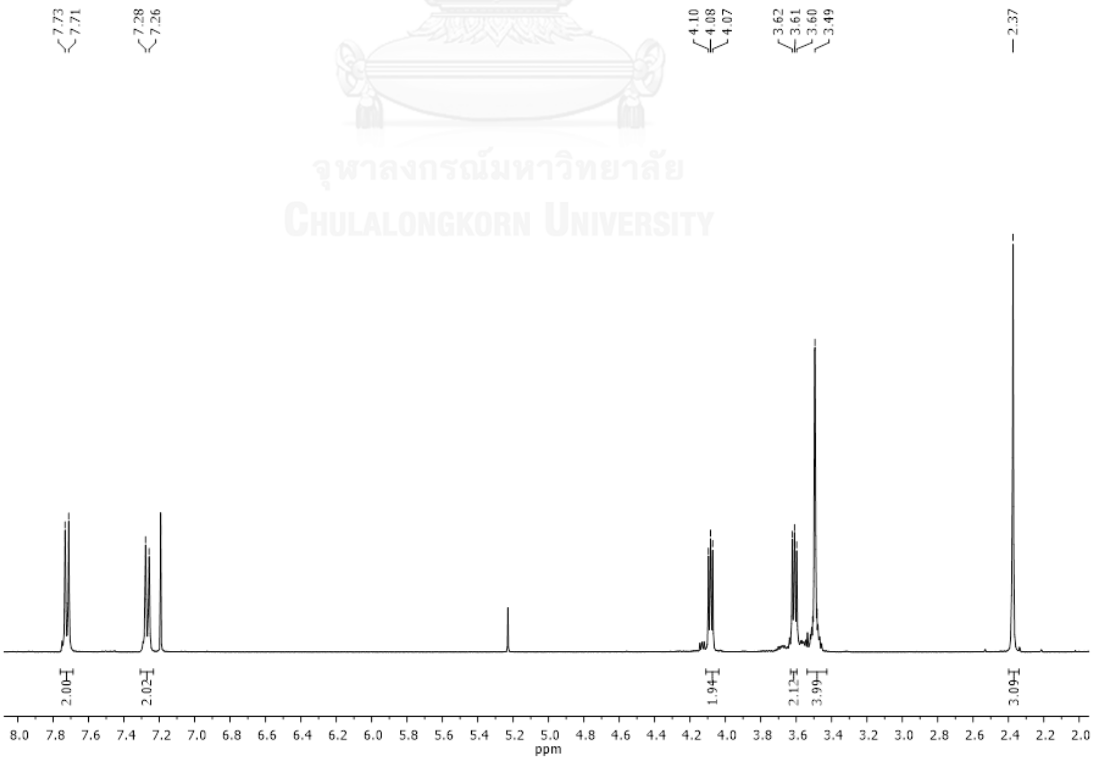

Figure A10 ^{1}H NMR of **3b** in $CDCl_3$

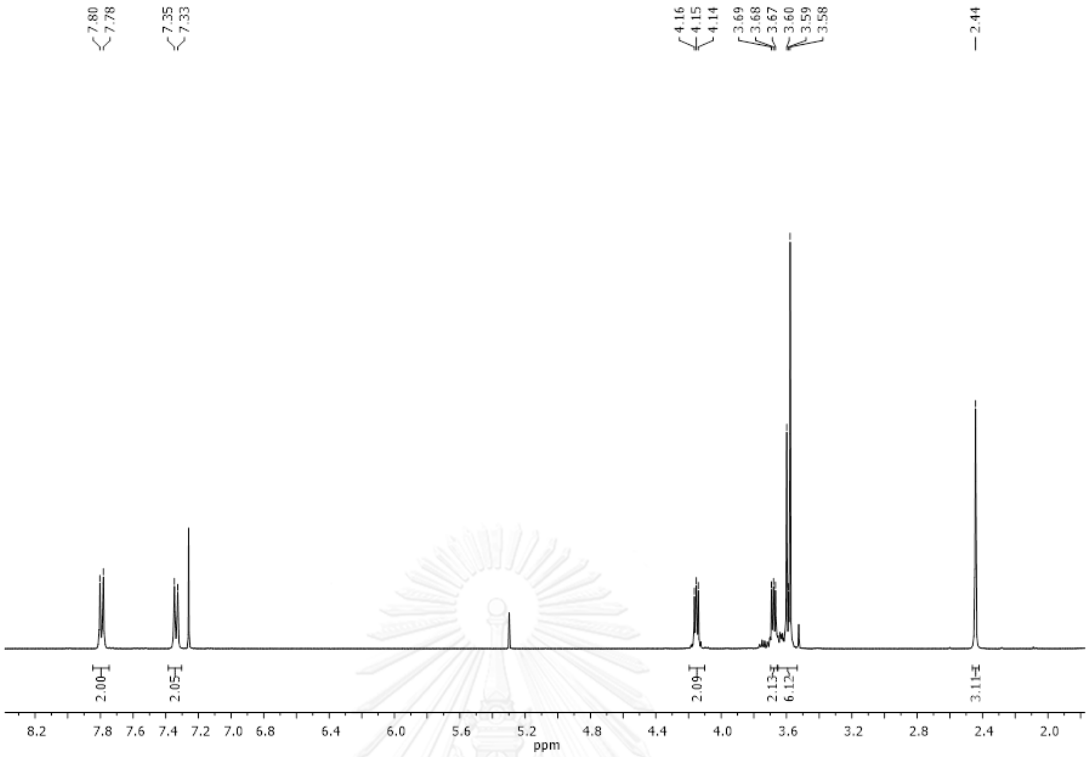

Figure A11 ^{1}H NMR of **3c** in $CDCl_3$

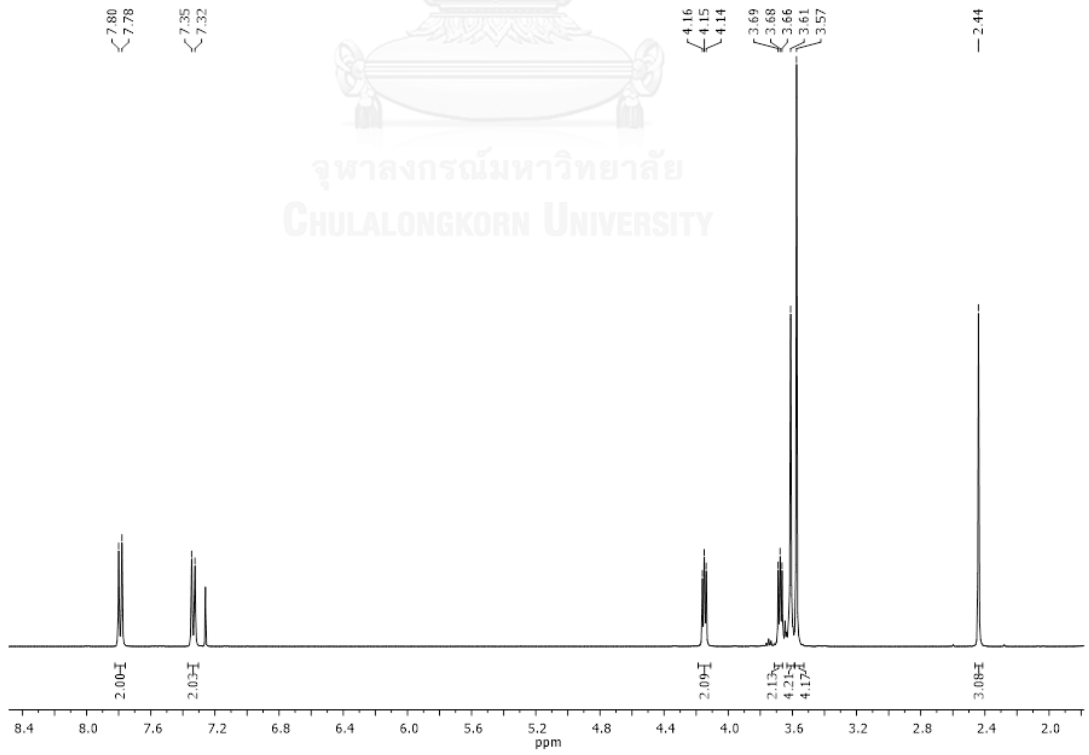

Figure A12 ^{1}H NMR of **3d** in $CDCl_3$

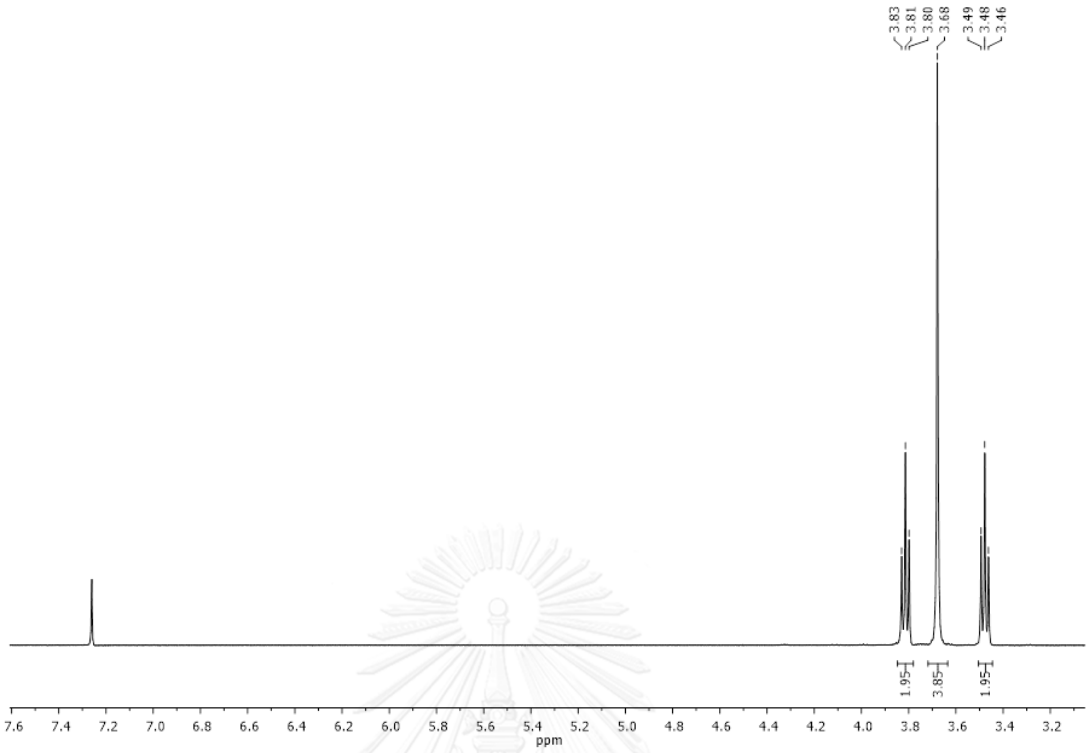

Figure A13 ^{1}H NMR of **4a** in $CDCl_3$

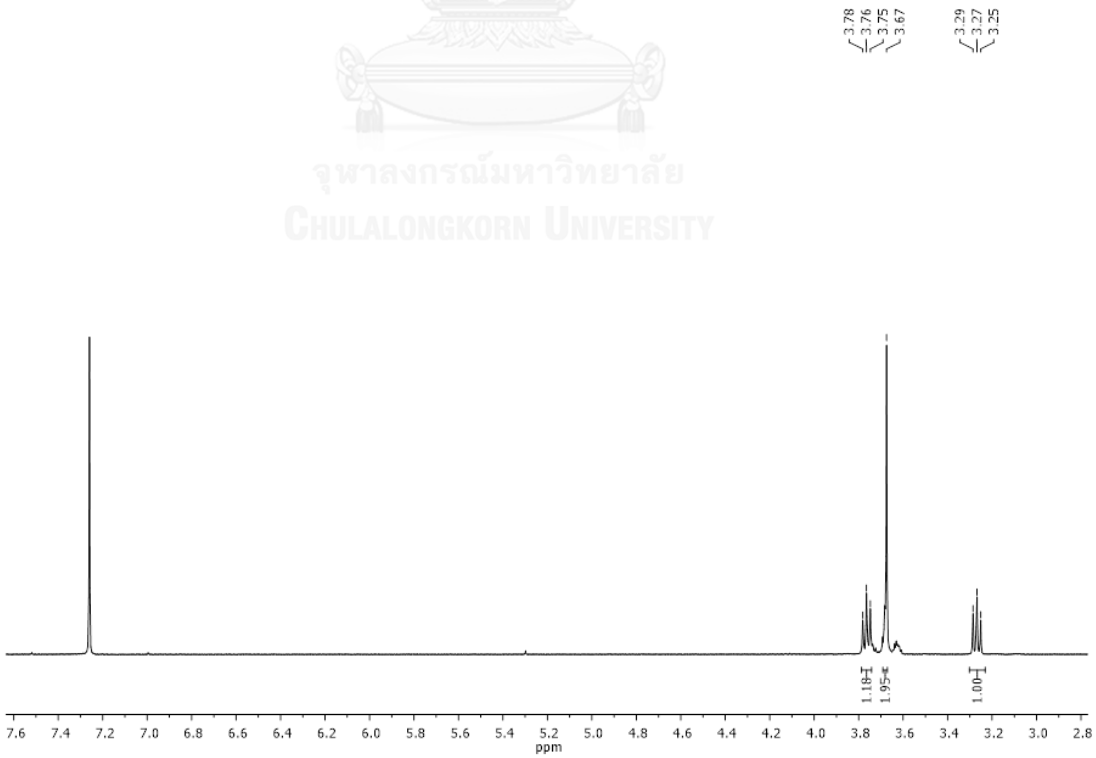

Figure A14 ^{1}H NMR of **4b** in $CDCl_3$

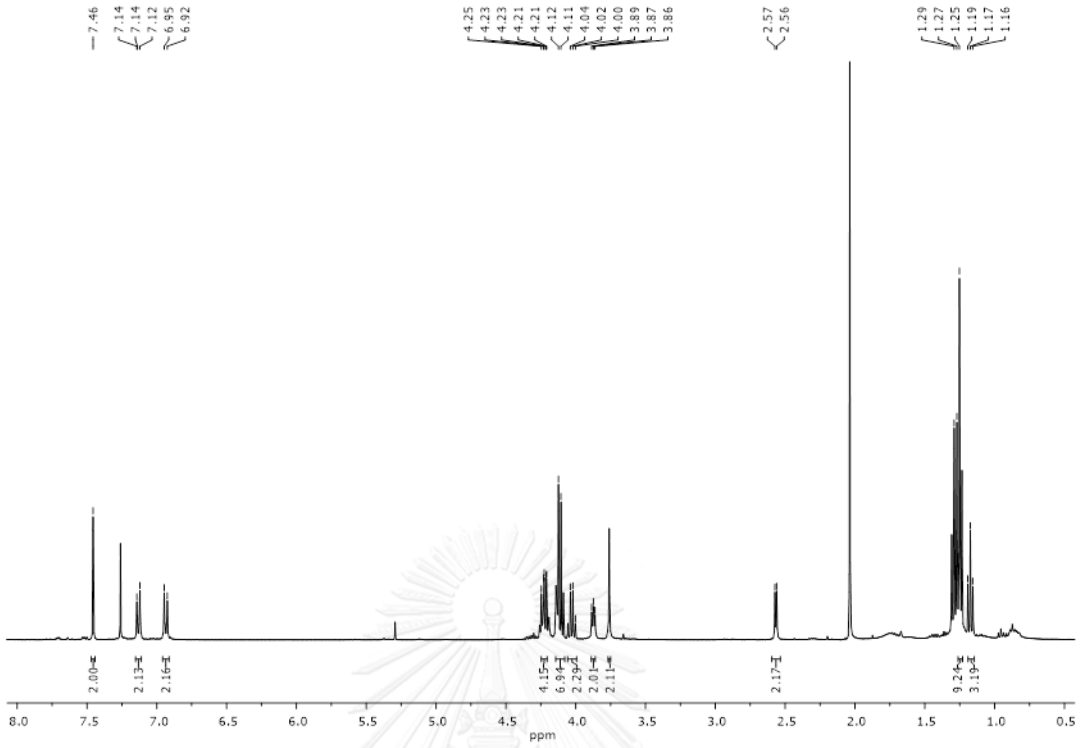

Figure A15 ^{1}H NMR of **5a** in $CDCl_3$

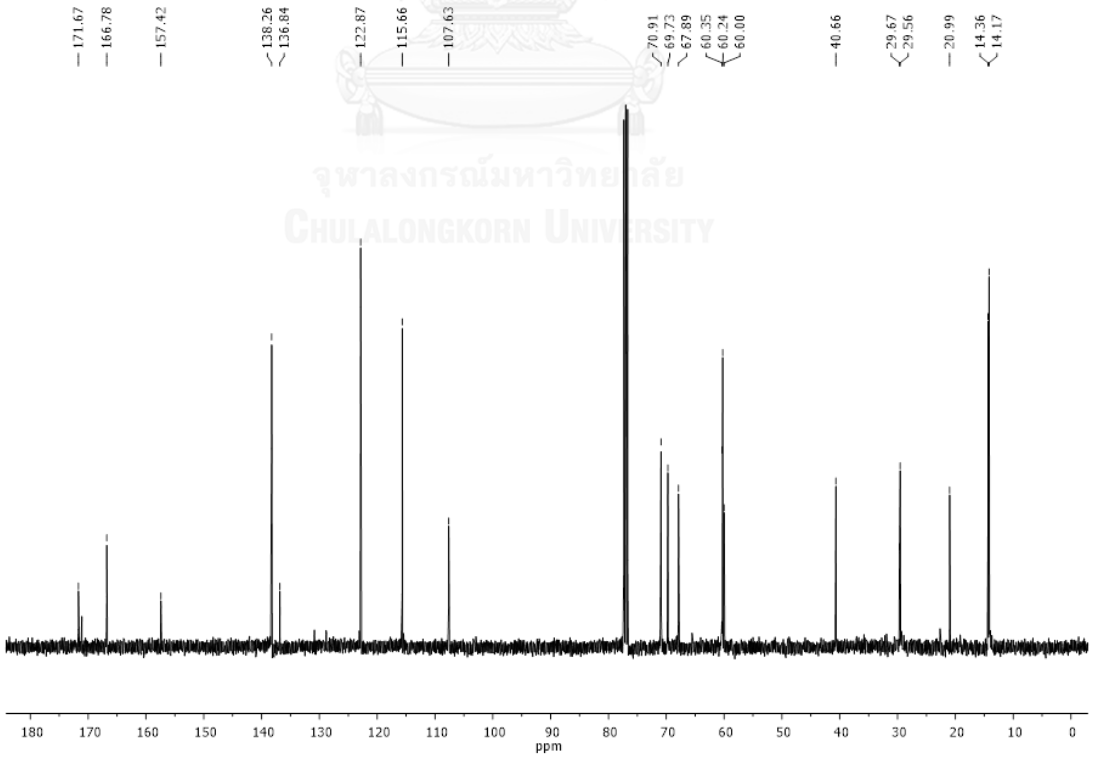

Figure A16 ^{13}C NMR of **5a** in $CDCl_3$

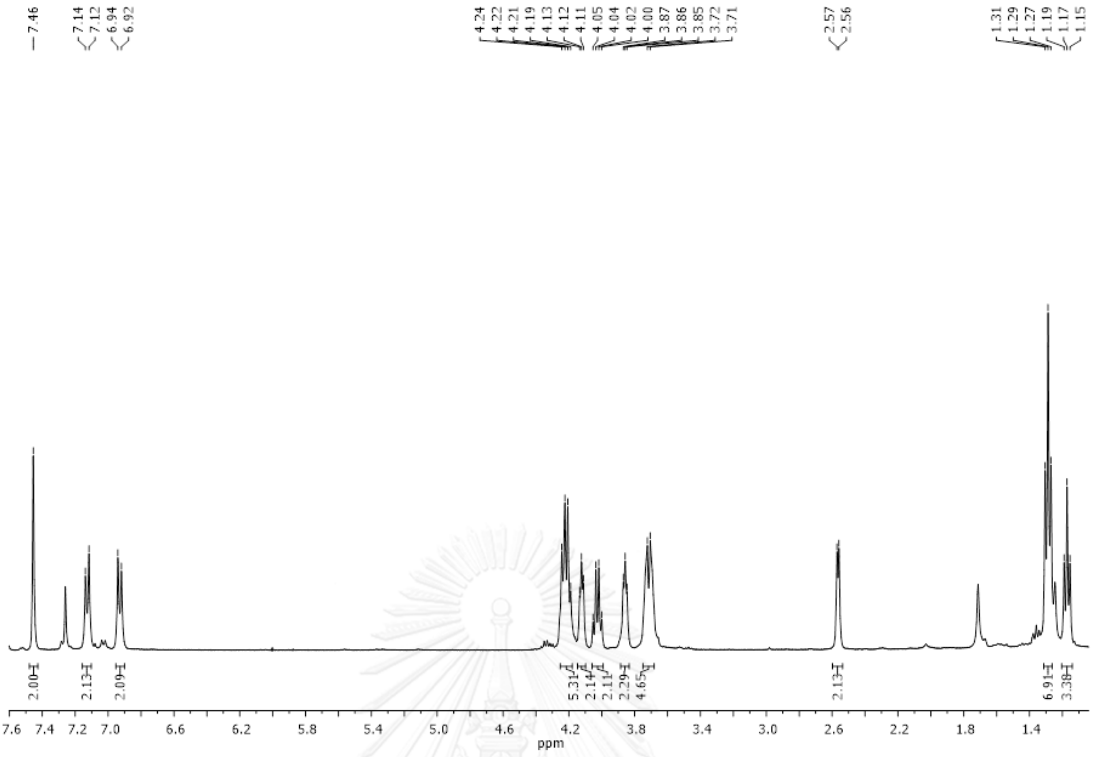

Figure A17 ^{1}H NMR of **5b** in $CDCl_3$

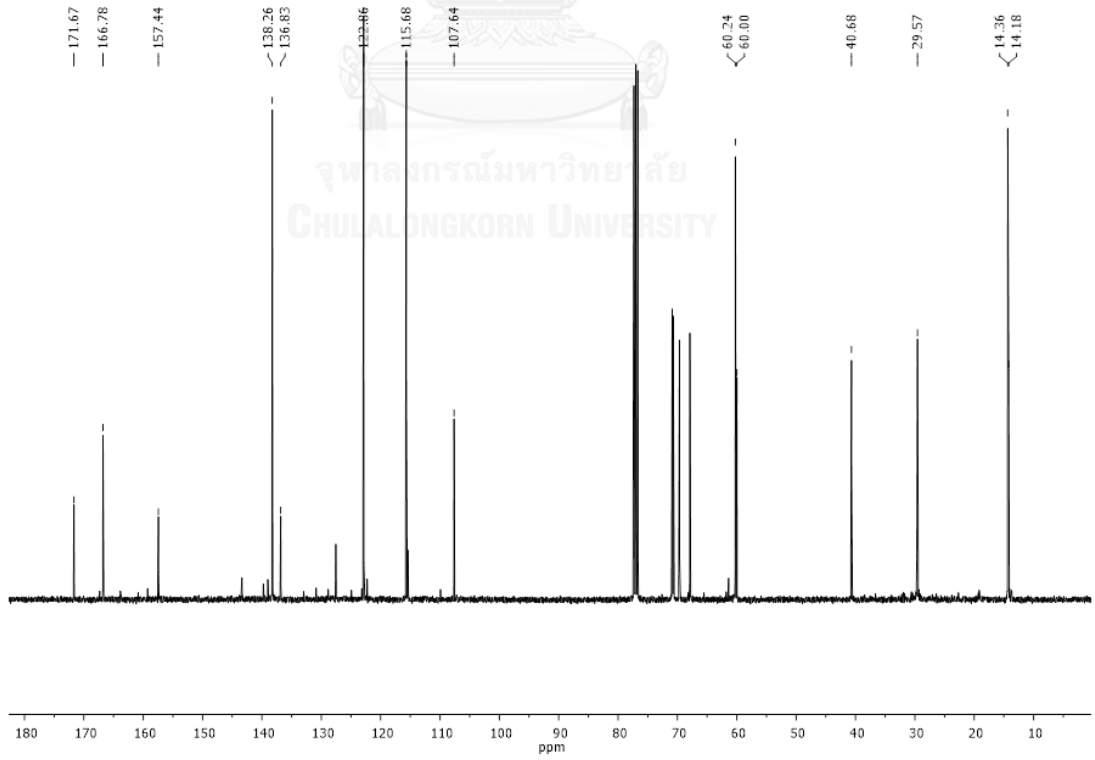

Figure A18 ^{13}C NMR of **5b** in $CDCl_3$

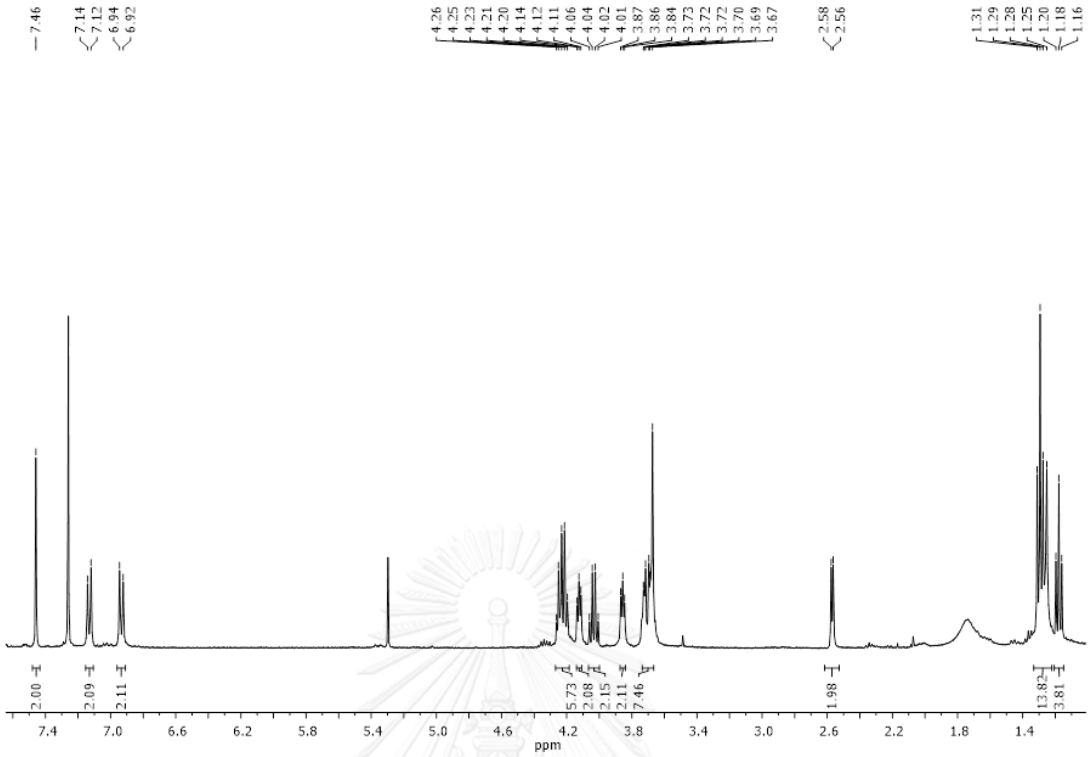

Figure A19 ^{1}H NMR of **5c** in $CDCl_3$

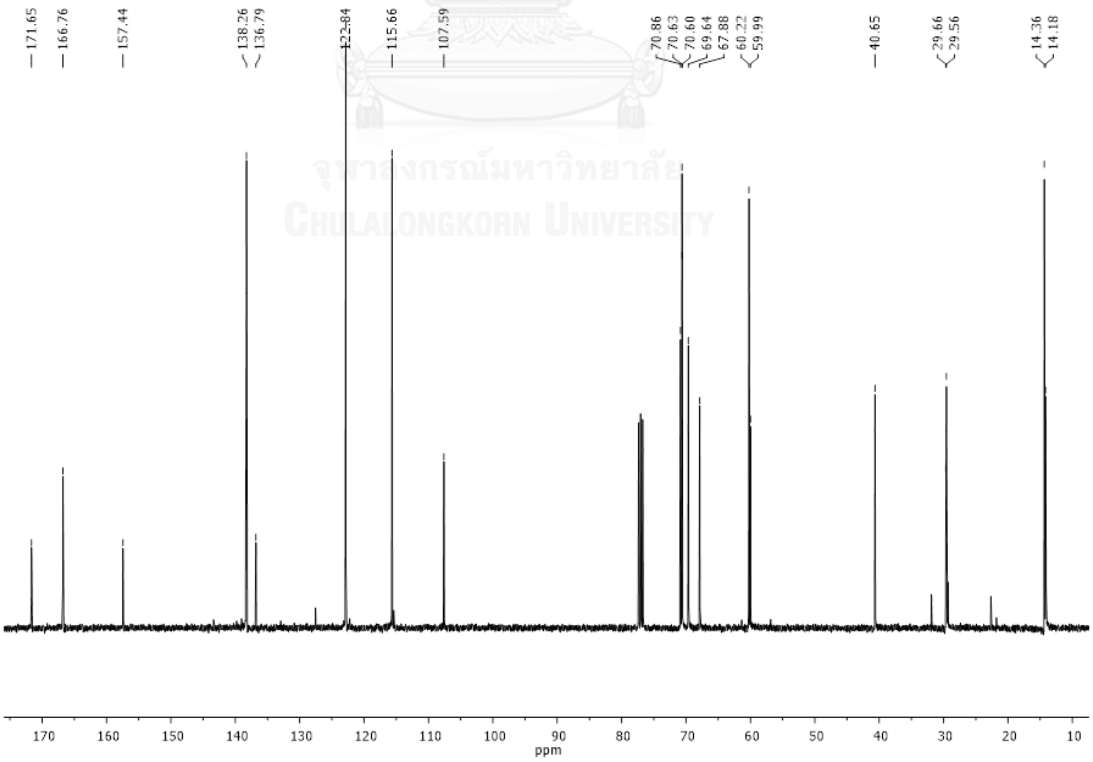

Figure A20 ^{13}C NMR of **5c** in $CDCl_3$

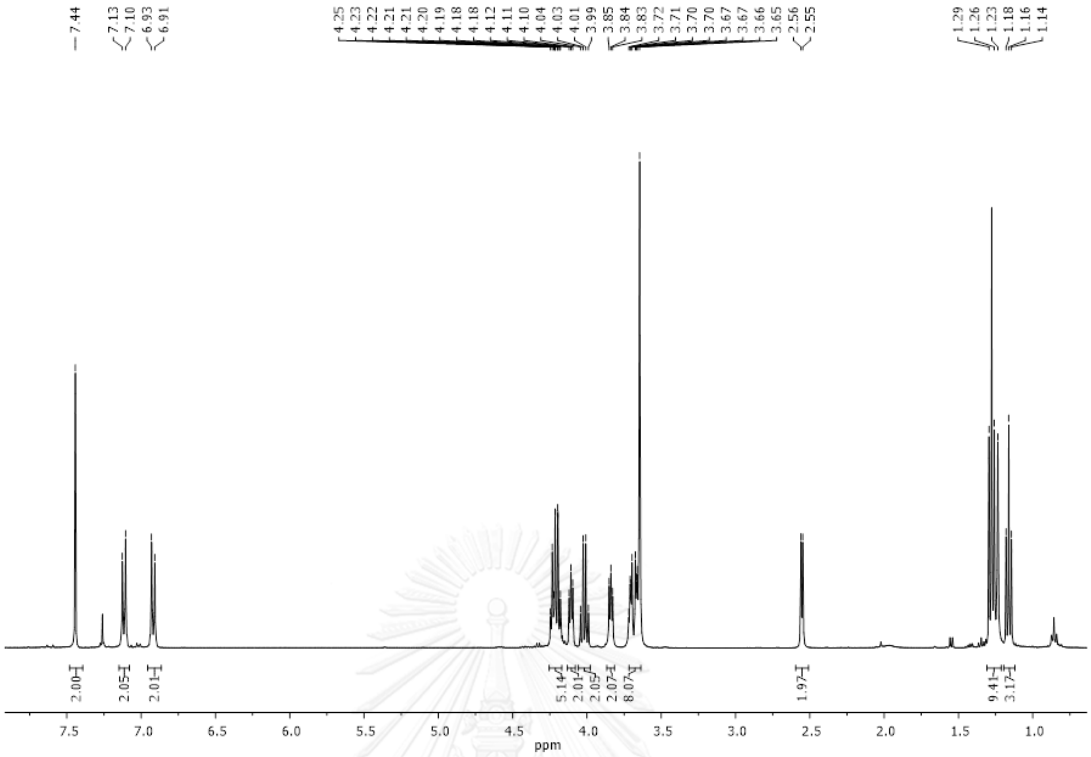

Figure A21 ^{1}H NMR of **5d** in $CDCl_3$

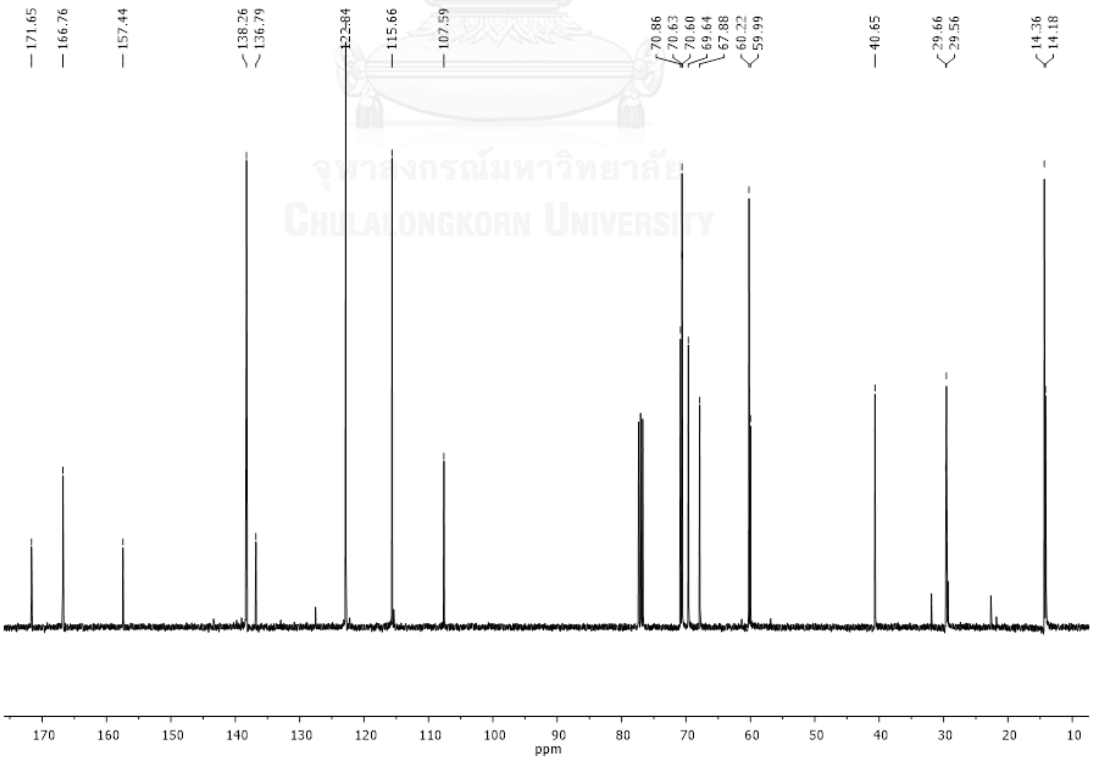

Figure A22 ^{13}C NMR of **5d** in $CDCl_3$

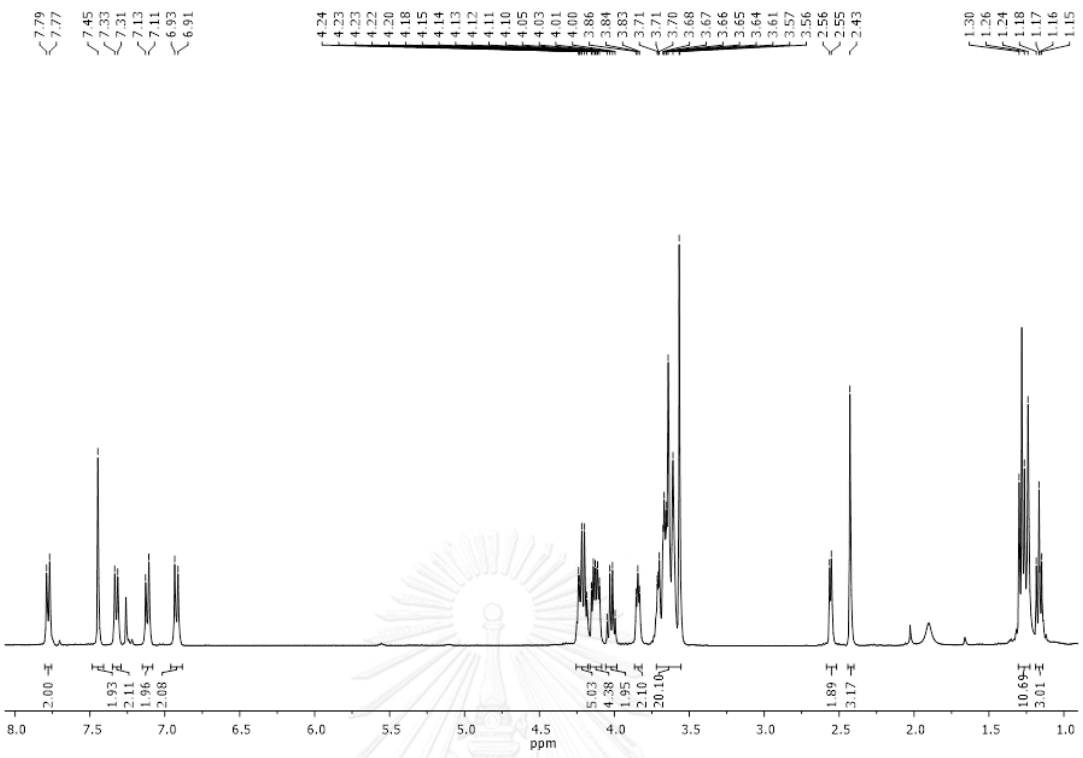

Figure A23 ^{1}H NMR of **6a** in $CDCl_3$

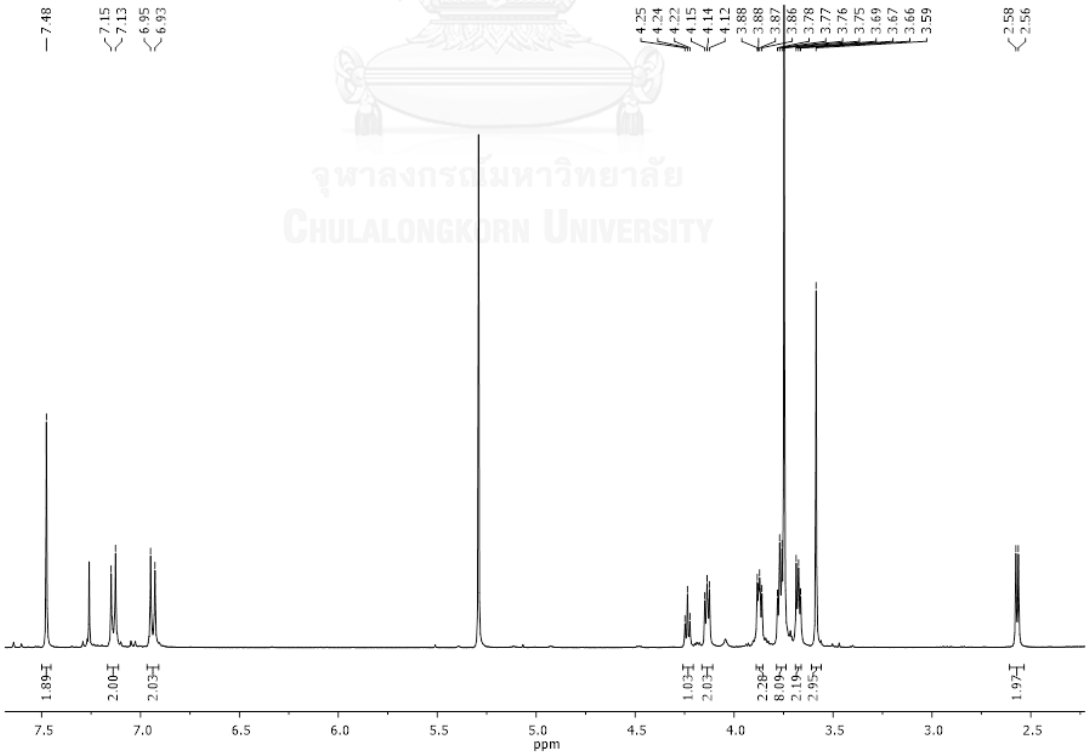

Figure A24 ^{1}H NMR of **6b** in $CDCl_3$

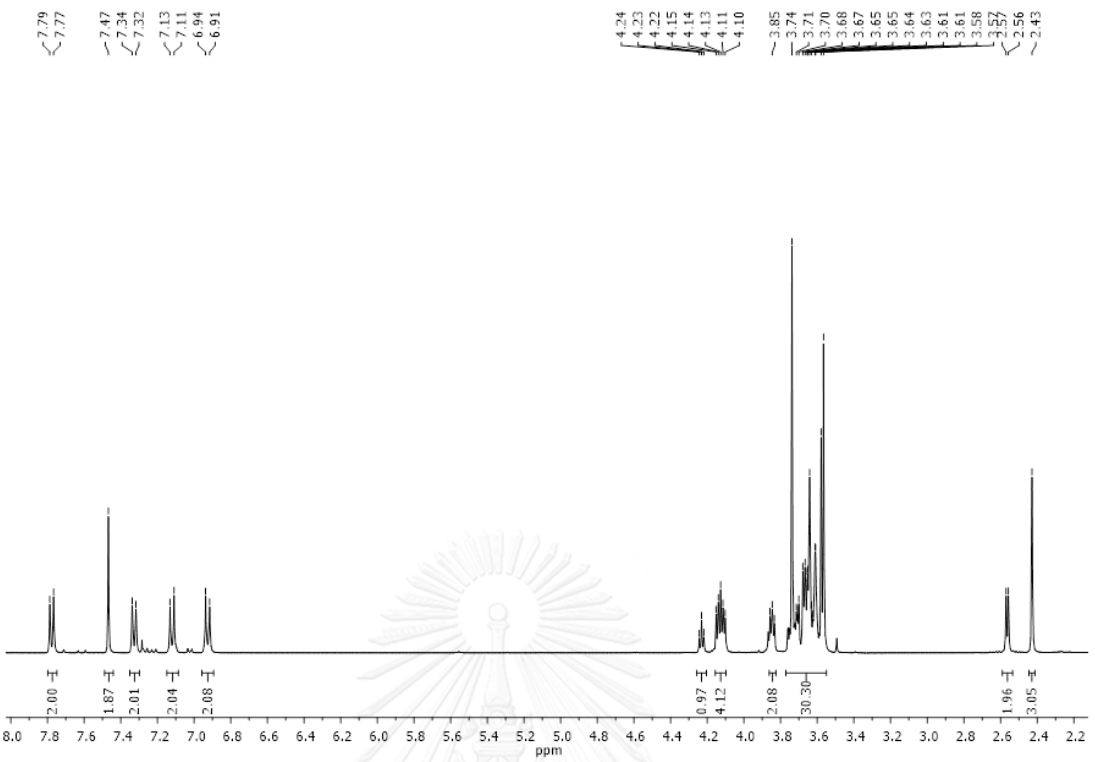

Figure A25 ^{1}H NMR of **6c** in $CDCl_3$

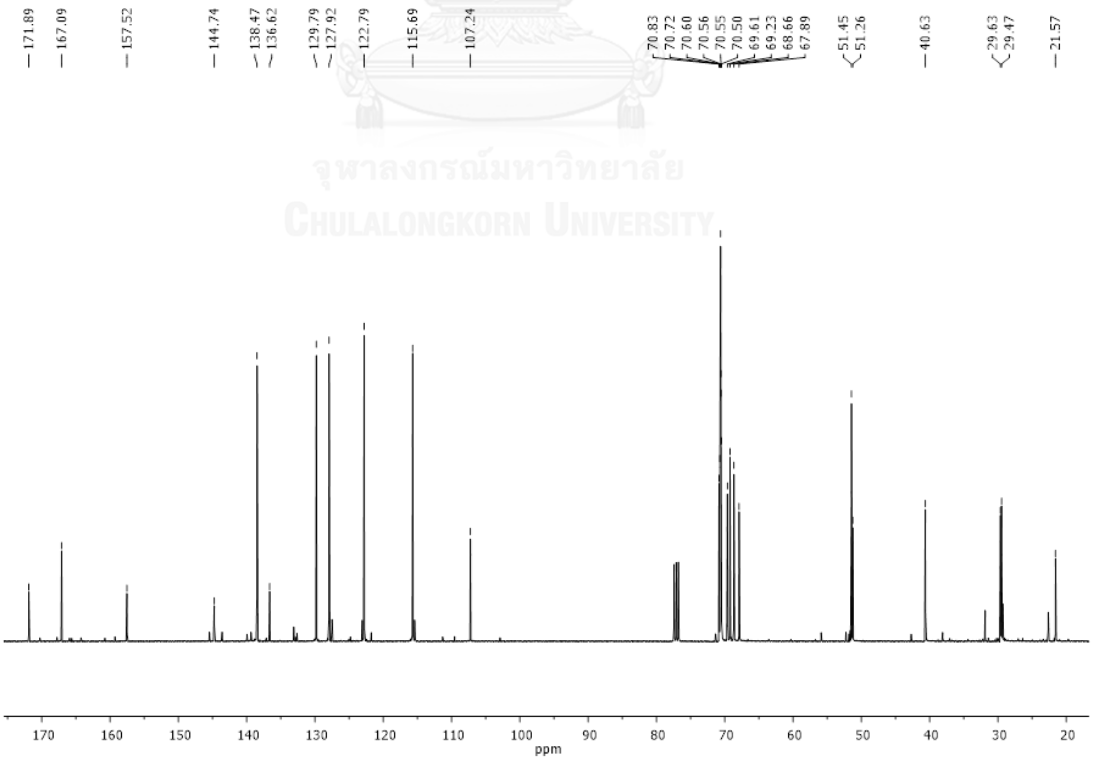

Figure A26 ^{13}C NMR of **6c** in $CDCl_3$

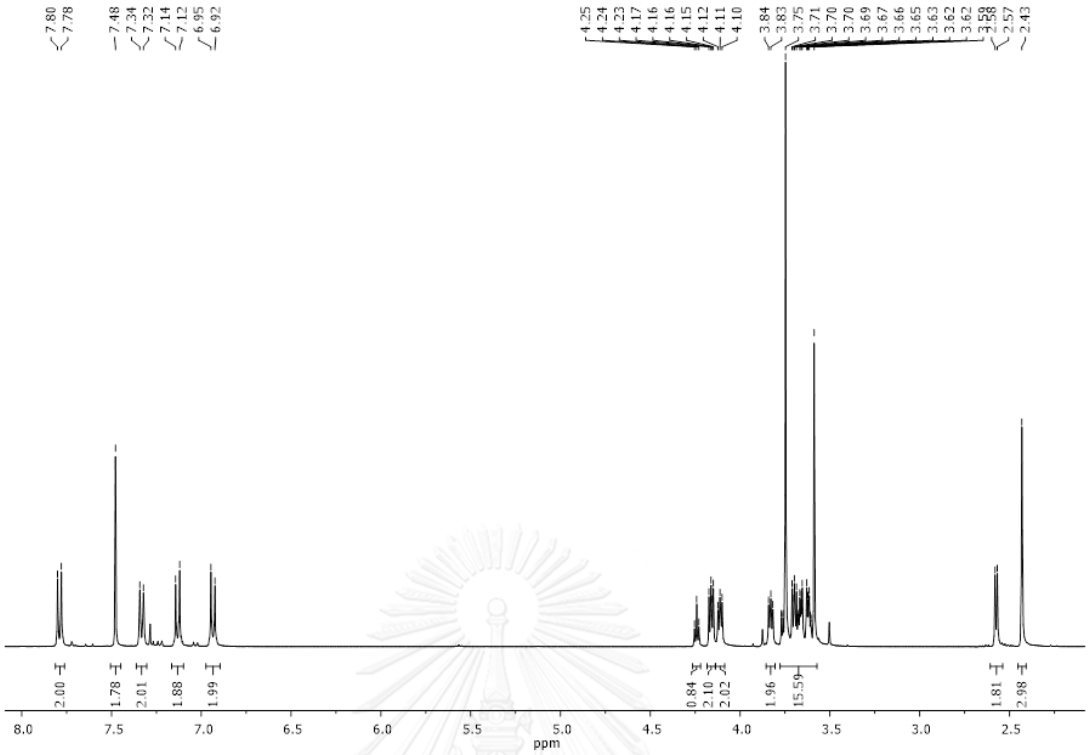

Figure A27 ^{1}H NMR of **6d** in $CDCl_3$

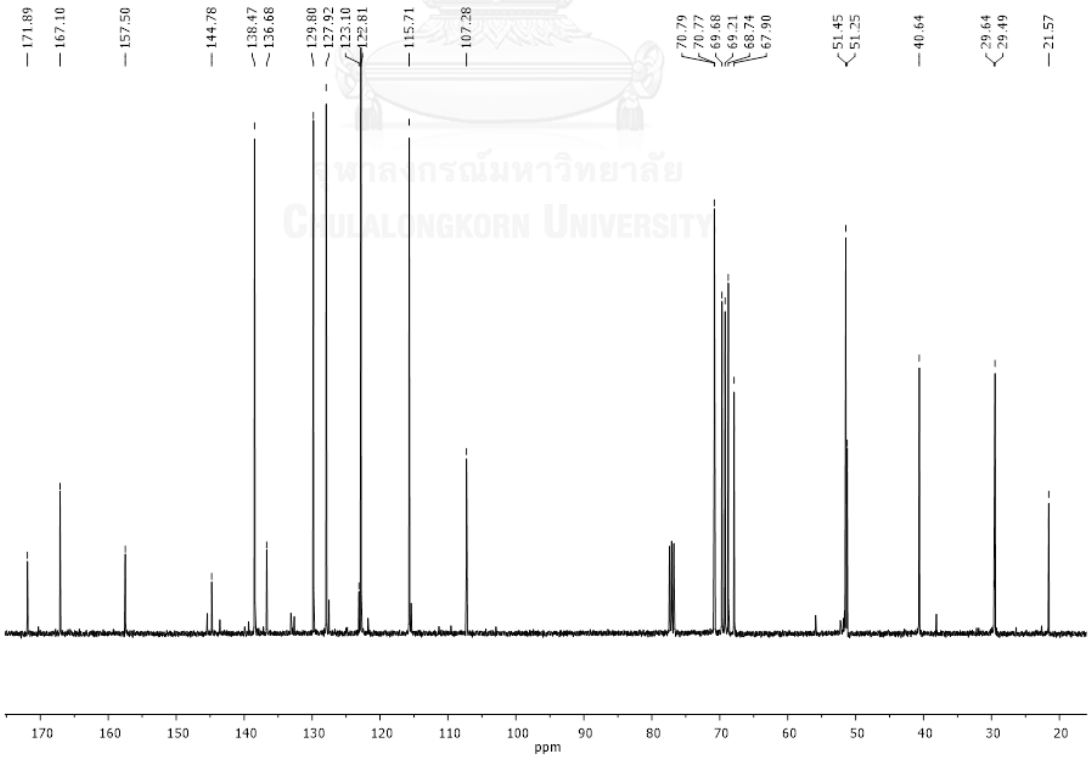

Figure A28 ^{13}C NMR of **6d** in $CDCl_3$

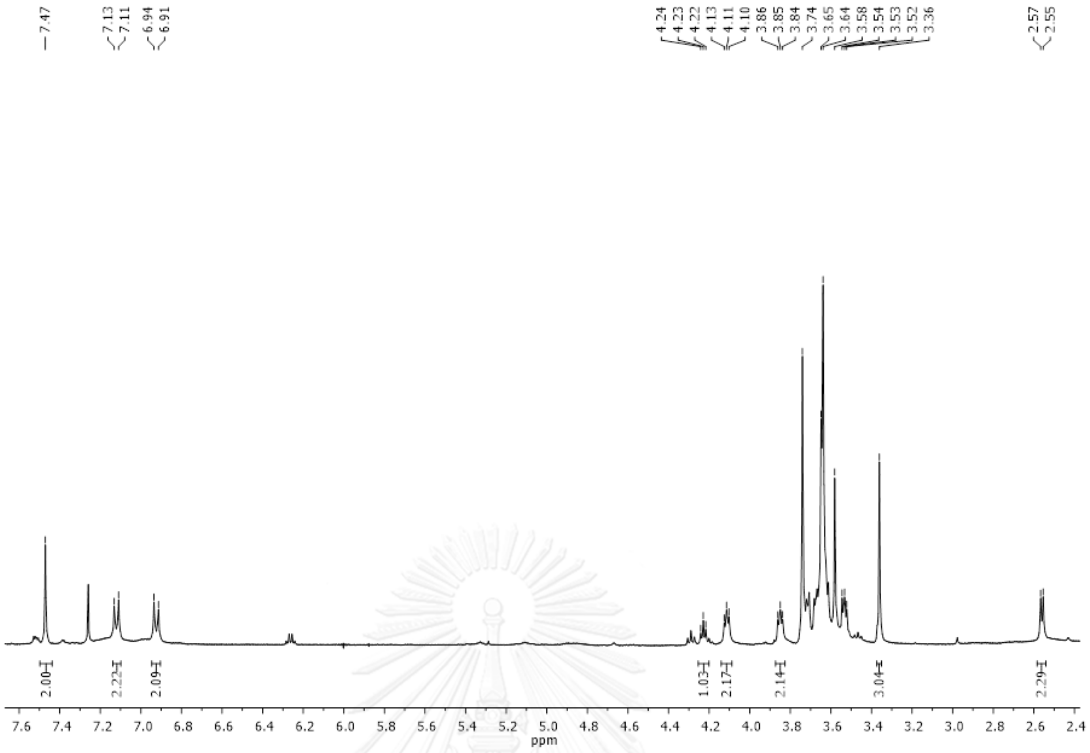

Figure A29 ^{1}H NMR of **7** in MeOD

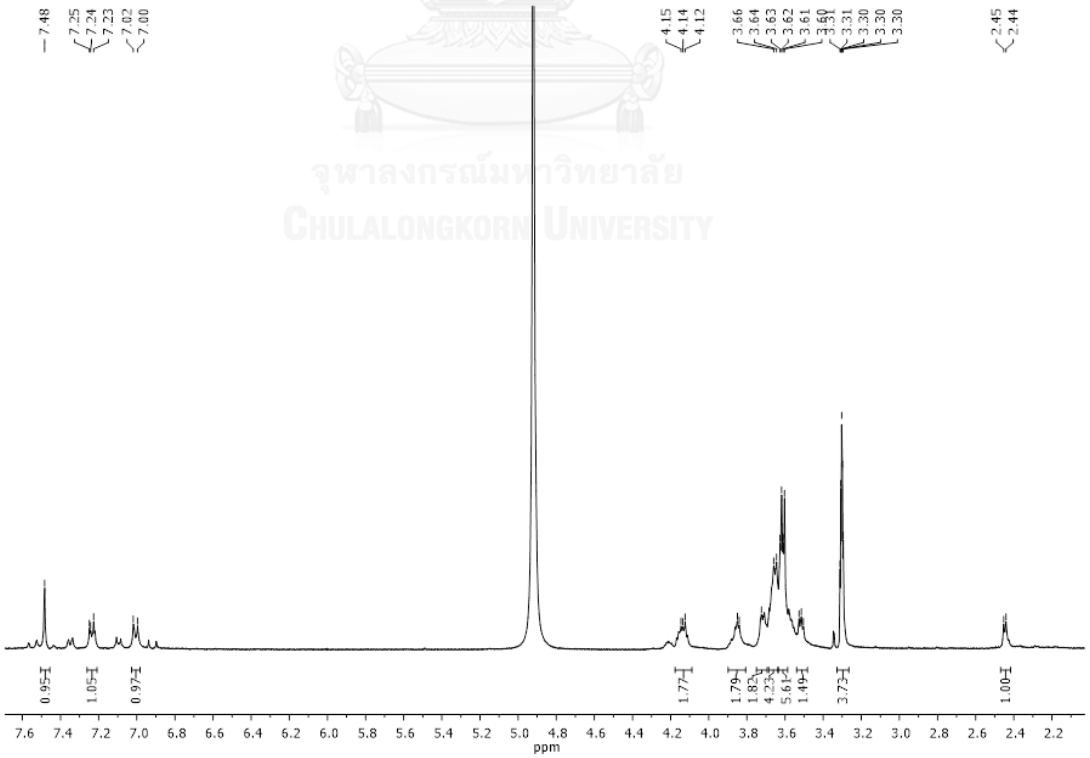

Figure A30 ^{1}H NMR of **8** in MeOD

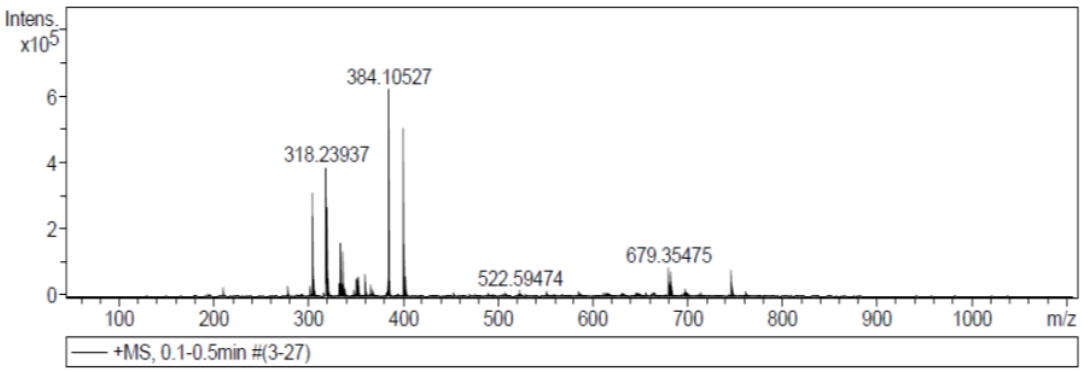

Figure A31 HRMS spectrum of **1c**

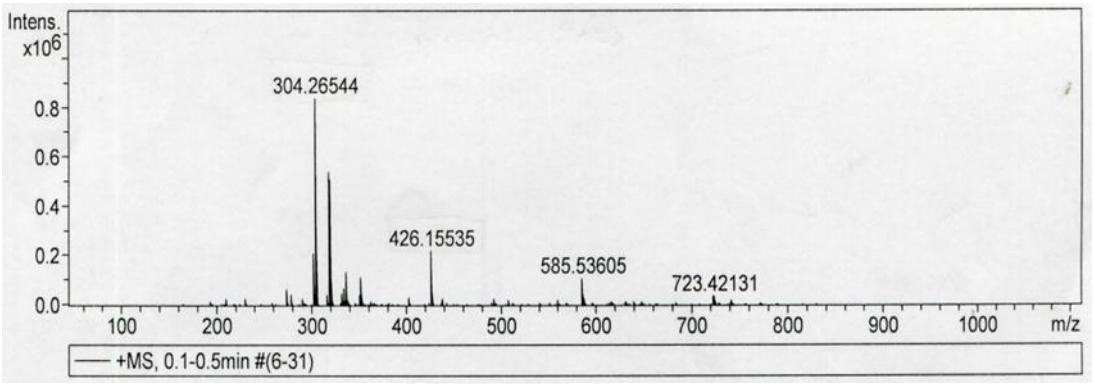

Figure A32 HRMS spectrum of **1d**

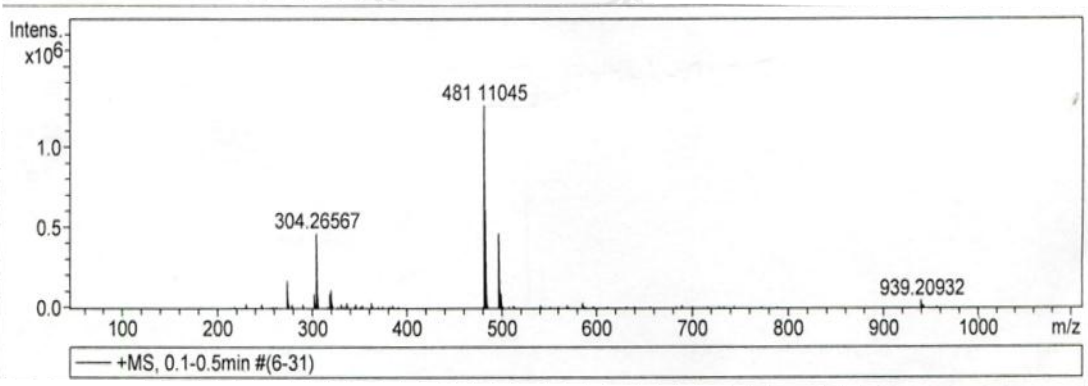

Figure A33 HRMS spectrum of **3a**

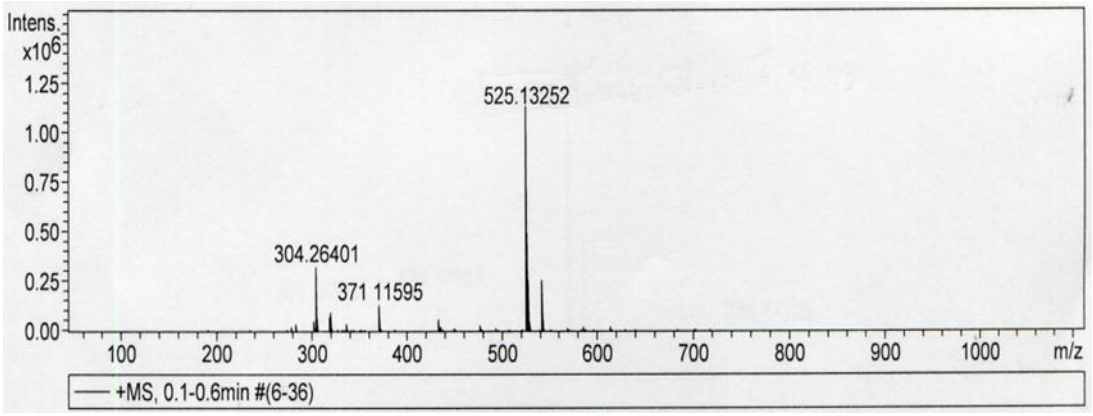

Figure A34 HRMS spectrum of **3b**

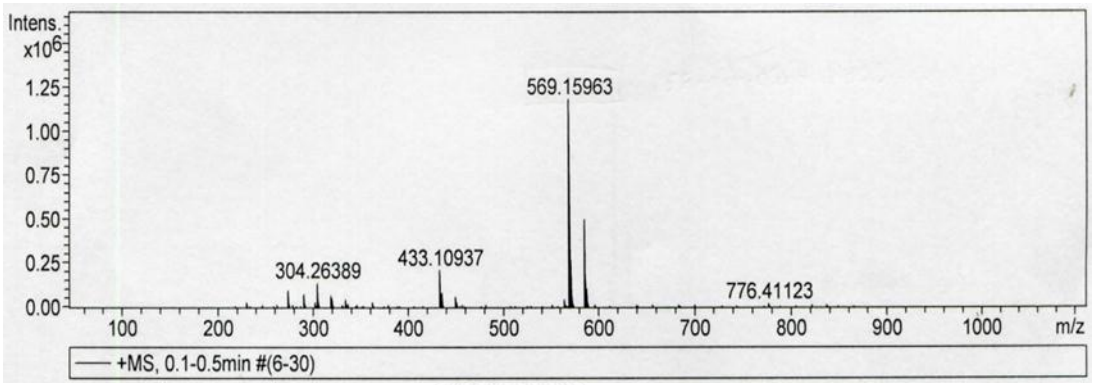

Figure A35 HRMS spectrum of **3c**

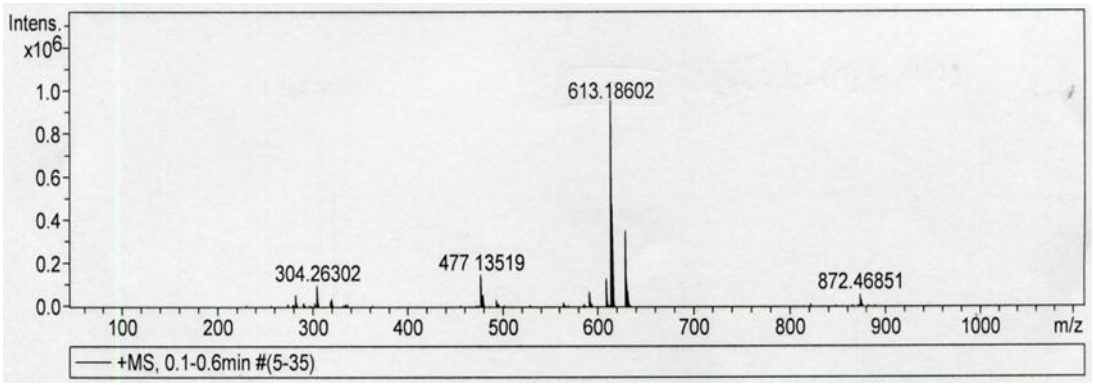

Figure A36 HRMS spectrum of **3d**

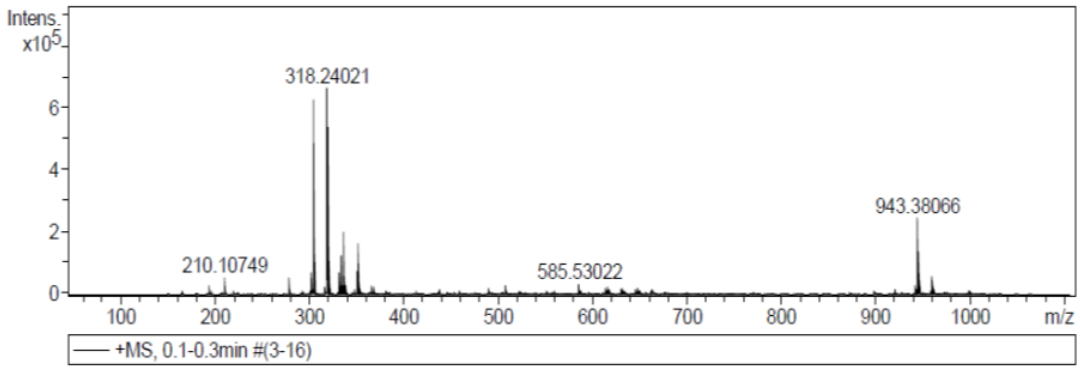

Figure A37 HRMS spectrum of **5a**

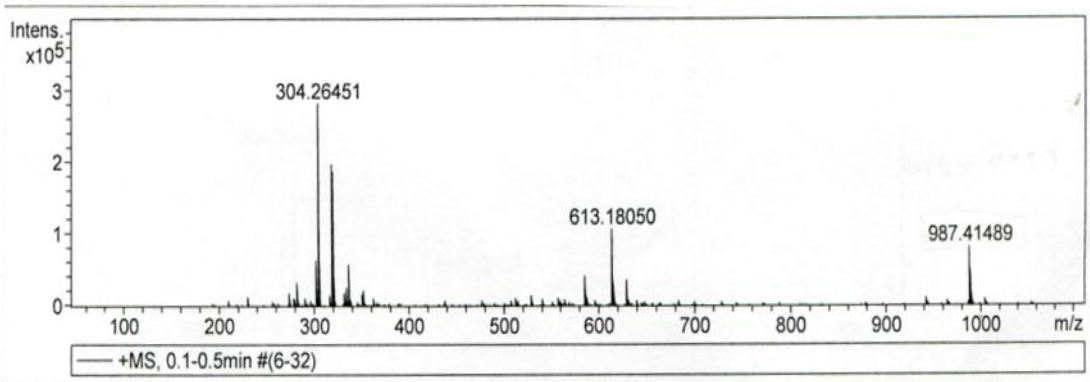

Figure A38 HRMS spectrum of **5b**

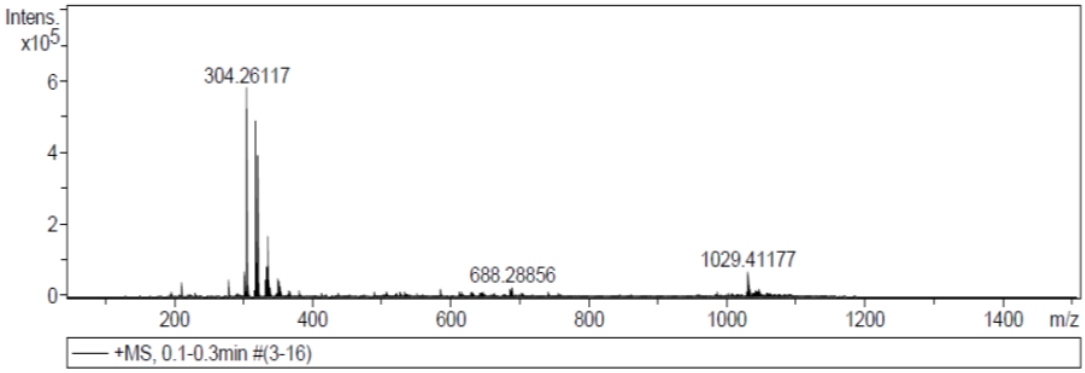

Figure A39 HRMS spectrum of **5c**

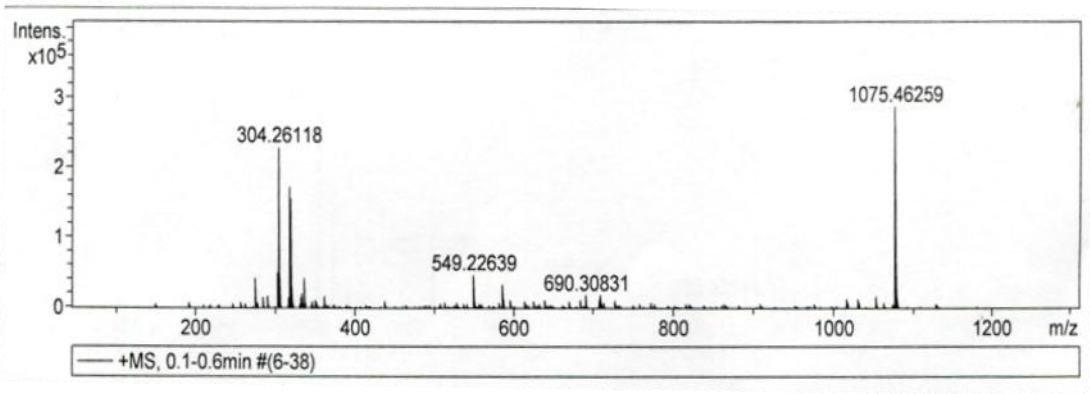

Figure A40 HRMS spectrum of **5d**

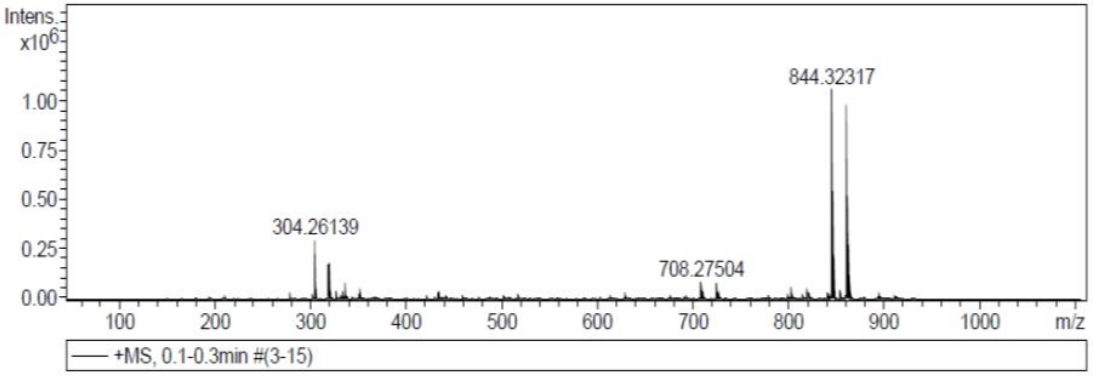

Figure A41 HRMS spectrum of **6a**

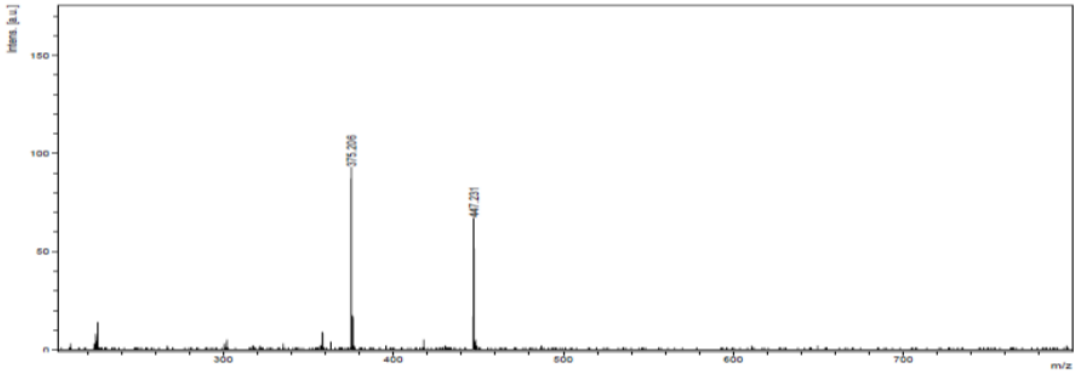

Figure A42 MALI-TOF spectrum of **6b**

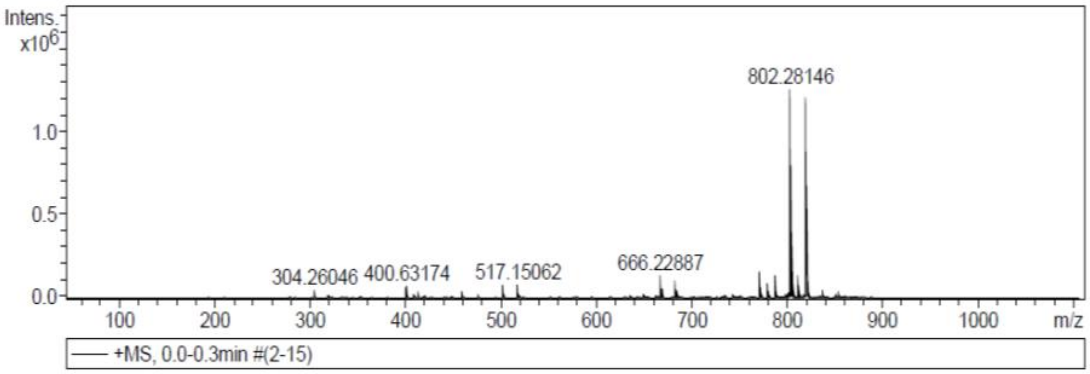

Figure A43 HRMS spectrum of **6c**

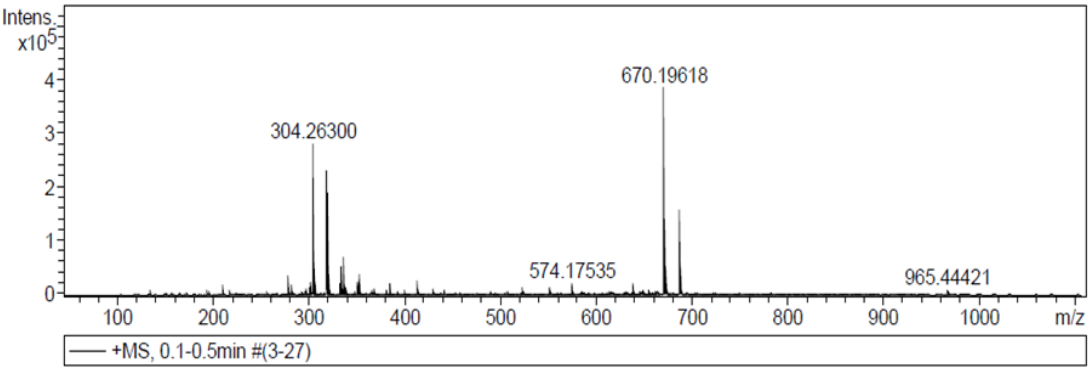

Figure A44 HRMS spectrum of **6d**

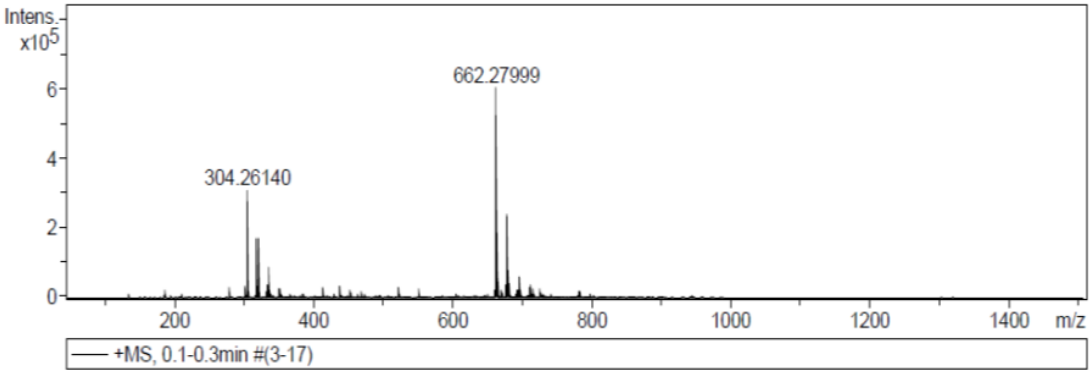

Figure A45 HRMS spectrum of **7**

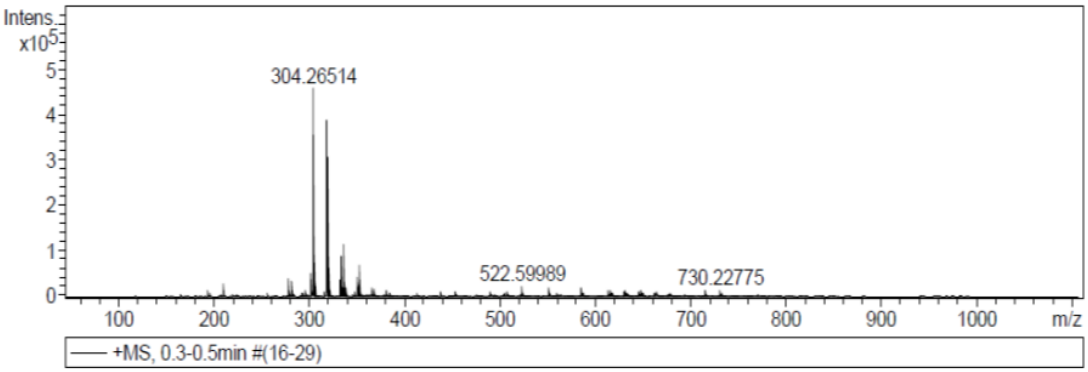

Figure A46 HRMS spectrum of **8**

VITA

Mr.Nattapong Srimuang was born on June 23th, 1988 in Sisaket, Thailand. He graduated with high school degree from Srinagarindra the princess mother school, Sisaket. He graduated in Bachelor Degree of Science, majoring in Chemistry from Khonkaen University in 2010. In 2011, He has been a graduate student in the program of organic chemistry, Faculty of Science, Chulalongkorn University and become a member of Material Advancement via Proficient Synthesis group (MAPS) under supervision of Assist. Prof. Dr. Anavat Ajavakom. During course of study, he received the scholarship from the Development and Promotion of Science and Technology Talents Project (DPST). He had presented his research in The 4th International Conference on Engineering and Applied Science (2014 ICEAS), Bexco, Sapporo, Japan.

His present address is 1512/21 Khukhan Road, Mueang Tai, Mueang, Sisaket, Thailand 33000.